Model driven analysis and design of a lactate sensing genetic circuit

Optimization of a biosensor to differentiate between healthy and colon cancer environments

By Josia Pool

Laboratory of Systems & Synthetic Biology

12 December 2022

Supervisor: Dr. Robert Smith

Abstract

Elevated lactate concentrations of 10 to 30 mM are linked to cancer, while healthy tissues have much lower concentrations of lactate in the range of 1.5 to 3 mM. For this reason, the iGEM 2022 team of Wageningen sought to use this phenomenon in order to create a living diagnostic tool for colorectal cancer: Colourectal. In this work, a mathematical model based on ordinary differential equations (ODE's) was constructed in order to characterize a lactate biosensor, and to explore strategies that can be used to improve the system's ability to discern cancerous lactate concentrations from healthy concentrations of lactate. Using Latin hypercube sampling and subsequent minimization, the model was fit to data. It was found that the operational range of the biosensor could be tuned by lowering the internal concentration of lactate. This can be achieved experimentally by overexpression of the enzyme lactate dehydrogenase. In order to improve the dynamic range of the system, the suggestion was made to implement a leak dampener in the form of a small RNA. The small RNA, which is inversely dependent on lactate, decreases any leaky expression of green fluorescent protein in low lactate concentrations.

Acknowledgements

I would like to thank everyone who was involved in iGEM Wageningen 2022, in particular Robert Smith and Nico Claassens for organizing everything. I also thank Bas Raats, for the nice discussions about lactate detection, the amazing figures and of course the experimental data from the lab. Finally, I would like to thank Rob again, for the great supervision, not just during my thesis but for all aspects of the iGEM project.

Authors declaration

I declare that the work in this dissertation was carried out in accordance with the requirements of the University's regulations and Code of Practice for Research Degree Programmes, and that it has not been submitted for any other academic awards. Except where indicated by specific reference in the text, the work is the candidate's own work. Work done in collaboration with, or with the assistance of, others, is indicated as such. Any views expressed in this dissertation are those of the author.

Signed: [Redacted]

Date: 12DEC22

Table of Contents

List of abbreviations

Abbreviation	Definition
ODE	Ordinary Differential Equation
FIT	Fecal Immunochemical Test
iGEM	Internationally Genetically Engineered Machine
E. coli	*Escherichia coli*
GFP	Green Fluorescent Protein
EC	Effective Concentration
CRISPR	Clustered Regularly Interspaced Short Palindromic Repeats
dCas	deactivated CRISPR associated protein
DNA	Deoxyribonucleic Acid
RNA	Ribonucleic acid
mRNA	Messenger RNA
tRNA	Transfer RNA
asRNA	Antisense RNA
sRNA	Small RNA
sgRNA	Single guide RNA
STAR	Small transcription activating RNA
qPCR	Quantitative Polymerase Chain Reaction
OD600	Optical Density (measured at 600nm)
SBOL	Synthetic Biology Open Language
RPU	Relative Promoter Units
FFN	Feed Forward Network

Chapter 1: Introduction

1.1: Societal relevance

Colorectal cancer is the third most common type of cancer and the second leading cause of cancer death worldwide, accounting for an estimated two million new cases and almost one million deaths in 2020[1]. Current diagnosis relies on periodic screening of the stool for blood and a follow-up colonoscopy. The fecal immunochemical test (FIT) however has a low positive predictive value for advanced adenoma and colorectal cancer (33.8% in 2021) [2]. This can cause unnecessary concern in potential patients and the performed colonoscopies are invasive and quite expensive. Furthermore, these tests are only performed once every two years, and there is the possibility that cancer develops in between screening periods [2]. Often when colon cancer symptoms are noticed the cancer is already in a later stage which makes treatment a lot more difficult than when it is detected early. The five-year survival rate for early state colorectal cancer is 91%, and for late stage it is 15% [3]. In conclusion, early detection of colorectal cancer is crucial to reduce colorectal cancer mortality rates.

1.2: Project Colourectal: A living diagnostic tool for detection of colorectal cancer

The iGEM Wageningen team of 2022 aims to create a living diagnostic tool for colorectal cancer, as an alternative for the FIT. The main goal of the project is to engineer a probiotic bacterial strain, *Escherichia coli* Nissle 1917 (*E. coli* Nissle 1917) to sense colorectal cancer biomarkers and report their presence by producing a color which presents itself in the stool. This allows the user to check the outcome of the test themselves, and the procedure is more user-friendly as the user will only need to take pills instead of having to collect a stool sample.

Detection of cancer is based on sensing two biomarkers: L-lactate and Matrix metalloproteinase 9. In this study the focus lies on the detection of L-lactate, hereby referred to as lactate. Lactate is produced in significantly higher amounts by cancer cells, even in oxygen rich environments. This phenomenon has been named the Warburg effect [4]. In healthy individuals the concentration of lactate in the colon ranges from 1.5 to 3 mM, while in cancerous environments lactate concentrations range from 10 to 30 mM [5,6].

Since lactate is naturally present in low concentrations, the aim is to construct a biosensor which can differentiate between low, healthy concentrations of lactate and high concentrations of lactate associated with cancer.

1.3: Biosensor for the detection of lactate produced by colorectal cancer

A biosensor is often characterized by its dose-response curve, where the response of the biosensor is plotted against the concentration of the sensed compound. Two terms are used to describe the performance of the biosensor: ‘operational range’ and ‘dynamic range’. The operational range is the range of concentrations where the biosensor response changes from its minimum signal to its maximum signal. The dynamic range (also known as the fold-change) is the difference between ‘OFF’ and ‘ON’ states [7]. See Figure 1 for an example.

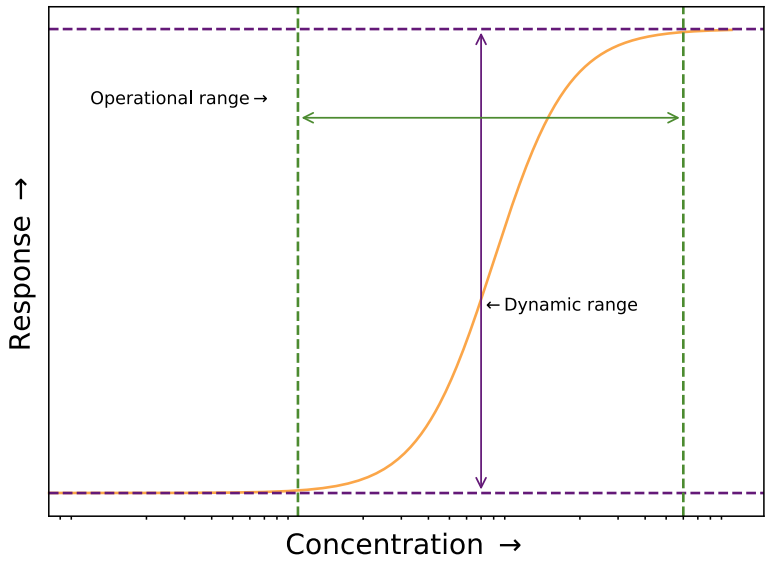

Figure 1: Example of a dose-response curve, where the dynamic range is shown in purple, and the operational range is shown in green.

The start of the operational range is considered the threshold at which the biosensor activates. Therefore, for differentiation between healthy and cancerous environments the ideal threshold concentration would be at the upper limit of healthy lactate concentrations. The end point of the operational range ideally would be around 10 mM, to ensure that in cancerous conditions the output is always at its maximum.

Additionally, the aim is to have a high dynamic range and a low minimum signal, also known as background expression. A higher dynamic range would make it easier for the user to visually differentiate between a negative and positive test. An example of what an ideal dose-response curve would look like can be seen in Figure 2.

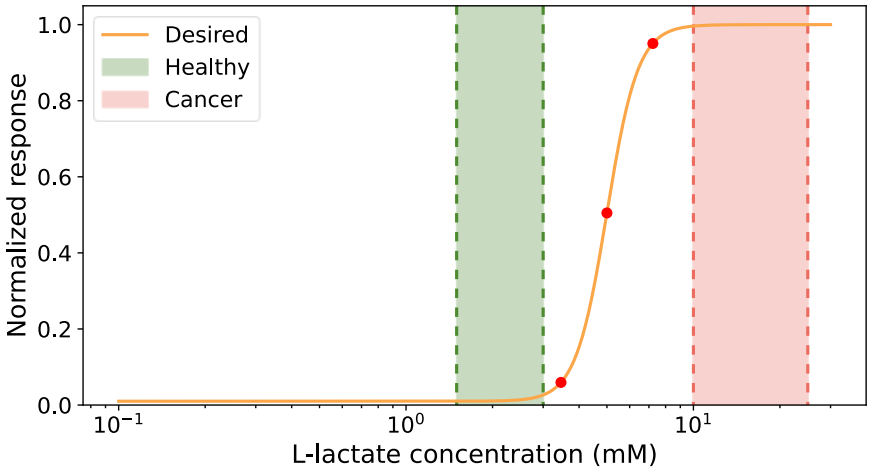

Figure 2: Example of an ideal dose-response curve for a biosensor that differentiates between healthy and cancerous colon environments. The operational range is between 3- and 10-mM lactate, and the dynamic range is maximal (0 to 1 when normalized). The red dots indicate the Effective Concentrations (EC) at which the response is 5%,50% and 95% of the dynamic range.

1.4: Lactate detection and utilization by *E. coli*

E. coli already has a system which can sense and utilize lactate, the 'lldPRD' operon. The operon encodes three proteins: LldP, LldR and LldD. LldP is a lactate permease which facilitates the transport of lactate into the cell by means of a proton motive force [8]. LldR is a regulatory transcription factor which binds to the promoter region of the lldPRD operon. The promoter region consists of two operator sites, O1 and O2 to which LldR can bind. Upon the presence of lactate, LldR binds to lactate and undergoes a conformational change. This causes the operator site O2 to be freed and LldR bound to the operator site O1 promotes transcription of the operon. A schematic view can be seen in

Figure 3.

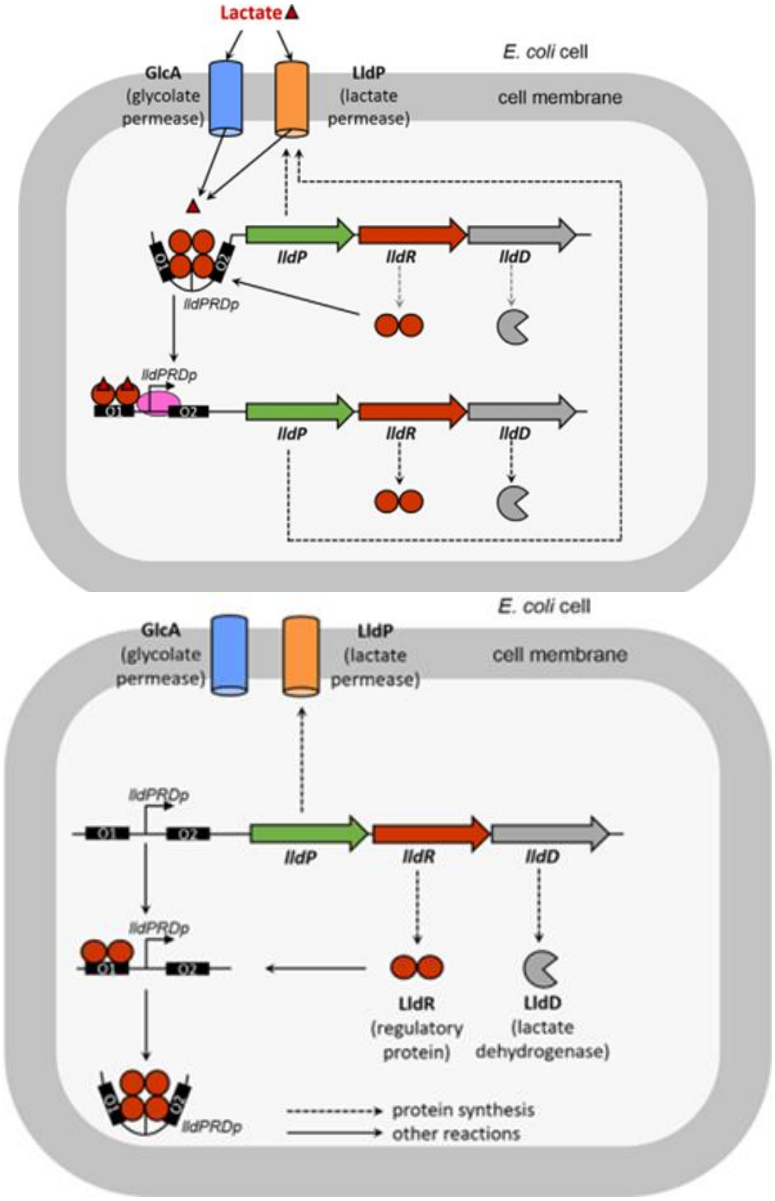

Figure 3: Native lactate utilization by the lldPRD operon in E. coli, the top figure shows the absence of lactate, where LldR blocks transcription and the top figure shows the presence of lactate where the O2 operator site is free and LldR promotes transcription. Image from [9]

lldD encodes a lactate dehydrogenase, which can convert lactate into pyruvate, allowing it to be used in other processes for growth and maintenance. Apart from the lactate permease there is another transport protein which is not regulated by lactate, named GlcA. This enzyme is located in the glycolate degradation operon and is upregulated by the presence of glycolate [10]. Both LldP and GlcA have the same possible substrates and similar affinities [8].

1.5: pALPaGA: A Lactate Promoter Operating in Glucose and Anoxia

The colon contains very little oxygen (from 0-6%) and many nutrients [11]. Unfortunately, the wild-type lldPRD promoter is affected by carbon catabolite repression, meaning that transcription of the operon is repressed in the presence of more energy-rich carbon sources. The promoter is also regulated by arcA, a regulatory protein that represses transcription in anoxic conditions.

Zúñ et al. 2021 [12] have created a lactate promoter sequence, named ALPaGA, that is less affected by carbon catabolite repression and repression by arcA in anaerobic conditions (see Figure 4).

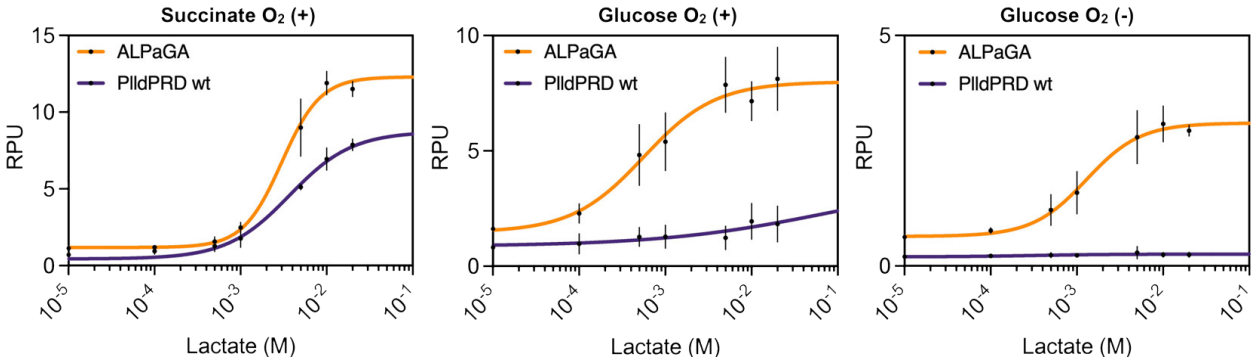

Figure 4: Comparison of pALPaGA and wild-type PlldPRD promoter in E. Coli Nissle 1917 from Zúñ et al. 2021 [12]*. Left panel: promoter response to lactate in aerobic conditions and succinate as carbon source. Middle panel: promoter response to lactate in aerobic conditions and glucose as carbon source. Right panel: Promoter response to lactate in anaerobic conditions and glucose as carbon source. Orange lines show the response of the ALPaGA promoter, and purple lines show the response of the wild-type promoter.*

This promoter enables sensing of lactate in a colonic environment. The promoter is not perfect however, because this promoter shows higher promoter leakage than the wildtype. This can be observed in Figure 4 where the measured relative promoter units (RPU) are greater for the ALPaGA promoter (orange line) than the wild-type promoter (purple line) when almost no lactate is present. Furthermore, the output is much lower compared to optimal conditions (succinate with oxygen), indicating that some repression may still be occurring: Note that while the graphs look similar, the y-axis range and measured RPU is smaller for conditions with glucose in aerobic (middle panel) and anaerobic conditions (right panel) compared to succinate in aerobic conditions (left panel).

For the purpose of detecting cancer, it should be noted that this promoter has an half maximal effective concentration (EC50) of 0.85-2 mM lactate, meaning that the biosensor will be at 50% of its maximum change at normal healthy concentrations of lactate. If the biosensor response is saturated too early, it will be impossible to visually differentiate between a positive and false result. It is therefore hypothesized that alterations are needed for the genetic circuit to function properly.

1.5: Gene regulation with CRISPRi and antisense RNA

The initial biosensor mechanism (Figure 5) that was designed for regulation of chromoprotein expression was based on Clustered Regularly Interspaced Short Palindromic Repeats interference (CRISPRi), where single guide RNA-bound deactivated CRISPR associated protein (dCas) constitutively represses the expression of a colored protein. To lift repression, an antisense RNA (asRNA) that is complementary to the guide RNA is used, which is under control of an engineered lldPRD promoter. The antisense strand can bind to the single guide RNA (sgRNA) preventing the CRISPRi-complex from binding to DNA, lifting repression and enabling transcription of chromoprotein [13,14].

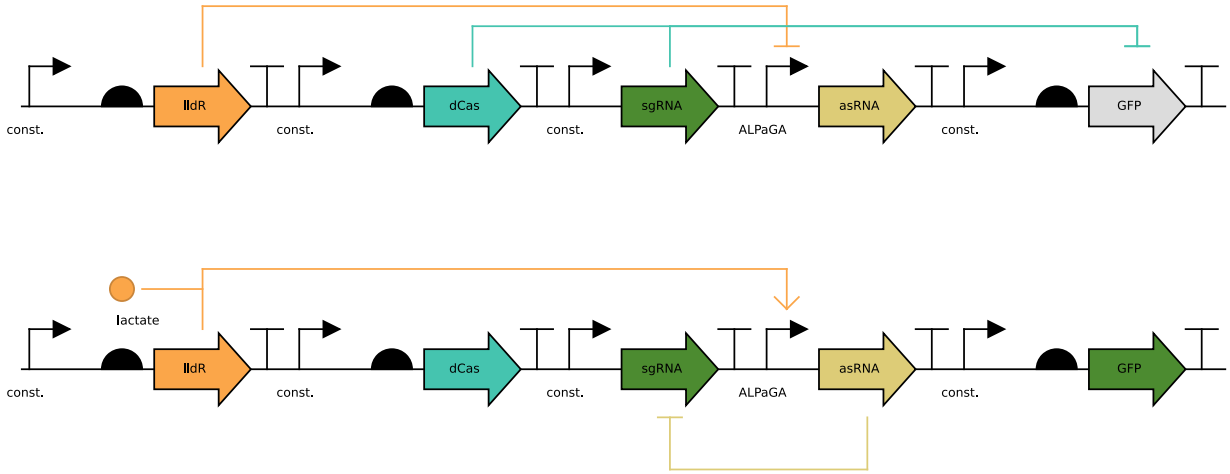

Figure 5: SBOL schematic of the initial lactate sensing system. Top: dCas12 and sgRNA are constitutively produced and repress a constitutively expressed reporter gene. An antisense is under control of lldR. Without lactate, transcription is repressed. Bottom: Upon sensing L-Lactate by binding transcription factor lldR, lldR promotes transcription of the antisense RNA which binds with the sgRNA inhibiting the dCas12-sgRNA complex. Once repression is lifted, GFP is produced.

The CRISPR interference system has the advantage that the system is programmable, orthogonal and lower in metabolic burden compared to regular transcription factors [15]. It would be relatively easy to alter the system if needed. There is however potential for off-target effects and dCas can be toxic when expressed in high amounts [16].

This genetic circuit is expected to work as a filter, where in low concentrations of lactate, the expression of antisense RNA is not enough to lift the repression of dCas9/sgRNA, and expression of reporter is off. Once lactate concentrations are increased, antisense RNA is produced more and will stop repression of the reporter gene. It is very likely that the operational range will not be as desired once the system is tested, which is why strategies to tune the operational range need to be explored.

1.6: Controlling the operational range: Examples from literature

There are various methods that could be used to improve or control the operational range of a biosensor. One method is directed evolution, in which a library of biosensor mutants is created and subsequently screened for the preferred functionality. This cycle can be repeated until a variant with a suitable operational range is found. This method has been used by Snoek et al. (2020) to obtain a biosensor with a broader operational range for *cis,cis*-muconic acid, after one round of directed evolution [17]. The

drawback of this technique is that it requires specialized equipment suitable for high-throughput screening.

Another method is simply switching out different components of the biosensor to evaluate what works best. For example, Rubens et al. (2016) tried out various promoters and ribosome binding sites in order to create hydrogen peroxide biosensors that varied in activation threshold [18].

It is also possible to modify the operational range of a biosensor by tuning the amount of ligand that is available. This has been done by introducing or overexpressing transport proteins, which actively transport the ligand outside or inside the cell. When the ligand is transported outside the cell, the internal concentration of ligand is reduced, which decreases the response of the biosensor relative to the total input. This shifts the operational range to higher concentrations. When the ligand is transported inside the cell, the biosensor response is increased relative to the total input, shifting the operational range to lower concentrations. Both approaches have been proven experimentally in various biosensors [19,20].

1.7: Controlling background expression and dynamic range with a feed forward loop

With the increased leakiness of the ALPaGA promoter it may be possible that due to background expression, the dynamic range will not be enough to visually differentiate between stool that is normal and stool that is colored due to a positive test. Therefore, strategies are needed to lower background expression and increase the dynamic range.

One method that can be used is the implementation of a leak dampener. As its name suggests it is a genetic circuit motif that reduces leaky gene expression. Leak dampener motifs are often coherent feed-forward loops, where the sensed component regulates a reporter gene and a leak dampener, which limits expression of the reporter gene in low concentrations of analyte.

One reported example of a leak dampener shown in Figure 6, published by Ho et al. (2021) used a suppressor tRNA and GFP containing stop codons to create a feedforward loop where in low concentrations of lactate, not enough tRNA is available and translation is stopped prematurely.

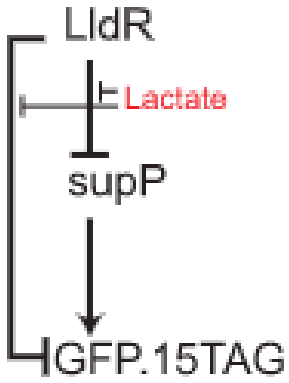

Figure 6: Example of a leak dampener feed-forward loop demonstrated by Ho et al. (2021) [5]*. In low concentrations of lactate, there is not enough tRNA (supP) which disrupts the translation of GFP.*

The use of a synthetic tRNA has drawbacks however, since ideally a free stop codon is needed to prevent read-through of other translated genes. Read-through during gene translation which could have unforeseen consequences. The genetic circuit design in Figure 5 does not contain a feed-forward motif,

since the GFP is not under control of a lactate dependent promoter. If it proves that this design has high background expression or a low dynamic range, changing the GFP promoter to be lactate dependent would be an easy method to incorporate a feed-forward motif in the genetic circuit design.

1.8: Mathematical modeling as method to explore system improvements

In short, the aim is to create a biosensor for lactate that only activates at specific concentrations. A 'conventional' lactate biosensor is unable to achieve this since the biosensors operational range will likely be unable to differentiate between healthy and cancerous lactate concentrations.

Tuning a biosensor to a specific operational range, in this case the range of lactate concentrations between healthy and cancerous levels, can be quite an experimental challenge. Therefore, a mathematical model is developed to characterize the system in two stages, first the lactate sensing-ability of the system is modelled using data from the lab, and then combined with a CRISPR system using previously published data. Afterwards, strategies for improving the system can be evaluated and predictions can be made on how the system should be tuned in practice to the desired operational range.

Specifically, sensitivity analysis can be performed to test what happens when parameters describing the system are changed. Using sensitivity analysis an informed decision is made for future genetic circuit designs. Sensitivity analysis has already been proven in the past to be a useful tool for predicting genetic circuit improvements [21].

This research has the following aims:

- Constructing a mathematical model that describes the designed genetic circuit based on experimental and published data.
- Evaluating the biosensors ability to differentiate between healthy and cancerous lactate environments.
- Comparing the CRISPRi/asRNA system with a generic lactate biosensor.
- Exploring strategies to improve the system if the operational range or dynamic range is not as desired.

Chapter 2: Methods

All code used to generate results is available on the GitLab of the Systems and Synthetic Biology group, at https://gitlab.com/wurssb/StudentProjects/lactate_threshold_circuit. All code should be compatible with python 3.6.9 or higher. Raw and processed data are also available.

2.1: Model explanation

All models are based on ordinary differential equations, which describe the components of the system as they change over time. To construct the model, a schematic was made in which all reactions and interactions thought possible for the initial biosensor constructed in the lab were included, which can be seen in Figure 7. The schematic made for the biosensor including the CRISPRi-asRNA system can be seen in Figure 8.

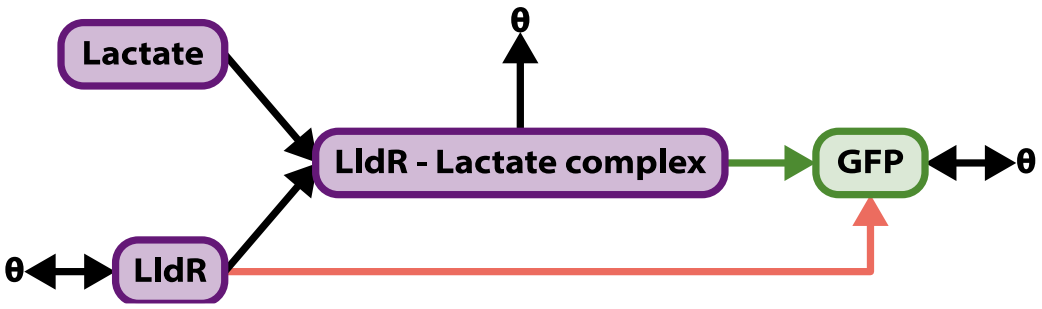

Figure 7: Schematic of the basic lactate sensing system. LldR represses GFP production but when LldR is bound to lactate, production of GFP is activated by the LldR-lactate complex instead. Black lines represent production/degradation. The red arrow represents transcription repression, and the green line represents transcription activation. Theta symbol represents the pool of amino acids and nucleotides, from which all species are produced and returned to once degraded or diluted.

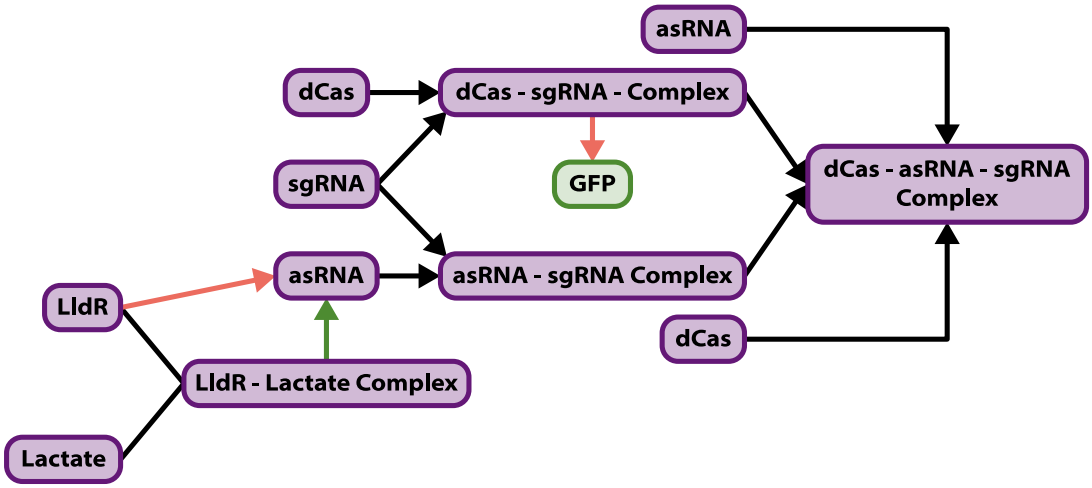

Figure 8: Schematic of the system with the CRISPRi-asRNA system included, where in low concentrations GFP is repressed by a CRISPRi complex. When lactate is present, a antisense RNA is expressed which disrupts the CRISPRi complex, enabling transcription of GFP. Black lines represent production/degradation. The red arrows represent transcription repression, and the green arrows represent transcription activation. Theta has been omitted for clarity.

The law of mass action was used to derive equations from these schematics, which is a general but effective way to approximate reaction kinetics [22]. A framework set out by Andrew D. Keller was used to describe the interactions between LldR and the lactate responsive promoter [23]. Assumptions were

made on how the transcription factor LldR and promoter interact, based on literature [24]. It is assumed that the promoter can be in three states:

- One where free LldR binds to the first operator site of the promoter, enabling weak transcription.
- One where free LldR forms a dimer and binds to both the first and second operator site, repressing transcription by forming a DNA loop as seen in Figure 3.
- Finally, LldR-lactate complex can bind to the first operator site, strongly activating transcription.

How this translates to an equation describing these assumptions can be seen in equation (11.

Considering that transcription and translation are affected by growth [25], the growth rate of the organism was included in terms that describe transcription and translation. This has been done before by Gutiérrez Mena et al. (2022) [26].

2.2: Model equations

2.2.1: CRISPRi-asRNA model

This model describes the rate of change of all RNA and protein species that are considered part of the system. All species are considered degradable, denoted by the k_d parameter. They are also diluted due to growth, which is denoted by the parameter μ. RNA species are transcribed at a certain rate, while proteins are translated from their corresponding mRNA transcripts.

There are also species which are formed by reactions unrelated to transcription or translation. In this model these are:

- CasComplex, which stands for the sgRNA-dCas complex referred to in Figure 8.
- asComplex, which corresponds to single guide RNA bound to antisense RNA.
- asCasComplex, which describes the sgRNA-dCas complex which is also bound to antisense RNA. It is assumed that this complex can form when antisense RNA binds to the sgRNA-dCas complex, and also when a dCas protein associates with single guide RNA bound to antisense RNA.

Since data on growth was not provided, it was assumed that the growth rate was always at its maximum and dilution due to growth was constant.

Terms in equation 1 to 34 have been color coded, showing transcription terms in orange, translation terms in green and degradation/dilution terms in red. Regulatory terms affected by the concentration of other model species (such as repression by sgRNA-dCas complex) have been colored purple. Finally, any reactions which turn one model species into another have been colored turquoise.

$$\frac{d[dCas_{mRNA}]}{dt} = k\_b_{dCas} - [dCas_{mRNA}](\mu + k\_d_{dcasmrna}) \quad (1)$$

$$\frac{d[dCas]}{dt} = k\_pt_{dCas}[dCas_{mRNA}] + k\_f_{1_{rv}}[CasComplex] - k\_f_{1_{fw}}[sgRNA][dCas] + k\_f_{4_{rv}}[asCasComplex] - k\_f_{4_{fw}}[dCas][asComplex] - [dCas](\mu + k\_d_{dcas}) \quad (2)$$

$$\frac{d[sgRNA]}{dt} = k\_b_{sgrna} + k\_f_{1_{rv}}[CasComplex] - k\_f_{1_{fw}}[sgRNA][dCas] - k\_f_{2_{fw}}[asRNA][sgRNA] + k\_f_{2_{rv}}[asComplex] - [sgRNA](\mu + k\_d_{sgrna}) \quad (3)$$

$$\frac{d[CasComplex]}{dt} = k\_f_{1_{fw}}[sgRNA][dCas] - k\_f_{1_{rv}}[CasComplex] - k\_f_{3_{fw}}[asRNA][CasComplex] + k\_f_{3_{rv}}[asCasComplex] - [CasComplex](\mu + k\_d_{cascomplex}) \quad (4)$$

$$\frac{d[asRNA]}{dt} = \frac{I^{n_{inducer}}}{kd_{asrna}^{n_{inducer}} + I^{n_{inducer}}} k\_p_{asrna} + k\_f_{2_{rv}} asComplex - k\_f_{2_{fw}}[asRNA][sgRNA] + k\_f_{3_{rv}}[asCasComplex] - k\_f_{3_{fw}}[asRNA][CasComplex] - [asRNA](\mu + k\_d_{asrna}) \quad (5)$$

$$\frac{d[asComplex]}{dt} = k\_f_{2_{fw}}[asRNA][sgRNA] - k\_f_{2_{rv}}[asComplex] + k\_f_{4_{rv}}[asCasComplex] - k\_f_{4_{fw}}[dCas][asComplex] - [asComplex](\mu + k\_d_{ascomplex}) \quad (6)$$

$$\frac{d[asCasComplex]}{dt} = k\_f_{3_{fw}}[asRNA][CasComplex] - k\_f_{3_{rv}}[asCasComplex] - k\_f_{4_{rv}}[asCasComplex] + k\_f_{4_{fw}}[dCas][asComplex] - [asCasComplex](\mu + k\_d_{ascascomplex}) \quad (7)$$

$$\frac{d[GFP_{mRNA}]}{dt} = k\_p_{gfpmrna} \frac{kd_{dcas}^{n_{cascomplex}}}{kd_{dcas}^{n_{cascomplex}} + [CasComplex]^{n_{cascomplex}}} - [GFP_{mRNA}](\mu + k\_d_{gfpmrna}) \quad (8)$$

$$\frac{d[GFP]}{dt} = k\_pt_{gfp}[GFP_{mRNA}] - [GFP](\mu + k\_d_{gfp}) \quad (9)$$

Parameter values and descriptions can be seen in the Appendix, Table 2.

2.2.2: Lactate model

Since data for growth was available, growth is modeled explicitly by a logistic function, shown in equation 10 below. μ_{max} stands for the maximum growth rate possible. t_c is the time at which maximum growth occurs, σ stands for the spread of the growth curve and cap is the maximum cell density possible at steady state.

$$\mu = \mu_{max} e^{-0.5\left(\frac{t-t_c}{\sigma}\right)^2} \left(1 - \frac{[C_x]}{cap}\right) \quad (10)$$

$$\text{ALPaGA} = \frac{k\_b_{alp} + (alp_{act1} + k\_b_{alp}) * alp\_k_{act1}[lldR] + (alp_{act2} + k\_b_{alp}) * alp\_k_{act2}[lldRcomplex]}{\gamma + alp\_k_{act1}[lldR] + alp\_k_{act2}[lldRcomplex] + alp_{k3}[lldR]^2} \quad (11)$$

$$\frac{d[lldR_{mRNA}]}{dt} = \frac{\mu}{\mu_{max}}(k\_op_{succ} + copy\_nr * k\_b_{p3}) - [lldr_{mRNA}](\mu + k\_d_{lldRmRNA}) \quad (12)$$

$$\frac{d[lldR]}{dt} = \mu * k\_pt_{lldR}[lldR_{mRNA}] - k\_f_{lldRcomplex}[lldR][Lactate]^2 - [lldR](\mu + k\_d_{lldR}) \quad (13)$$

$$\frac{d[lldRcomplex]}{dt} = k\_f_{lldRcomplex}[lldR][Lactate]^2 - [lldRcomplex](\mu + k\_d_{lldRcomplex}) \quad (14)$$

$$\frac{d[GFP_{mRNA}]}{dt} = \frac{\mu}{\mu_{max}} * copy\_nr * ALPaGA - [GFP_{mRNA}](\mu + k\_d_{gfpmRNA}) \quad (15)$$

$$\frac{d[GFP]}{dt} = \mu * k\_pt_{gfp}[GFP_{mRNA}] - [GFP](\mu + k\_d_{gfp}) \quad (16)$$

$$\frac{d[Cx]}{dt} = \mu[Cx] \quad (17)$$

Parameter values and descriptions can be seen in the Appendix, Table 3.

2.2.3: Combined model

Models were combined by replacing the asRNA production with the terms for the ALPaGA promoter, using the same equation for describing the ALPaGA promoter as equation (11. The cell density and growth rate μ follows the equations described in equations (17 and (10 respectively. Parameters for growth rate dependency were added for terms of the CRISPRi model that describe transcription or translation. Because growth is now time dependent, parameters of the CRISPRi model were rescaled accordingly.

Any transcription terms of the CRISPRi model were multiplied by the copy number, since it was assumed that if such a construct was made, it would all be on the same plasmid. For any overlapping parameters such as those related to GFP degradation the value of lactate model was chosen.

$$\frac{d[dCas_{mRNA}]}{dt} = \frac{\mu}{\mu_{max}}(k\_b_{dcas} * copy\_nr) - [dCas_{mRNA}](k\_d_{dcasmrna} + \mu) \tag{18}$$

$$\frac{d[dCas]}{dt} = \mu * k\_pt_{dCas}[dCas_{mRNA}] + k\_f_{1_{rv}}[CasComplex] - k\_f_{1_{fw}}[sgRNA][dCas] + k\_f_{4_{rv}}[asCasComplex] - k\_f_{4_{fw}}[dCas][asComplex] - [dCas](\mu + k\_d_{dcas}) \tag{19}$$

$$\frac{d[sgRNA]}{dt} = \frac{\mu}{\mu_{max}} k\_b_{sgrna} * \ copy\_nr + k\_f_{1_{rv}}[CasComplex] - k\_f_{1_{fw}}[sgRNA][dCas] - k\_f_{2_{fw}}[asRNA][sgRNA] + k\_f_{2_{rv}}[asComplex] - [sgRNA](\mu + k\_d_{sgrna}) \tag{20}$$

$$\frac{d[CasComplex]}{dt} = k\_f_{1_{fw}}[sgRNA][dCas] - k\_f_{1_{rv}}[CasComplex] - k\_f_{3_{fw}}[asRNA][CasComplex] + k\_f_{3_{rv}}[asCasComplex] - [CasComplex](\mu + k\_d_{cascomplex}) \tag{21}$$

$$\frac{d[asRNA]}{dt} = \frac{\mu}{\mu_{max}} * copy\_nr * ALPaGA + k\_f_{2_{rv}}[asComplex] - k\_f_{2_{fw}}[asRNA][sgRNA] + k\_f_{3_{rv}}[asCasComplex] - k\_f_{3_{fw}}[asRNA][CasComplex] - [asRNA](k\_d_{asrna} + \mu) \tag{22}$$

$$\frac{d[asComplex]}{dt} = k\_f_{2_{fw}}[asRNA][sgRNA] - k\_f_{2_{rv}}[asComplex] + k\_f_{4_{rv}}[asCasComplex] - k\_f_{4_{fw}}[dCas][asComplex] - [asComplex](\mu + k\_d_{ascomplex}) \tag{23}$$

$$\frac{d[asCasComplex]}{dt} = k\_f_{3_{fw}}[asRNA][CasComplex] - k\_f_{3_{rv}}[asCasComplex] - k\_f_{4_{rv}}[asCasComplex] + k\_f_{4_{fw}}[dCas][asComplex] - [asCasComplex](\mu + k\_d_{ascascomplex}) \tag{24}$$

$$\frac{d[lldR_{mRNA}]}{dt} = \frac{\mu}{\mu_{max}}(k\_op_{succ} + copy\_nr * k\_b_{p3}) - [lldr_{mRNA}](\mu + k\_d_{lldRmRNA}) \tag{25}$$

$$\frac{d[lldR]}{dt} = \mu * k\_pt_{lldR}[lldR_{mRNA}] - k\_f_{lldRcomplex}[lldR][Lactate]^2 - [lldR](\mu + k\_d_{lldR}) \tag{26}$$

$$\frac{d[lldRcomplex]}{dt} = k\_f_{lldRcomplex}[lldR][Lactate]^2 - [lldRcomplex](\mu + k\_d_{lldRcomplex}) \tag{27}$$

$$\frac{d[GFP_{mRNA}]}{dt} = \frac{\mu}{\mu_{max}} * copy\_nr * k\_p_{gfpmrna} * \frac{kd_{dcas}^{n_{cascomplex}}}{kd_{dcas}^{n_{cascomplex}} + [CasComplex]^{n_{cascomplex}}} - [GFP_{mRNA}](\mu + k\_d_{gfpmRNA}) \tag{28}$$

$$\frac{d[GFP]}{dt} = \mu * k\_pt_{gfp}[GFP_{mRNA}] - [GFP](\mu + k\_d_{gfp}) \quad (29)$$

Parameter values and descriptions can be seen in the Appendix, Table 4.

2.2.4: Model improvements

Feedforward network

All equations were equal to those described in the combined model equations (18 to (29, only $k\_p_{gfpmrna}$ was replaced by $ALPaGA$ in the equation describing GFP_{mRNA} as shown below in equation 30.

$$\frac{d[GFP_{mRNA}]}{dt} = \frac{\mu}{\mu_{max}} * copy\_nr * ALPaGA * \frac{kd_{dcas}^{n_{cascomplex}}}{kd_{dcas}^{n_{cascomplex}} + [CasComplex]^{n_{cascomplex}}} - [GFP_{mRNA}](\mu + k\_d_{gfpmRNA}) \quad (30)$$

sRNA leak dampener switch

To describe the production and regulation of sRNA using CRISPR interference, the following equations were derived:

$$\frac{d[sRNA]}{dt} = \frac{\mu}{\mu_{max}} k\_b_{srna} * copy\_nr * \frac{kd_{dcas}^{n_{cascomplex}}}{kd_{dcas}^{n_{cascomplex}} + [CasComplex2]^{n_{cascomplex}}} - [sRNA](k\_d_{srna} + \mu) \quad (31)$$

CasComplex2 stands for the CRISPRi complex that forms when dCas is bound to the second guide RNA which targets the small RNA.

$$\frac{d[CasComplex2]}{dt} = k\_f_{5_{fw}}[sgRNA2][dCas] - k\_f_{5_{rv}}[CasComplex2] - [CasComplex2](\mu + k\_d_{cascomplex}) \quad (32)$$

$$\frac{d[sgRNA2]}{dt} = \frac{\mu}{\mu_{max}} * copy\_nr * ALPaGA + k\_f_{5_{rv}}[CasComplex2] - k\_f_{5_{fw}}[sgRNA2][dCas] - [sgRNA2](\mu + k\_d_{sgrna2}) \quad (33)$$

To add sRNA mediated degradation of GFP_{mRNA}, a sRNA dependent degradation term was added to the equation describing GFP_{mRNA}, as shown in equation 34 below.

$$\frac{d[GFP_{mRNA}]}{dt} = \frac{\mu}{\mu_{max}} * \text{copy\_nr} * ALPaGA * \frac{kd_{dcas}^{n_{cascomplex}}}{kd_{dcas}^{n_{cascomplex}} + [CasComplex]^{n_{cascomplex}}} - [GFP_{mRNA}]\left(\mu + k\_d_{gfpmRNA} + k\_d_{gfpmrna2} * \frac{[sRNA]}{kd_{srna} + [sRNA]}\right) \quad (34)$$

Parameter values and descriptions can be seen in the Appendix, Table 5.

2.3: Experiment simulation

Simulation of the ordinary differential equations was done with SciPy 1.9.0 [27], which uses lsoda as a solver. SciPy was also used to interpolate simulation results in order for scoring the model and calculating EC values.

2.3.1: Initial system and combined model

First, 24 hours of 'overnight' growth without lactate was simulated. After simulating, the starting OD600 was diluted back to its initial value (0.05). Afterwards, the concentration of lactate was changed, and the system was simulated for 21 hours. This mimics what was done in the lab: First a pre-culture, which is then diluted and measured over time in a plate reader. In the initial conditions for the pre-culture everything started at 0, except the cell population which was set to 0.05 OD.

2.3.2: CRISPRi-asRNA model

Since the data starts in what was assumed a steady state where no dCas or sgRNA is present, the initial condition of GFP was approximated by setting the differential equations to zero and solving for GFP:

$$\frac{d[GFP_{mRNA}]}{dt} = 0 = k\_p_{g\text{fpmRNA}} - [GFP_{mRNA}](\mu + k\_d_{gfpmrna}) \tag{35}$$

$$[GFP_{mRNA}] = k\_p_{gfpmRNA}/(\mu + k\_d_{gfpmrna}) \tag{36}$$

$$\frac{d[GFP]}{dt} = k\_pt_{gfp} * [GFP_m RNA] - [GFP](\mu + k\_d_{gfpmrna}) = 0 \tag{37}$$

$$k\_pt_{gfp} * \ k\_p_{gfpmRNA}/(\mu + k\_d_{gfpmrna}) - [GFP](\mu + k\_d_{gfpmrna}) = 0 \tag{38}$$

$$[GFP] = k\_pt_{gfp} * \ k\_p_{gfpmRNA}/\left((\mu + k\_d_{gfp})(\mu + k\_d_{gfpmrna})\right) \tag{39}$$

This set the initial concentration of GFP. The system was then simulated for a total of 18 hours, where at time of induction the inducer concentration was changed to 5 mM.

2.4: Data acquisition and processing

2.4.1: Lactate biosensor data

Experimental absorbance (OD600) and fluorescence data was obtained by Bas Raats, a fellow iGEM team member who tested the ALPaGA promoter described in Zúñ et al. 2021 [12] in a plate-reader experiment. For model fitting, data was used from testing in aerobic conditions with succinate as carbon source, one of the conditions tested by Zúñ et al. 2021 shown in Figure 4. Fluorescence data was divided by the absorbance to correct fluorescence for the cell volume. The data was then processed for model fitting by calculating the average and standard deviation over all replicates. Some datapoints had an almost nonzero standard deviation, which would cause the optimization algorithm to focus solely on these datapoints. To solve this problem, any standard deviations below 10^{-6} were set to 1.

2.4.2: CRISPRi/asRNA

Fluorescence data (of which an example can be seen in Figure 9) from Lee et al. (2016) [13] was extracted manually using WebPlotDigitizer [28]. Three time-series data of 18 hours were extracted, where dCas9 and a single guide RNA were induced at t=0. Antisense RNA was induced at variable time points, at 7, 9 and 11 hours. Due to the manual extraction, it was at times not possible to extract the error due to overlap of the error bar with the plotted points. In this case, an error of 1% was assumed.

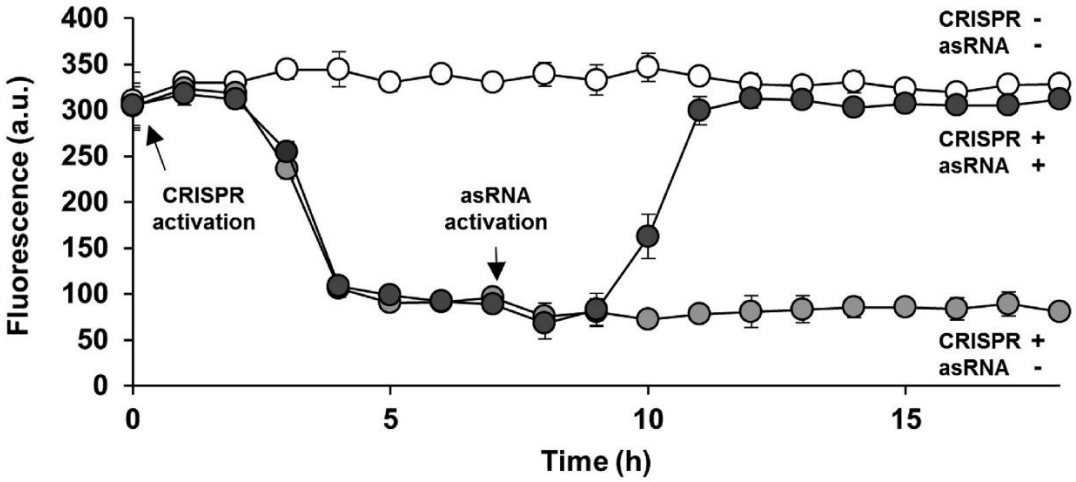

Figure 9: Example of data from Lee et al. (2016), where CRISPR interference was activated at t=0 and an antisense RNA was activated at t=7h (Dark grey dots)

2.5: Model fitting and optimization

Latin hypercube sampling (using the python package pyDOE 0.3.8 [29]) was used to generate parameter set samples. To fit the model to data, one million parameter sets were simulated, and the top 1000 scoring parameter sets were selected for optimization by the minimization algorithm L-BFGS-B in python using SciPy. Upper and lower bounds for L-BFGS-B minimization were ±10% the original values from the Latin hypercube sample.

To score parameter sets, the weighted sum of squared errors was calculated between the data and the simulation, as seen in equation 40 below.

$$Score(j) = \sum_{i=t_0}^{t_f} \frac{\left(Fluorescence_{sim}(i,j) - Fluorescence_{data}(i)\right)^2}{\sigma_i^2} \quad (40)$$

For a specific parameter set **j**, where for timepoint t_0 to the final timepoint t_f, the difference between simulated and experimental timepoints is calculated, squared, divided by the variance of the data ($\boldsymbol{\sigma_i^2}$) and summed together.

For models using time-dependent growth, the absorbance data was first fitted to the growth equations (10 and 17) using one million Latin hypercube samples. The best scoring values obtained were then fixed during the simulations of the full model Latin hypercube samples. Bounds for L-BFGS-B were the same for growth parameters and all other parameters.

2.6: Model evaluation

To evaluate the operational and dynamic range of the models, a range of 100 concentrations were sampled logarithmically, from $10^{-1.5}$ to $10^{1.5}$ millimolar (50 concentrations from 10^{-1} to $10^{1.7}$ for one-at-a-time analysis). After simulation of the concentration range, the end points were used to create a dose-response curve. The operational range was obtained by interpolation of the response to yield the concentration where the dose-response curve was at 5, 50 and 95% of its maximum: the EC5, EC50 and EC95. The EC5 was defined as the beginning of the operational range, and the EC95 was defined as the end.

The dynamic range was calculated as the fold-change of the dose-response curve, shown in equation 41 below.

$$Fold\ change\ = \frac{max(response) - min(response)}{min(response)} \tag{41}$$

Background expression was defined as the minimal response.

2.7: Sensitivity analysis

To make predictions about how the system should be changed, one-at-a-time parameter sensitivity analysis was performed. A sample list was created where each parameter of the model was increased and decreased by a maximum of factor 10 one at a time and simulated to see what effect it would have on the dose-response curve. For each tested sample, the EC5, EC50 and EC95 were calculated and plotted on the dose-response curve. Dynamic range was calculated as the fold-change of the dose-response curve, shown in equation 41.

Chapter 3: Results

3.1: Models fitted to data

In order to be able to analyze what improvements could be made to the lactate sensing system shown in Figure 5, the model of CRISPRi/asRNA interaction (as described in 2.2.1: CRISPRi-asRNA model) and the lactate sensing model (as defined in 2.2.2: Lactate model) have to be fitted to data separately and then combined. This was done by the method described in chapter 2.5: Model fitting and optimization.

3.1.1: CRISPRi/asRNA model fits the data

Model fitting and optimization of the CRISPRi/asRNA model resulted in the curves seen in Figure 10 below. On the left, data was plotted where antisense RNA was induced after seven hours (Orange) against a simulation of the model with the best scoring parameter set (Turquoise). On the right data was plotted where antisense RNA was induced at 9 hours against a simulation.

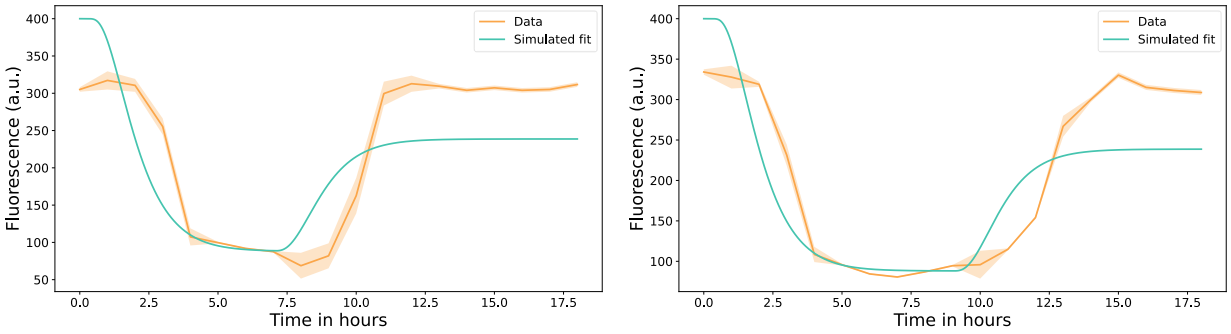

Figure 10: CRISPRi/asRNA model fit against training data from Lee et al. (2016) [13]*. Left panel: asRNA induced at t=7h. Right panel: asRNA induced at t=9h. Orange line: Data, orange shaded regions represent the error bars. Turquoise: Simulation.*

The simulated model shows the same behavior as the data, where after t=0 the fluorescence decreases due to the expression of dCas9 and a single guide RNA. After time of induction, antisense RNA gets expressed and the amount of fluorescence starts to increase. The data is delayed compared to the simulation. When a time delay of one hour was implemented at t=0 and time of induction, the score of the model improved from 13047 to 8896. The resulting simulation can be seen in Figure 11, which now lines up with the decrease and increase of fluorescence that the data shows. The rationale for a time delay was that upon t=0 and time of induction, the cells are diluted and provided with a medium containing different inducers, after which the cells need to acclimatize to their new conditions.

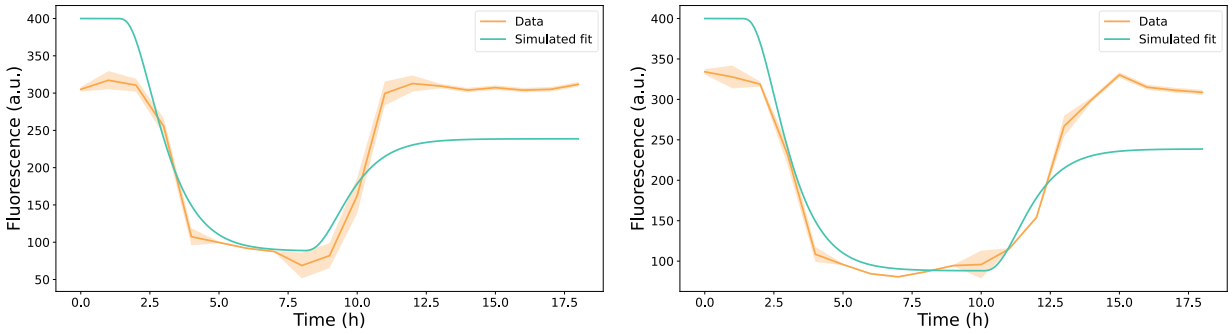

Figure 11: Model fit against training data from Lee et al. (2016) [13]*, with an implemented time delay of one hour at t=0 and induction of antisense RNA. Left panel: asRNA induced at t=7h. Right panel: asRNA induced at t=9h. Orange line: Data, orange shaded regions represent the error bars. Turquoise: Simulation.*

The model fit was also validated by using a dataset that was not used in the model, shown in Figure 12 below. Comparing this simulation with the data also matched, indicating that the model correctly captures the behavior of the CRISPRi/asRNA system.

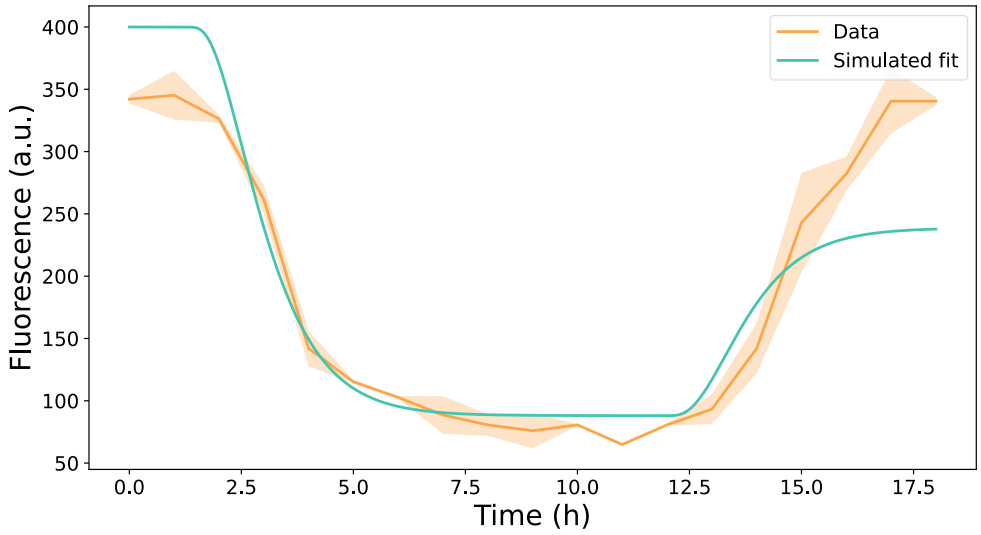

Figure 12: Delayed CRISPRi/asRNA model fit against validation data where asRNA was induced at t=11h. Orange line: Data, orange shaded regions represent the error bars. Turquoise: Simulation.

3.1.2: Lactate model fits the data

After fitting and optimization of the lactate model described in 2.2.2: Lactate model, the dose-response curve of the data (orange) and model (turquoise) were plotted against each other, which can be seen in Figure 13.

The model matches measured concentrations from 0.05 mM to 5 mM lactate well but falls short when simulated at a concentration of 20 mM. The dose-response curve of the model has a EC95 concentration of around 7.6 mM, while the data suggests that at 20 mM the response is still not saturated. This anomaly will be discussed in 4.2: .

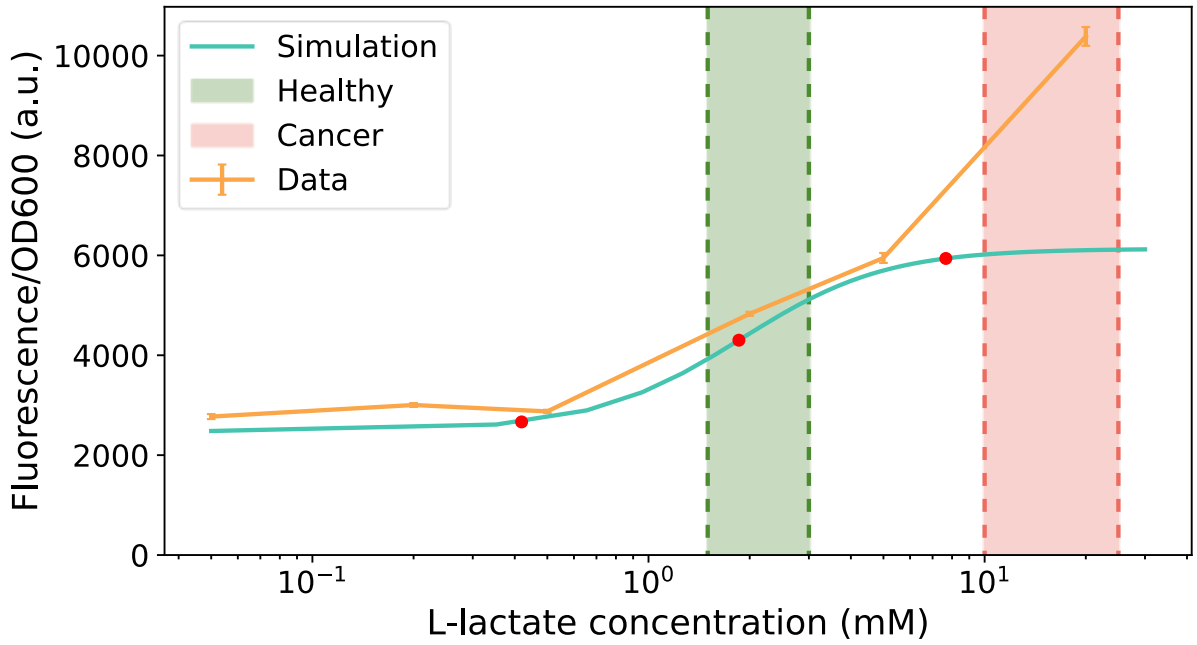

Figure 13: Comparison of dose-response curves from the data (orange line) and the Lactate model (turquoise line). Red dots are the calculated EC5, EC50 and EC95 of the model. The green area indicates the range of healthy lactate concentrations, while the red area indicates the range of cancerous concentrations.

3.2: Combining models does not result in the desired behavior

After the models were fit to data, they were combined to simulate the response to lactate when a CRISPRi/asRNA system was included. The resulting dose-response curve was compared to the original biosensor, which is shown in Figure 14. Here it can be seen that both systems are quite similar in terms of response, with their EC values (red dots) being very close together. The background expression, here considered as the concentrations below the healthy concentrations of lactate (green area) is slightly higher with a CRISPRi/asRNA system. Both systems do not have the operational range necessary to distinguish healthy lactate concentrations from cancerous lactate concentrations, since in healthy concentrations the system is already at 50% of their maximum response while the desired response would be below 5% of the maximum response.

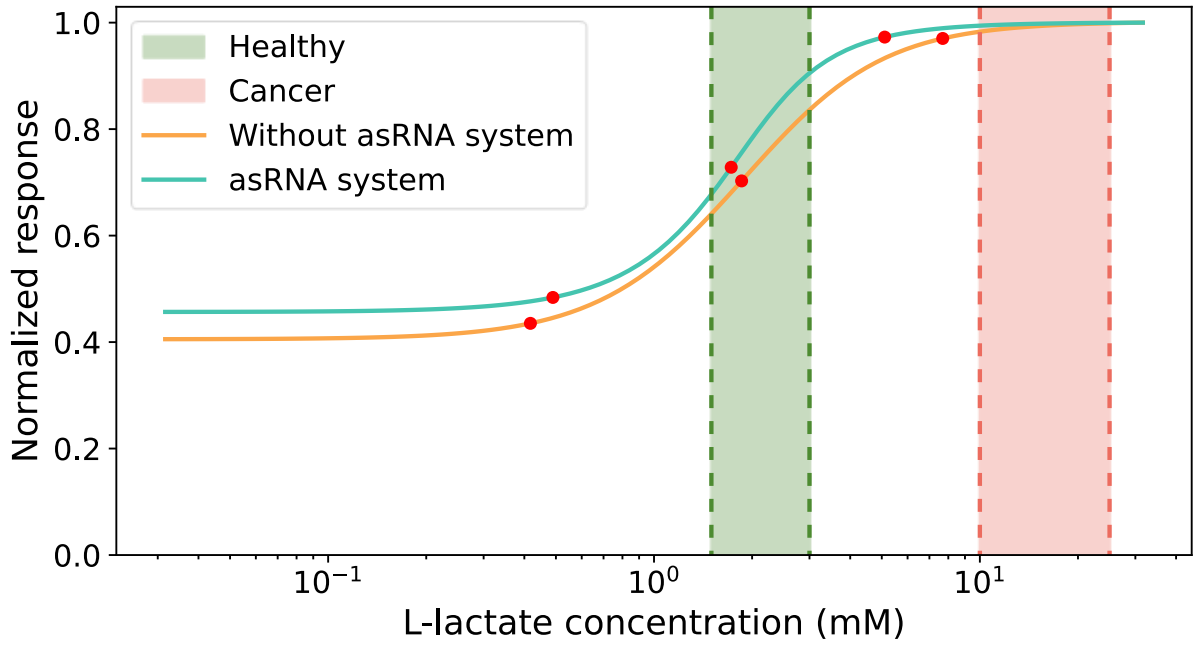

Figure 14: Comparison of the lactate sensing models with (Turquoise line) and without (Orange line) CRISPRi-asRNA system, with the EC5, EC50 and EC95 marked with red dots. Fluorescence was normalized by dividing each curve by its maximum. Ret dots indicate the calculated EC5, EC50 and EC95. The green zone shows the range of healthy lactate concentrations, while the red zone shows lactate concentrations associated with cancer.

While the comparison suggests that the addition of a CRISPRi/asRNA system is not beneficial, there is more room for system improvement since there are more components which can be fine-tuned to improve the operational range and limit background expression.

3.3: Improving the system: Operational range

In order to identify how the system can be improved, one-at-a-time sensitivity analysis was performed to analyze how the system would change if one parameter was perturbed. A full summary of this analysis can be found in Appendix 2: Sensitivity analysis results of the combined model. These subchapters highlight the most important parameters concerning the operational range. A summary of the sensitivity analysis and the results for each parameter can be found in Appendix 2: Sensitivity analysis results of the combined model.

3.3.1: Internal lactate concentration to tune operational range

From the sensitivity analysis of the combined model the parameter $k\_f_{lldrcomplex}$ has the biggest effect on increasing the operational range, as shown in Appendix 2.1: Summarized sensitivity analysis results. Decreasing this parameter with a factor of 10 increased the EC5 from 0.5 mM to 1.55 mM. $k\_f_{lldrcomplex}$ is a parameter in the model which describes the rate of complex formation between lactate and lldr. From the sensitivity analysis it was revealed that changes to this parameter directly influenced the operational range, as shown in Figure 15 below. When $k\_f_{lldrcomplex}$ is decreased, the operational range shifts to higher concentrations (Orange line).

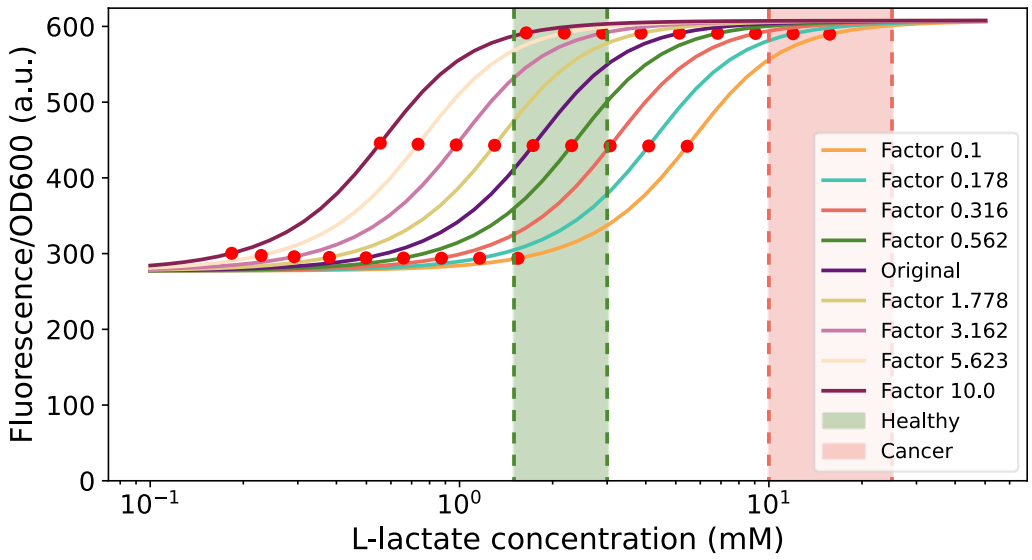

Figure 15: One-at-a-time sensitivity analysis result for $k\_f_{lldrcomplex}$, showing what happens to the original dose-response curve (in dark blue) when the parameter is decreased (right of the original curve) and increased (left of the original curve). Red dots indicate the EC5, EC50 and EC95 of each respective curve.

Without complex protein engineering this parameter is unlikely to be able to be changed experimentally. The term that contains this parameter, $k\_f_{lldrcomplex} * [LldR] * [lactate]^2$, could be changed, by either changing the lldR or lactate concentration. Reducing the amount of lldR may have effects on regulation of the ALPaGA promoter, and lactate is only involved in this model term. This makes changing the lactate concentration the best choice.

3.3.2: asRNA parameters do not affect operational range

One of the experimental hypotheses in the beginning of the project was that by changing the binding strength of antisense RNA and single guide RNA, the biosensors operational range could be tuned to the desired range of 3 to 10 mM. The results of sensitivity analysis shown in Figure 16 suggests however that the change in operational range is minimal compared to the rest of the parameters shown in Appendix Figure 22. Especially $k\_f_{2_{fw}}$ to $k\_f_{4_{rv}}$ have almost no effect on the EC5, which describe kinetic parameters that are related to the binding affinity between the single guide RNA and antisense RNA.

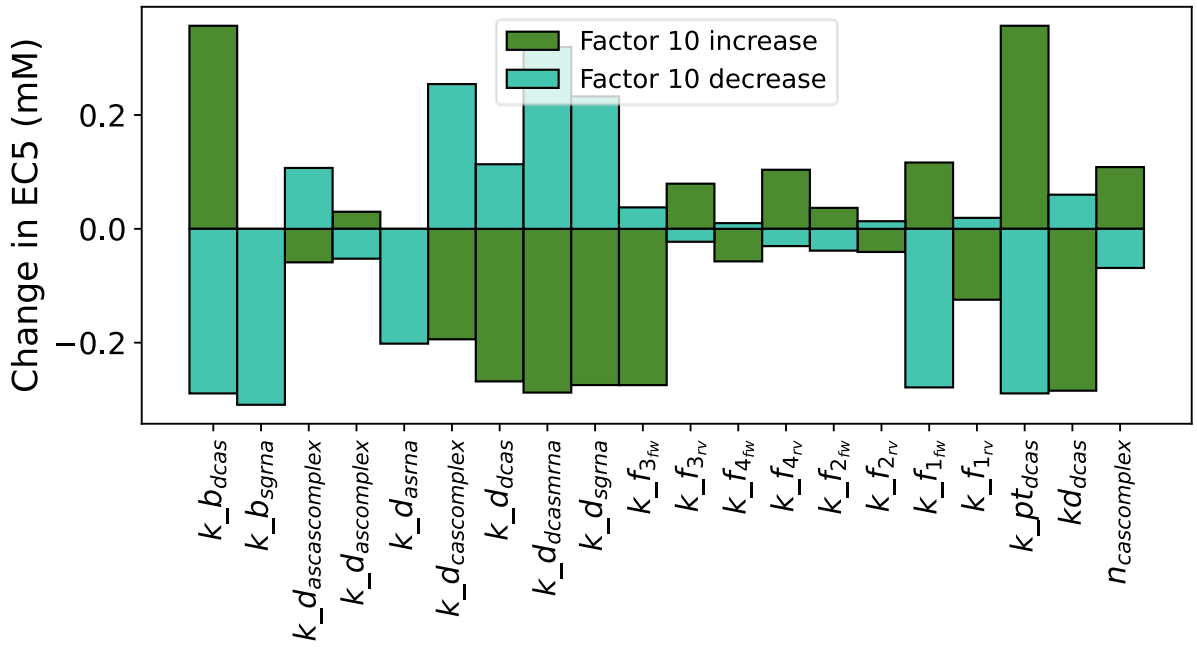

Figure 16: Effect of decreasing (Turquoise bars) or increasing (Green bars) CRISPRi/asRNA related parameters with a factor of 10 on the EC5 of the combined model.

3.4: Improving the system: Background expression and dynamic range

Having found strategies for improving the operational range, the focus now shifts to decreasing the background expression of the lactate sensing system. Ideally the system would have zero background expression at a lactate concentration lower than 3 mM.

3.4.1: Introduction of a Feed-forward loop reduces background expression

As described in the introduction, feed forward loops are genetic circuit motifs that are shown in literature to reduce background expression and subsequently increase the dynamic range of a genetic circuit [5,30].

By switching from a constitutive GFP promoter to the lactate-dependent ALPaGA promoter, a feed-forward motif is created in the system shown in Figure 17.

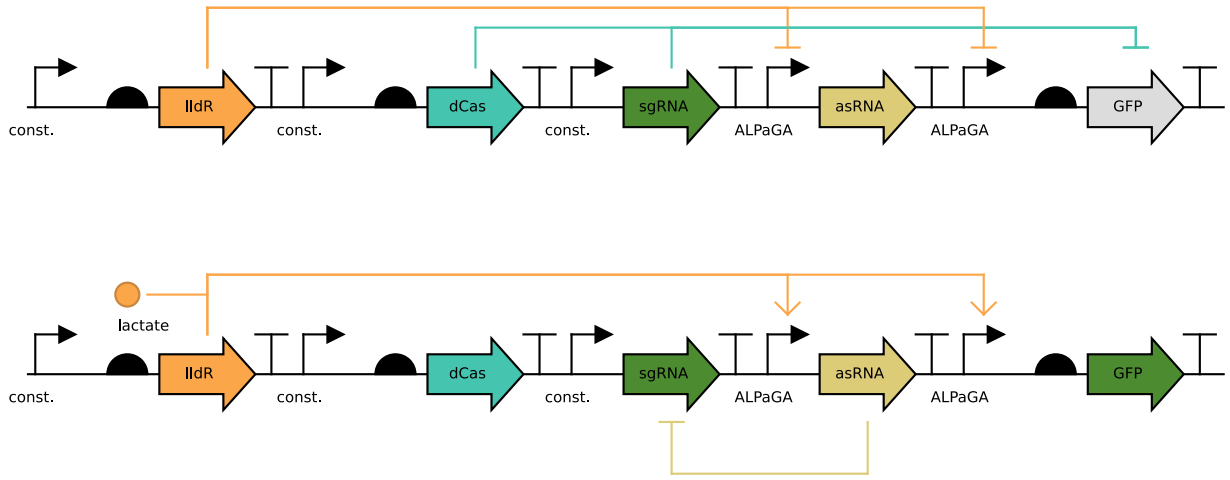

Figure 17: Switching out the constitutive GFP promoter for ALPaGA creates a feed-forward loop, where in the 'OFF' state transcription is both repressed by a CRISPRi complex and lldR. In the 'ON' state, repression is lifted and transcription of GFP is activated.

Replacing the constitutive promoter with ALPaGA enables the double repression of GFP in low lactate concentrations but activates the system more when high concentrations of lactate are present. The dose-response curve of this model is shown in Figure 18 as the red line, where introducing the feed-forward motif reduced the background expression more than two-fold compared to without (orange line).

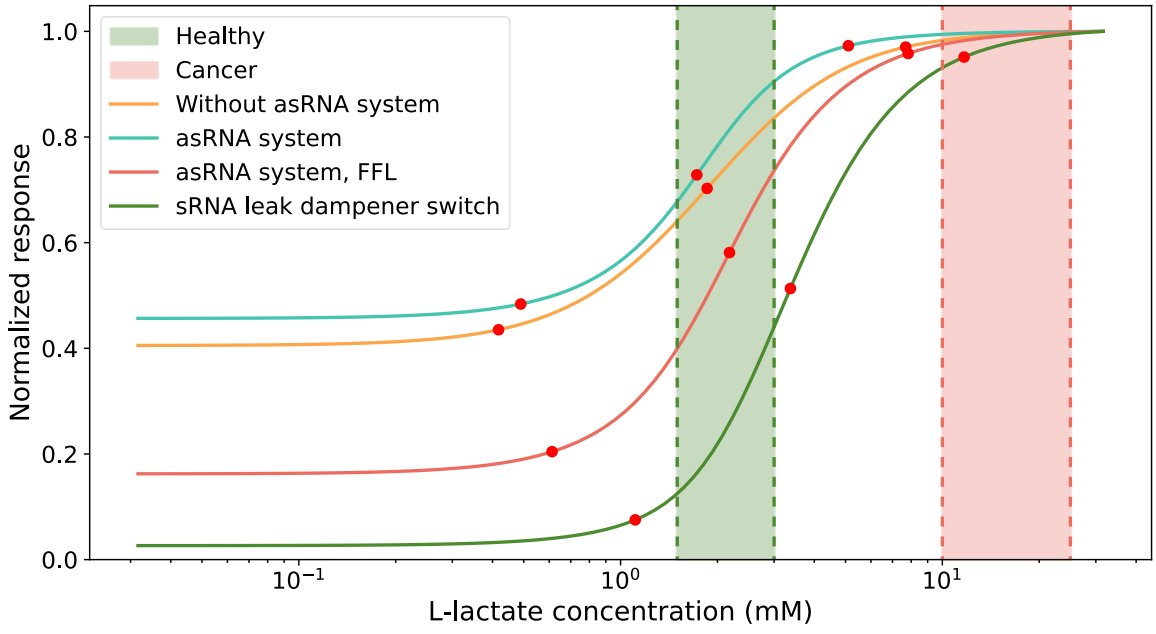

Figure 18: Comparison of dose-response curves from the tested models. Orange: Lactate model without the CRISPRi/asRNA system., Turquoise: Dose-response curve of the combined model. , Red: Dose-response when GFP is under pALPaGA instead of a constitutive promoter, Dark green: Dose-response of the sRNA leak dampener model. The green and red area highlight the range of healthy and cancerous lactate concentrations respectively. Red dots indicate the EC5, EC50 and EC95 respectively.

3.4.2: sRNA as leak dampener

The background expression of the improved system shown in the previous section could still be decreased further. One-at-a-time sensitivity analysis was performed to evaluate the effect of each parameter on the background expression, of which a summary can be seen in Appendix Figure 23.

One of the most effective ways to decrease the background expression of the system that the one-at-a-time analysis showed was that when the degradation of GFP mRNA is increased, the background expression would be lower. The effect on the background expression can be seen in Figure 19, where if $k\_d_{gfpmrna}$ is increased by a of 10, the background expression goes down from ~300 a.u. (dark blue line). to less than 100 a.u. (purple line).

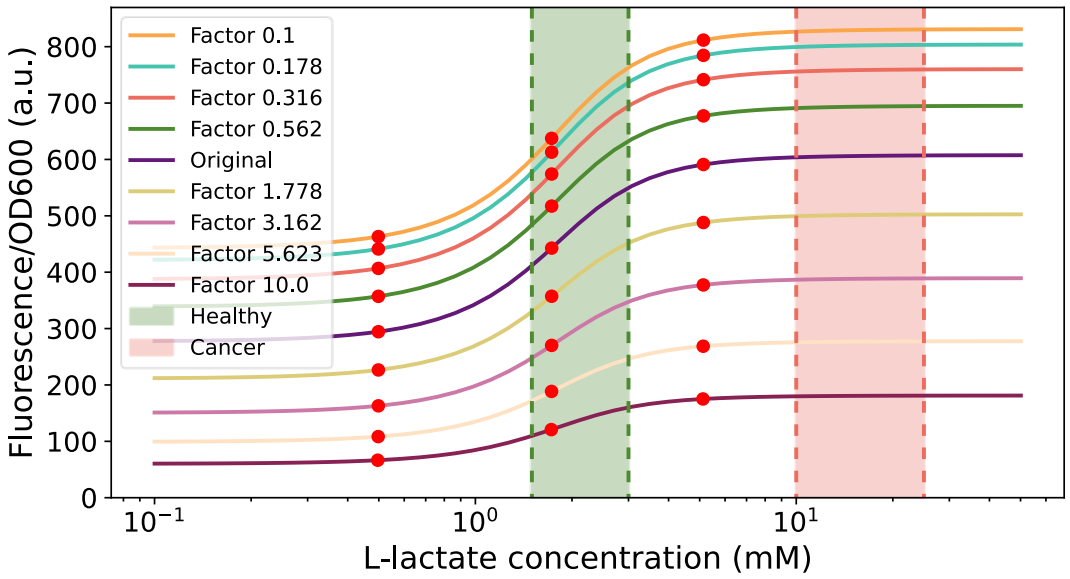

Figure 19: One-at-a-time sensitivity analysis result for $k\_d_{gfpmrna}$, showing what happens to the original dose-response curve (in dark blue) when the parameter is decreased (above the original curve) and increased (below the original curve). The green and red area highlight the range of healthy and cancerous lactate concentrations respectively. Red dots indicate the EC5, EC50 and EC95 respectively.

Increasing the degradation rate of GFP mRNA would be possible by implementing a small RNA that is partly complementary to the start of mRNA transcript, which is also known as RNA interference (RNAi) [31].

The use of RNAi might solve the problem of background expression since it is another layer of repression: CRISPRi and lldR repress on a transcriptional level while RNAi represses on a translational level.

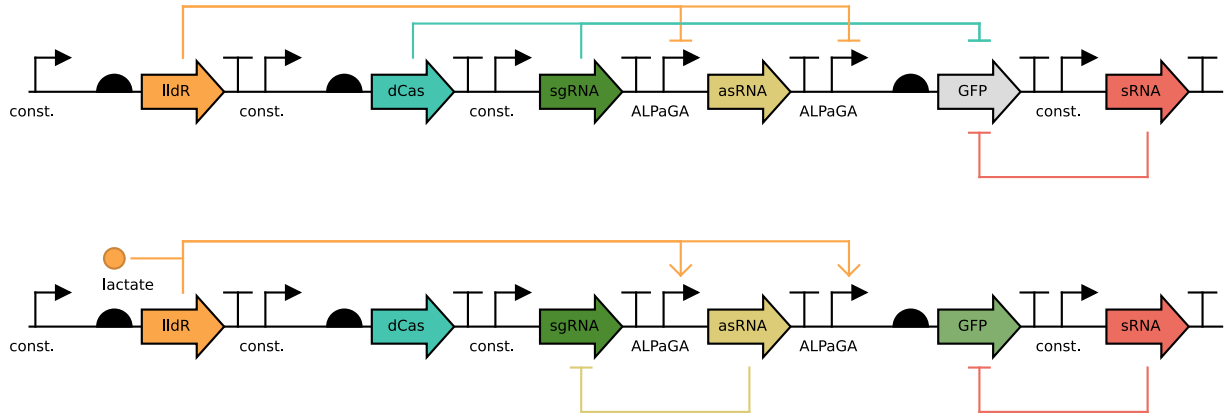

Figure 20: Top: sRNA as a leak dampener for GFP in the 'OFF' state, where GFP is repressed by CRISPRi, and any leaked transcript is degraded by a small RNA. Bottom: sRNA lacks any regulation which can result in lower expression of GFP in the 'ON' state.

How a constitutively expressed sRNA could be implemented in the biosensor can be seen in Figure 20. The issue of using a constitutively expressed small RNA however, would be that the degradation of GFP mRNA transcript is also increased in high lactate conditions, lowering the dynamic range as shown in the bottom line of Figure 19. This indicates the need for a mechanism that is dependent on lactate.

3.4.3: sRNA lactate dependent switch eliminates background expression

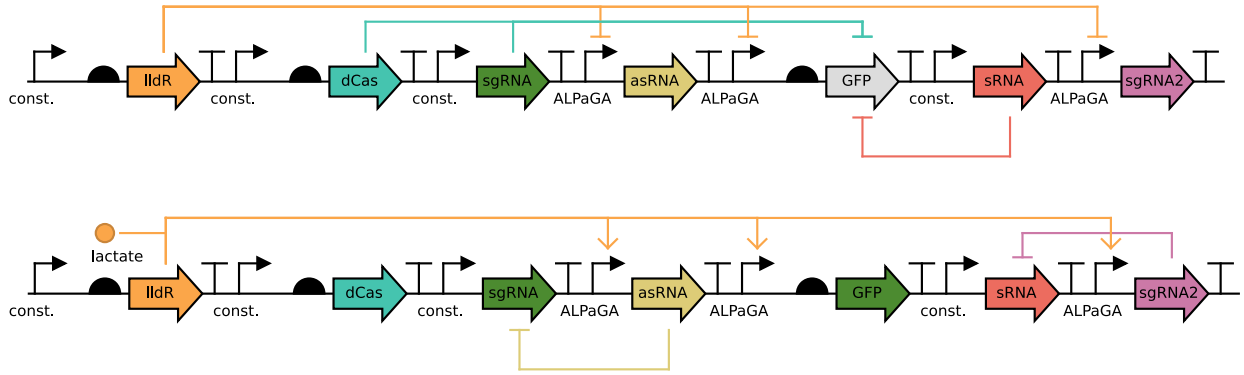

Figure 21: Top: sRNA lactate dependent circuit in the 'OFF' state, where GFP is repressed by CRISPRi, and any leaked transcript is degraded by a small RNA. Bottom: sRNA dependent circuit in the 'ON' state, where GFP is free to be expressed. sRNA is inhibited by a CRISPRi complex, due to the introduction of a second guide RNA (in pink).

In order for the sRNA to be lactate dependent, a single guide RNA under control of ALPaGA is introduced. This guide RNA, in combination with dCas targets the sRNA and inverts the lactate signal and represses the expression of sRNA in high concentrations of lactate (Figure 21). The repression of sRNA when lactate is present should mitigate any loss of dynamic range due to the small RNA enabled degradation. To compare the systems, the dose-response curve of each model was plotted (Figure 18). The green line corresponds to the sRNA lactate dependent switch which shows virtually no background expression as opposed to the other models.

Table 1 shows the calculated operational and dynamic range of each tested model. While the goal of the sRNA switch was to reduce background expression, the operational range also shifted more towards higher concentrations.

Table 1: Comparison of the operational, dynamic range and background expression for tested models

Model	**Operational Range (EC5-95)**	**Dynamic range (Fold-change)**	**Background expression**
Lactate model	0.42-7.67 mM	1.47	0.364
Combined model	0.49-5.10 mM	1.19	0.399
Combined model, FFN	0.61-7.83 mM	5.16	0.145
sRNA leak dampener	1.11-11.68 mM	36.7	0.0265

Chapter 4: Discussion

To summarize the results, two models were fitted separately with each their respective dataset. One model describes the dynamics of CRISPRi and antisense RNA. The second model describes a basic lactate biosensor. Afterwards the models were combined in order to simulate a lactate biosensor that employs the CRISPRi/asRNA system to regulate expression. The combined system did not have the operational and dynamic range that is desired as a biosensor for distinguishing between healthy lactate levels and the levels of lactate associated with cancer. One-at-a-time analysis was performed to yield the best parameters that can improve the operational and dynamic range. $k\_f_{lldrcomplex}$, was the best parameter for the operational range, which is the rate at which lactate and LldR form a complex. This rate is also affected by the lactate concentration which is why the suggestion was made to reduce the internal lactate concentration. For the improvement of the dynamic range, it was suggested to introduce a feedforward loop motif by making the GFP promoter lactate dependent. In addition to, a lactate dependent small RNA was implemented, which would sequester GFP mRNA and increasing the degradation rate $k\_d_{gfpmrna}$ of the mRNA transcript in lower concentrations of lactate.

4.1: Model evaluation

After fitting to data, the CRISPRi/asRNA model matched the data, but after implementation of a time-delay there were still discrepancies between them. Namely at the start the model initial fluorescence is higher and the end of the simulation is lower than the data. Leaky CRISPRi expression may explain why the CRISPRi/asRNA model starts with a higher initial GFP concentration. Leaky expression is not considered in the initial conditions of the model. If leaky expression of CRISPRi were taken into account, it would result in a lower initial condition for GFP. This could also explain why when asRNA is induced, the model reaches a lower plateau than the data. This is also supported by experiments from Lee et al. 2016, where they show that sgRNA transcript is present even when not induced [13].

The lactate model also had a discrepancy: The model fits the measured fluorescence from where 0.05mM to 5mM lactate was present, but not where the lactate concentration was 20 mM. It may be possible that the model is overfitted to lower concentrations, since 0.05mM to 5mM consist of 5 measured concentrations, but then there is only one dataset for higher concentrations. Ideally, more measurements in between 5 and 20mM would be preferred to fix this issue. It may also be possible that reducing the amount of low concentration datasets used for fitting the model would make the model fit better for higher concentration, although with less data the model would likely be less accurate than doing more measurements. The data to obtained by Zúñ et al. 2021 shows that the biosensor response levels off around 10 to 20 mM lactate [12]. Therefore, it could be assumed that at 20 mM, the dose-response curve is saturated. The measured data points do not capture the exact concentration where the biosensor response saturates. If this 'transition period' from the 'OFF' to 'ON' state is measured accurately, it would be more likely that the model would have a better fit to the data after optimization.

The predicted fluorescence from the combined model is likely not accurate. Since different datasets were used for the final model, which were measured in different labs with different equipment, equipment parameters etc. Nonetheless the improvements suggested can be a valid strategy to improve the biosensor, as this mostly affect the output of the model and not the general behavior. It would have been better to construct the full design and gather data on this system instead, but that would require a lot of time experimentally which turned out to be unfeasible in the timeframe of this project.

In addition, it would have been preferable to use experimental data from anaerobic conditions with glucose as a carbon source for the lactate model, however due to the anaerobic conditions, the green fluorescent protein does not mature over time. This resulted in almost no fluorescence until after 16 hours where oxygen was increased. The increase in oxygen enables the maturation of GFP which causes a spike in fluorescence. The sudden spike in fluorescence made this time-series data unusable. Therefore, data was chosen from the biosensor in aerobic conditions, which is not the case in the colon, where the biosensor would operate. It is likely that the biosensor would give a lower response in anaerobic conditions, as the ALPaGA promoter gives a lower response in anaerobic conditions as shown in Figure 4.

4.2: Evaluation of results

To tune the operational range of the lactate sensing system, it is suggested to decrease the internal concentration of lactate in the cell. In literature, the strategy for decreasing internal concentrations was to increase the export of analyte outside of the cell [7]. However, the known native transporter proteins for lactate (lldP and glcA) import lactate into the cell instead of exporting [8]. Therefore, another strategy for tuning the internal lactate concentrations in the cell was needed.

Instead of exporting to decrease internal lactate concentrations, it is also possible to convert lactate through the use of lactate dehydrogenase [32]. This enzyme converts lactate to pyruvate, lowering the internal concentration of lactate in the cell. Overexpression of this enzyme would be much easier than attempting to engineer the lactate transporters to export instead. The conversion of lactate to pyruvate also gives an advantage to the living diagnostic, enabling it to grow better in cancerous environments.

To improve the dynamic range of the combined model a small RNA was introduced. sRNA repression of GFP mRNA was modeled by a sRNA dependent degradation term, sRNA however also blocks translation of the mRNA to protein. The blocking of GFP translation by sRNA was not taken into account for in the model, so it may be that in practice the addition of an sRNA dependent on lactate proves more effective than predicted.

4.3: Recommendations for future research

To have more information about the system, it would be nice to have more data. One example would be to measure substrate and/or lactate consumption with High Performance Liquid Chromatography (HPLC). This would give more information on how and what *E. coli* Nissle uses for growth. qPCR or transcriptomics could also be used to get information about the transcripts of all RNA components of the system. Transcriptomics has been proven valuable for the debugging of genetic circuits and would be especially useful for a system that contains multiple RNA-based regulators [33].

To better approximate the conditions in the colon it is recommended that the genetic circuit is tested in a continuous bioreactor. It could also be used to more easily study the effects of lactate perturbations that could simulate the effects of dietary lactate. The data gathered in these experiments could be used to build a more accurate model.

One recommendation for a genetic circuit element to include in future designs would be a small transcription activating RNA (STAR), developed by Westbrook et al. (2017) [34]. This RNA stabilizes a secondary DNA structure in which transcription and translation are enabled. Without the STAR present both RNA polymerase and the ribosome are unable to initiate transcription and translation respectively. This dual regulation control improved the dynamic range of their genetic circuit from 10-fold to a 923-fold

change induction compared to a genetic circuit with an RNA which only activated transcription of reporter protein.

In conclusion, a mathematical model describing a lactate sensing system was fitted to data. This system was not optimal for the detection of colorectal cancer, so a strategy has been developed for optimizing the lactate biosensor. Namely by tuning the operational range by decreasing the internal concentration of lactate. This can be done experimentally by overexpression of lactate dehydrogenase. Background expression and increase of the dynamic range can be improved by addition of a leak dampener in the form of a small RNA which turns off in higher concentrations of lactate. These strategies may help to create a better lactate biosensor for the detection of cancer in the future.

Appendix

Appendix 1: Model parameter values and descriptions

Table 2: Parameter descriptions and values for the CRISPRi/asRNA model

Name	Description	Values	Units
$\mathrm{k\_b_{dcas}}$	Constitutive production of dCas	7.422	mM/h
$\mathrm{k\_b_{sgrna}}$	Constitutive production of sgRNA	4.49	mM/h
$k\_p_{gfpmrna}$	Max production rate of GFP_mRNA	0.674	mM/h
k_p_{asrna}	Max production rate of asRNA	7.511	mM/h
$k\_d_{ascascomplex}$	Degradation rate of asCasComplex	5.331	1/h
$k\_d_{ascomplex}$	Degradation rate of asRNA-sgRNA complex	10.793	1/h
k_d_{asrna}	Degradation rate of asRNA	5.751	1/h
$k\_d_{cascomplex}$	Degradation rate of sgRNA-Cas complex	1.151	1/h
k_d_{dcas}	Degradation rate of dCas protein	5.076	1/h
$k\_d_{dcasmrna}$	Degradation rate of dCas mRNA	2.389	1/h
k_d_{sgrna}	Degradation rate of sgRNA	1.389	1/h
$\mathrm{k\_d_{gfpmrna}}$	Degradation rate of GFP mRNA	0.344	1/h
k_d_{gfp}	Degradation rate of GFP	0.002	1/h
k_pt_{dcas}	Proportionality constant of dCas9 translation	6.854	1
k_pt_{gfp}	Proportionality constant of GFP translation	6.605	1
$k\_f_{3_{fw}}$	Formation rate of asCasComplex	6.016	1/mM.h
$k\_f_{3_{rv}}$	Dissociation rate of asCascomplex	1.1	1/h
$k\_f_{4_{fw}}$	Formation rate of asCasComplex but dCas comes last	6.426	1/mM.h
$k\_f_{4_{rv}}$	Dissociation rate of asCasComplex but dCas comes last	1.76	1/h
$k\_f_{2_{fw}}$	Formation rate of asRNA-sgRNA complex	3.281	1/mM.h
$k\_f_{2_{rv}}$	Dissociation rate of asRNA-sgRNA complex	7.799	1/h
$k\_f_{1_{fw}}$	Formation rate of dCas-sgRNA complex	9.631	1/mM.h
$k\_f_{1_{rv}}$	Dissociation rate of CasComplex	0.855	1/h
kd_{dcas}	Dissociation constant of CasComplex with DNA	1.142	mM
kd_{asrna}	Dissociation constant of inducer and asRNA promoter	7.792	mM
$n_{cascomplex}$	Hill coefficient dCas repression	4	1
$n_{inducer}$	Hill coefficient asRNA inducer	1	1
as_{input}	Concentration of inducer	0(uninduced)/5(induced)	mM
μ	Growth/dilution rate	1.2	1/h
$scale$	Scaling factor which scales GFP to the amount of fluorescence	166.73	1

Table 3: Parameter descriptions and values for the Lactate model

Name	Description	Values	Units
alp_{act1}	activated production of pALPaGA when activated by monomeric LldR	3.904	mM/OD.h
alp_{act2}	activated production of pALPaGA when activated by the LldR-lactate complex	22.127	mM/OD.h
k_b_{alp}	basal production by the pALPaGA promoter	7.8	mM/OD.h
alp_k_{act1}	binding affinity of LldR monomeric LldR	42.532	mM
alp_k_{act2}	binding affinity of LldR-lactate complex	67.022	mM
alp_{k3}	Repression strength of LldR-dimer	1.933	mM
cap	Maximum cell density	0.234	OD
$copy\_nr$	Copy number of the plasmid	5.199	1
$\mathrm{k\_b_{p3}}$	Constitutive production of LldR on the plasmid	38.422	mM/OD.h
k_d_{gfp}	Degradation rate of GFP protein	0.003	1/h
$k\_d_{gfpmrna}$	Degradation rate of GFP mRNA	0.067	1/h
k_d_{LldR}	Degradation rate of LldR	3.758	1/h
$k\_d_{LldRcomplex}$	Degradation rate of LldR-lactate complex	0.768	1/h
$k\_d_{LldRmrna}$	Degradation rate of LldR mRNA	7.939	1/h
$k_{f_L} ldRcomplex$	Formation rate of LldR-lactate complex	0.234	1/mM^2.OD.h
k_op_{succ}	Production rate of LldR from the operon	2.784	mM/OD.h
k_pt_{gfp}	Proportionality constant of GFP translation	0.705	1
k_pt_{LldR}	Proportionality constant of LldR translation	8.91	1
μ_{max}	Maximal specific growth rate	0.405	1/h
γ	Dilution factor	4.462	1
$scale$	Scaling factor, which incorporates unmodeled fluorescence production and dilution effects	59.633	1
σ	Spread of the growth curve	4.292	h
t_c	Time where maximal growth is reached	10.423	h

Table 4: Parameter descriptions and values for the Combined Model / Feed forward network

Name	Description	Value	Unit
alp_{act1}	activated production of pALPaGA when activated by monomeric LldR	3.904	mM/OD.h
alp_{act2}	activated production of pALPaGA when activated by the LldR-lactate complex	22.172	mM/OD.h
k_b_{alp}	basal production by the pALPaGA promoter	7.8	mM/OD.h
alp_k_{act1}	binding affinity of LldR monomeric LldR	42.532	mM
alp_k_{act2}	binding affinity of LldR-lactate complex	67.022	mM
alp_{k3}	Repression strength of LldR-dimer	1.933	mM
cap	Maximum cell density	0.234	OD
$copy\_nr$	Copy number of the plasmid	5.199	1
k_b_{dcas}	Constitutive production of dCas	33.117	mM/OD.h
k_b_{p3}	Constitutive production of LldR on the plasmid	38.422	mM/OD.h
k_b_{sgrna}	Constitutive production of sgRNA	20.034	mM/OD.h
$k\_d_{ascascomplex}$	Degradation rate of asCasComplex	5.331	1/h
$k\_d_{ascomplex}$	Degradation rate of asRNA-sgRNA complex	10.793	1/h
k_d_{asrna}	Degradation rate of asRNA	5.751	1/h
$k\_d_{cascomplex}$	Degradation rate of sgRNA-Cas complex	1.151	1/h
k_d_{dcas}	Degradation rate of dCas protein	5.076	1/h
$k\_d_{dcasmrna}$	Degradation rate of dCas mRNA	2.389	1/h
k_d_{gfp}	Degradation rate of GFP protein	0.003	1/h
$k\_d_{gfpmrna}$	Degradation rate of GFP mRNA	0.067	1/h
k_d_{LldR}	Degradation rate of LldR	3.758	1/h
$k\_d_{LldRcomplex}$	Degradation rate of LldR-lactate complex	0.768	1/h
$k\_d_{LldRmrna}$	Degradation rate of LldR mRNA	7.939	1/h
k_d_{sgrna}	Degradation rate of sgRNA	1.389	1/h
$k\_f_{1_{fw}}$	Formation rate of dCas-sgRNA complex	2.158	1/mM.OD.h
$k\_f_{1_{rv}}$	Dissociation rate of CasComplex	0.855	1/h
$k\_f_{2_{fw}}$	Formation rate of asRNA-sgRNA complex	0.735	1/mM.OD.h
$k\_f_{2_{rv}}$	Dissociation rate of asRNA-sgRNA complex	7.799	1/h
$k\_f_{3_{fw}}$	Formation rate of asCasComplex	1.348	1/mM.OD.h
$k\_f_{3_{rv}}$	Dissociation rate of asCascomplex	1.1	1/h
$k\_f_{4_{fw}}$	Formation rate of asCasComplex but dCas comes last	1.44	1/mM.OD.h
$k\_f_{4_{rv}}$	Dissociation rate of asCasComplex but dCas comes last	1.76	1/h
$k\_f_{LldRcomplex}$	Formation rate of LldR-lactate complex	0.234	1/mM^2.OD.h
k_op_{succ}	Production rate of LldR from the operon	2.784	mM/OD.h
$k\_p_{gfpmrna}$	Max production rate of GFP_mRNA	3.007	mM/OD.h
k_pt_{dcas}	Proportionality constant of dCas9 translation	6.854	1

k_pt_{gfp}	Proportionality constant of GFP translation	0.705	1
k_pt_{LldR}	Proportionality constant of LldR translation	8.91	1
kd_{dcas}	Dissociation constant of CasComplex with DNA	5.096	mM
μ_{max}	Maximal specific growth rate	0.405	1/h
$n_{cascomplex}$	Hill coefficient dCas repression	4	1
γ	Dilution factor	4.462	1
$scale$	Scaling factor, which incorporates unmodeled fluorescence production and dilution effects	59.633	1
σ	Spread of the growth curve	4.292	h
t_c	Time where maximal growth is reached	10.423	h

Table 5: Parameters added for the sRNA leak dampener model

Name	**Description**	**Value**	**Unit**
k_b_{srna}	Max production rate of sRNA	30	mM/OD.h
k_d_{srna}	Degradation rate of sRNA	2	1/h
k_d_{sgrna2}	Degradation rate of sgRNA2	1.389	1/h
$k\_d_{gfpmrna2}$	Maximum GFP mRNA degradation rate mediated by sRNA	10	1/h
kd_{srna}	Dissociation constant of sRNA and GFP mRNA	0.05	mM
$\mathrm{k\_f}_{5_{fw}}$	Formation rate of dCas-sgRNA2 complex	5	1/mM.OD.h
$k\_f_{5_{rv}}$	Dissociation rate of dCas-sgRNA2 complex	0.855	1/h

Appendix 2: Sensitivity analysis results of the combined model

Appendix 2.1: Summarized sensitivity analysis results

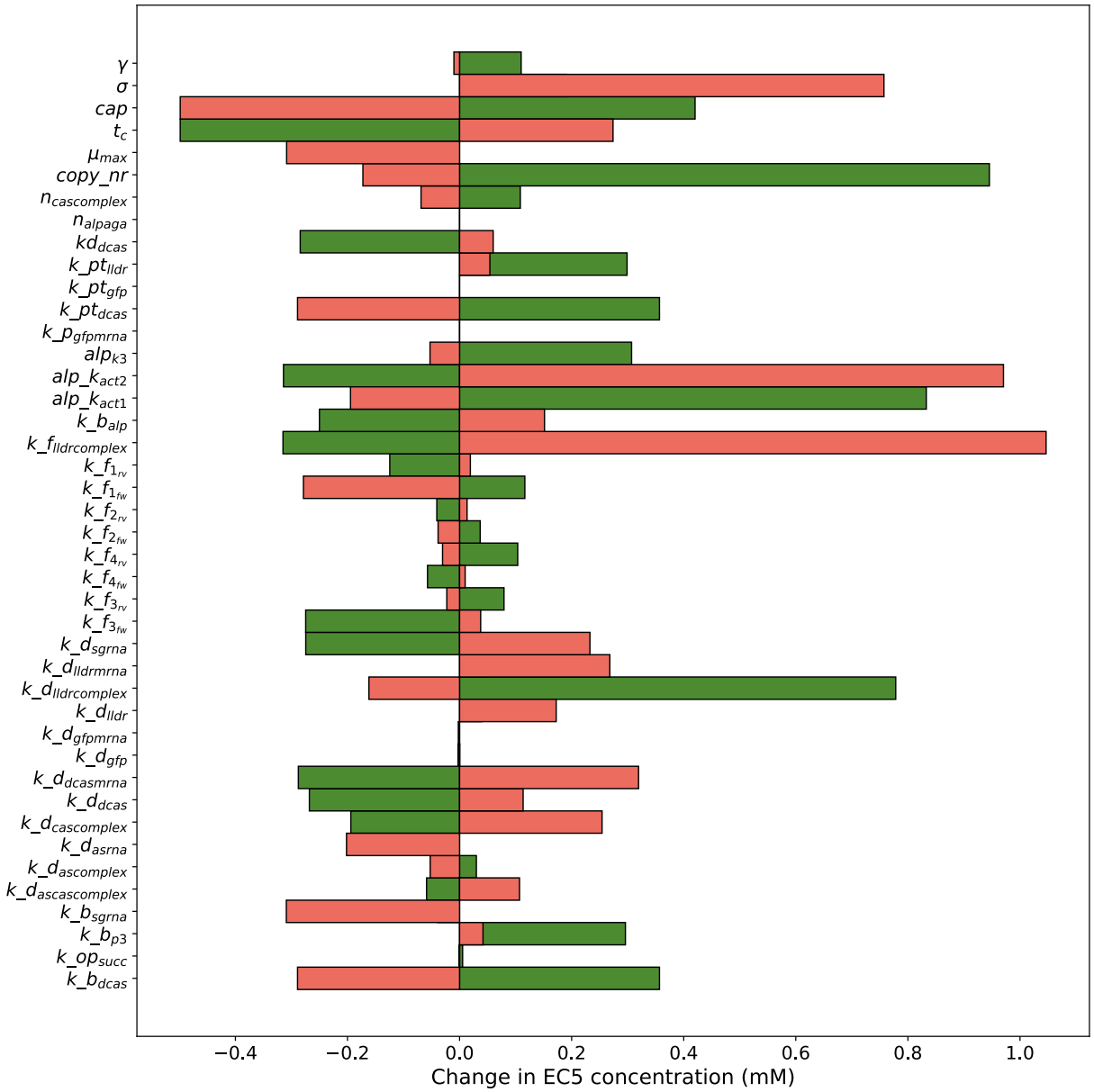

Figure 22: Summary of one-at-a-time sensitivity results, which show how parameters affect the operational range, plotted as the change in EC5 when the parameter is decreased (red) or increased(green) by a factor of 10. alp_{act1} and alp_{act2} were omitted because they skewed the chart due to wrong interpolation.

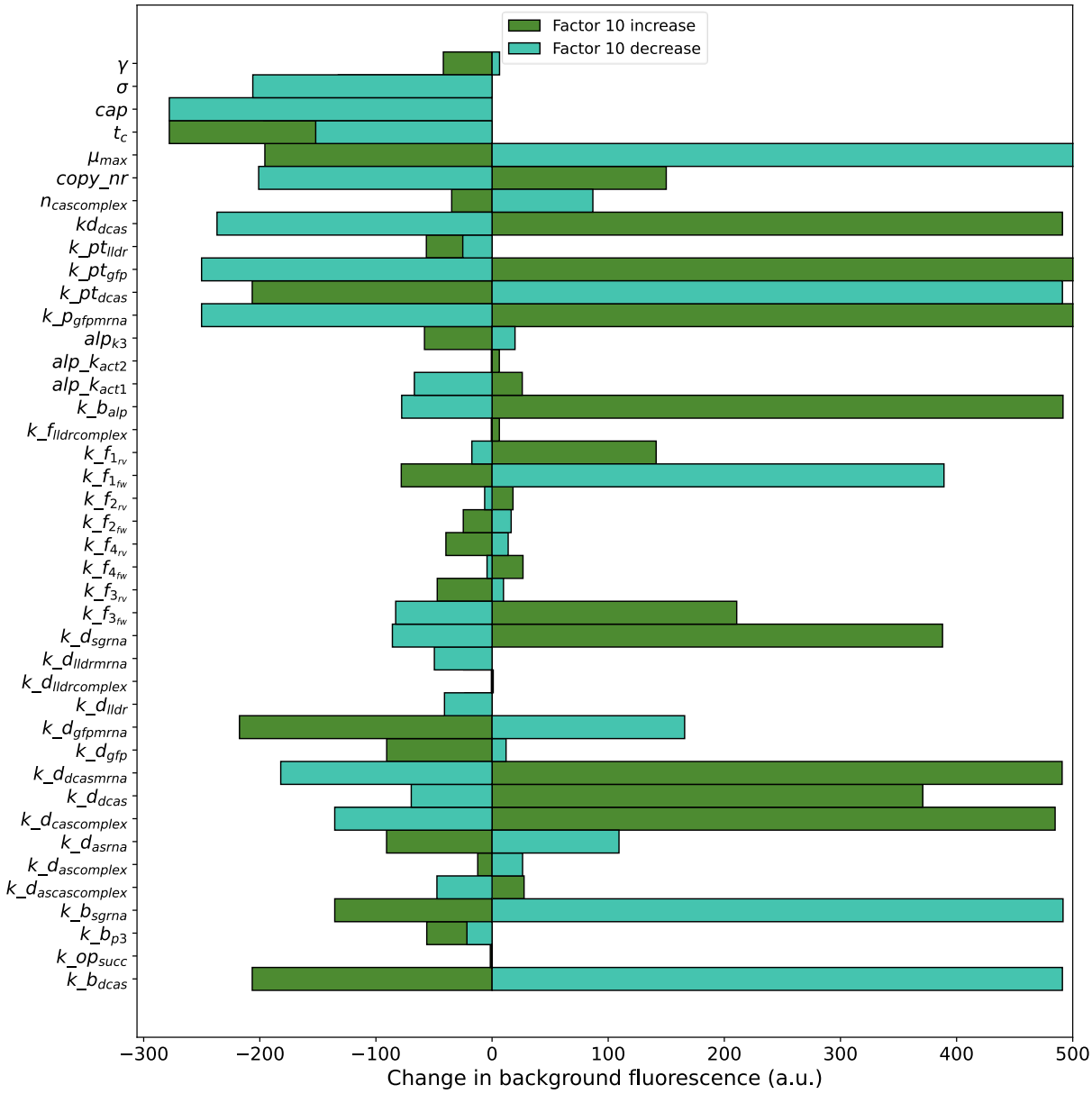

Figure 23: Summary of one-at-a-time sensitivity results, which show how parameters affect the dynamic range, plotted as the change in background expression when the parameter is decreased (turquoise) or increased(green) by a factor of 10. alp_{act1} and alp_{act2} were omitted because they skewed the chart due to wrong interpolation. The x-axis was cut off around 500 since the interest lies in decreasing the background expression.

Appendix 2.2: One at a time analysis plots of each parameter

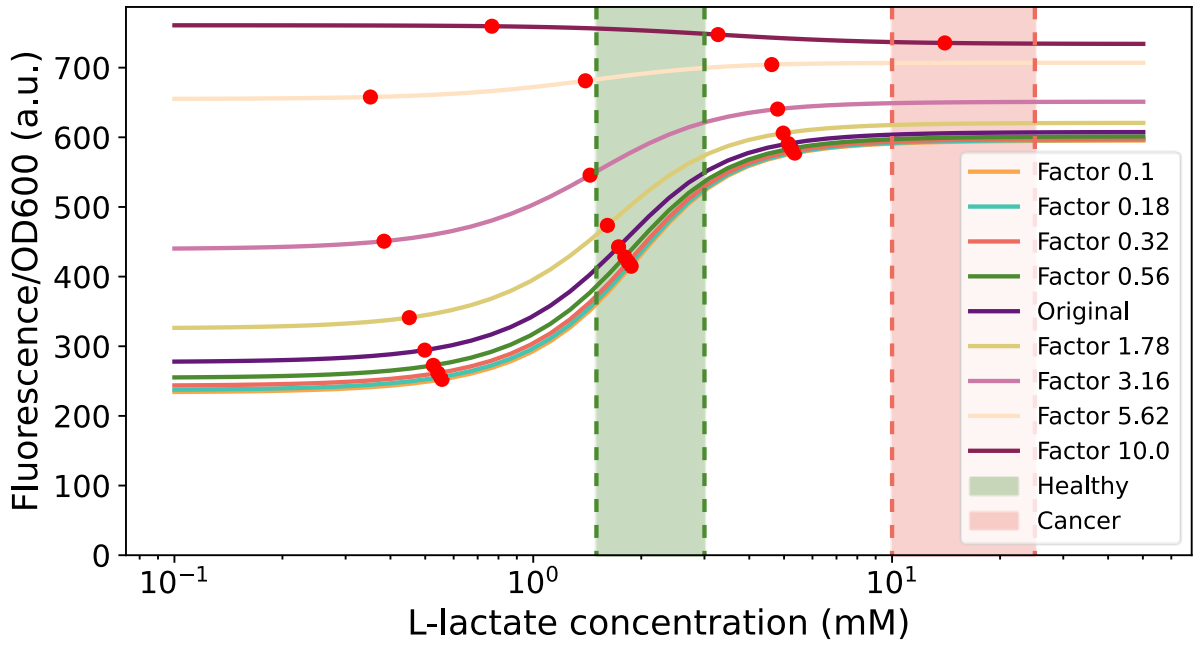

Figure 24: One-at-a-time sensitivity analysis result for alp_{act1}, showing what happens to the original dose-response curve (in dark blue) when this parameter is decreased (orange line) or increased (purple line). The green and red area highlight the range of healthy and cancerous lactate concentrations respectively. Red dots indicate the EC5, EC50 and EC95 respectively.

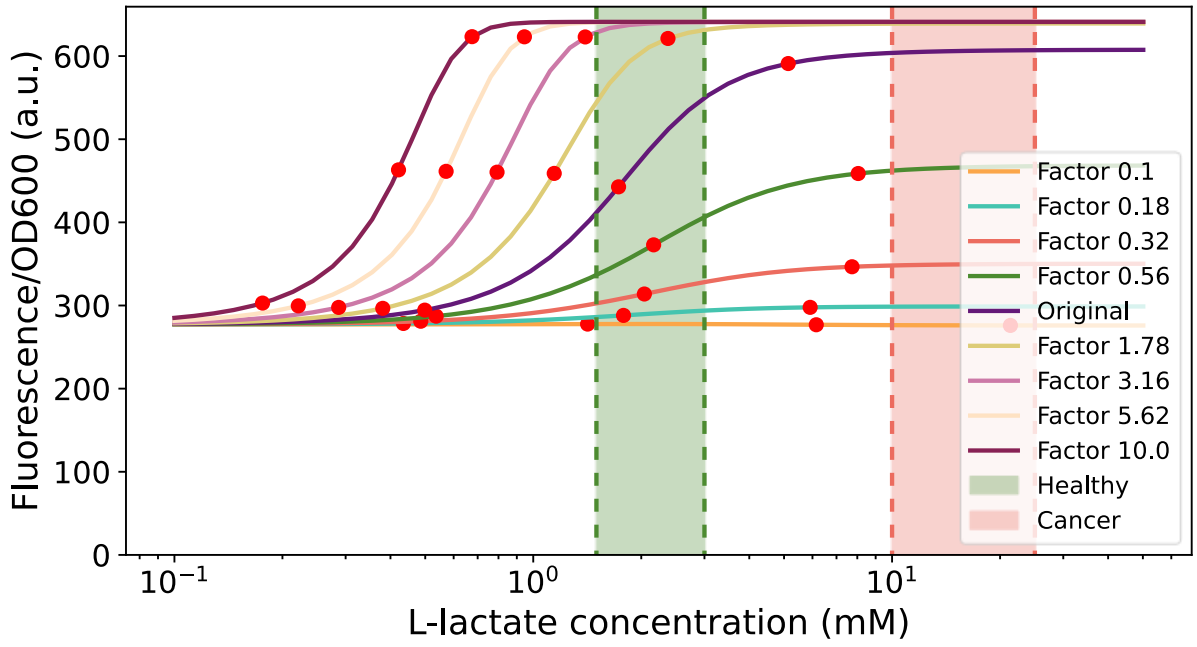

Figure 25: One-at-a-time sensitivity analysis result for alp_{act2}, showing what happens to the original dose-response curve (in dark blue) when this parameter is decreased (orange line) or increased (purple line). The green and red area highlight the range of healthy and cancerous lactate concentrations respectively. Red dots indicate the EC5, EC50 and EC95 respectively.

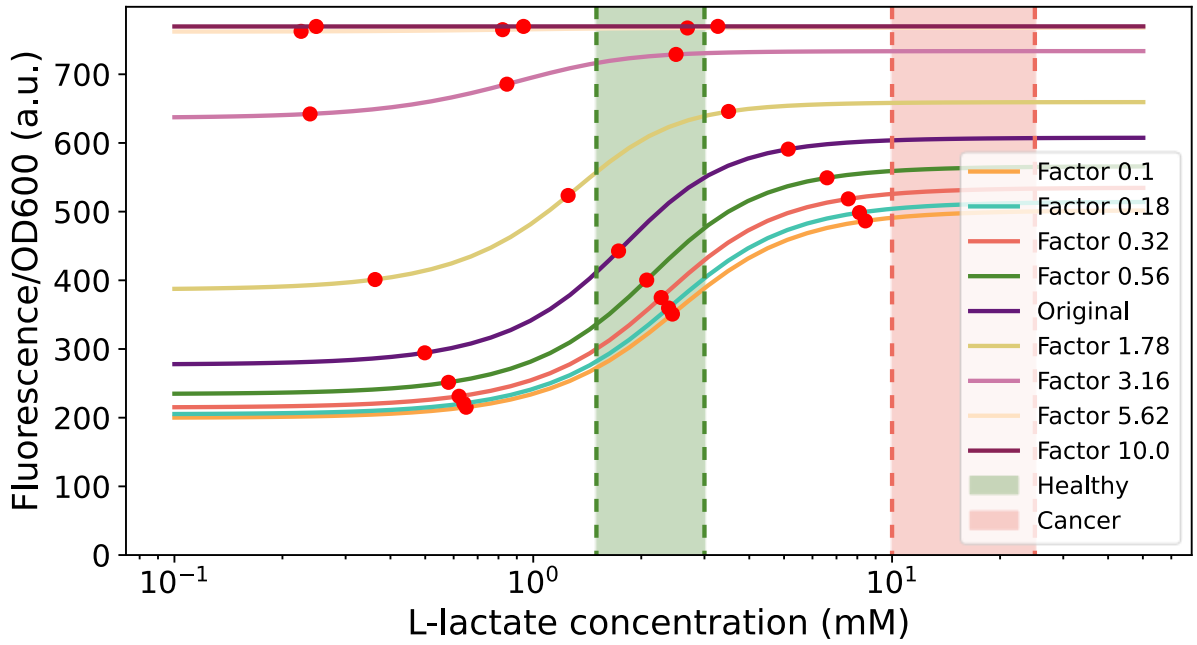

Figure 26: One-at-a-time sensitivity analysis result for k_b_{alp}, showing what happens to the original dose-response curve (in dark blue) when this parameter is decreased (red line) or increased (purple line). The green and red area highlight the range of healthy and cancerous lactate concentrations respectively. Red dots indicate the EC5, EC50 and EC95 respectively.

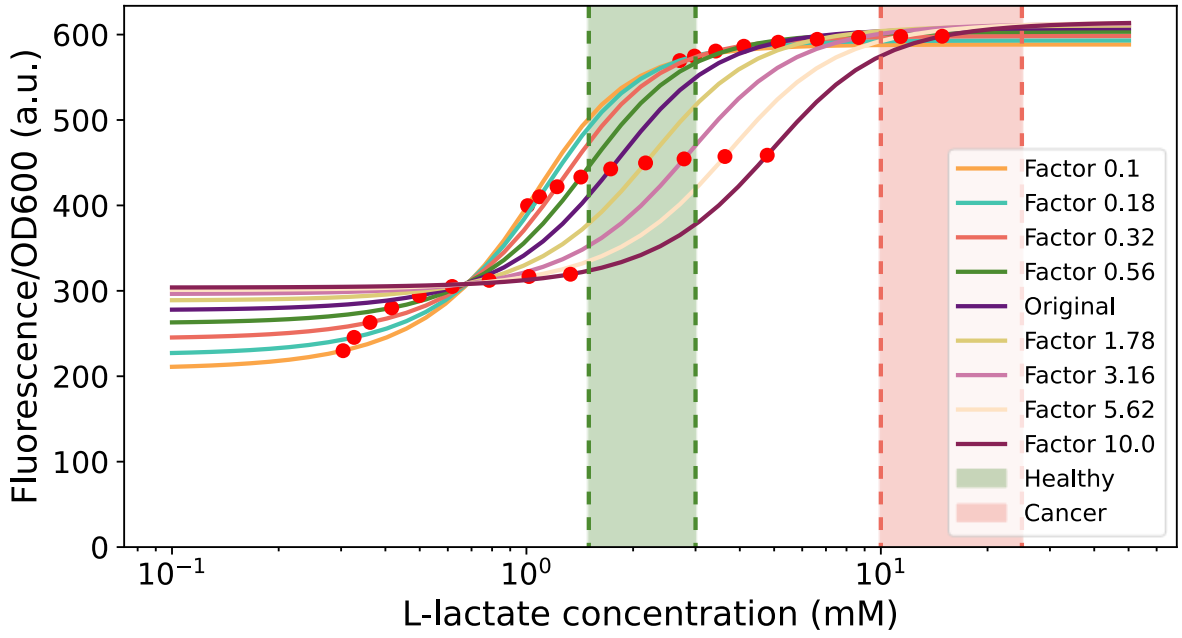

Figure 27: One-at-a-time sensitivity analysis result for alp_k_{act1}, showing what happens to the original dose-response curve (in dark blue) when this parameter is decreased (red line) or increased (purple line). The green and red area highlight the range of healthy and cancerous lactate concentrations respectively. Red dots indicate the EC5, EC50 and EC95 respectively.

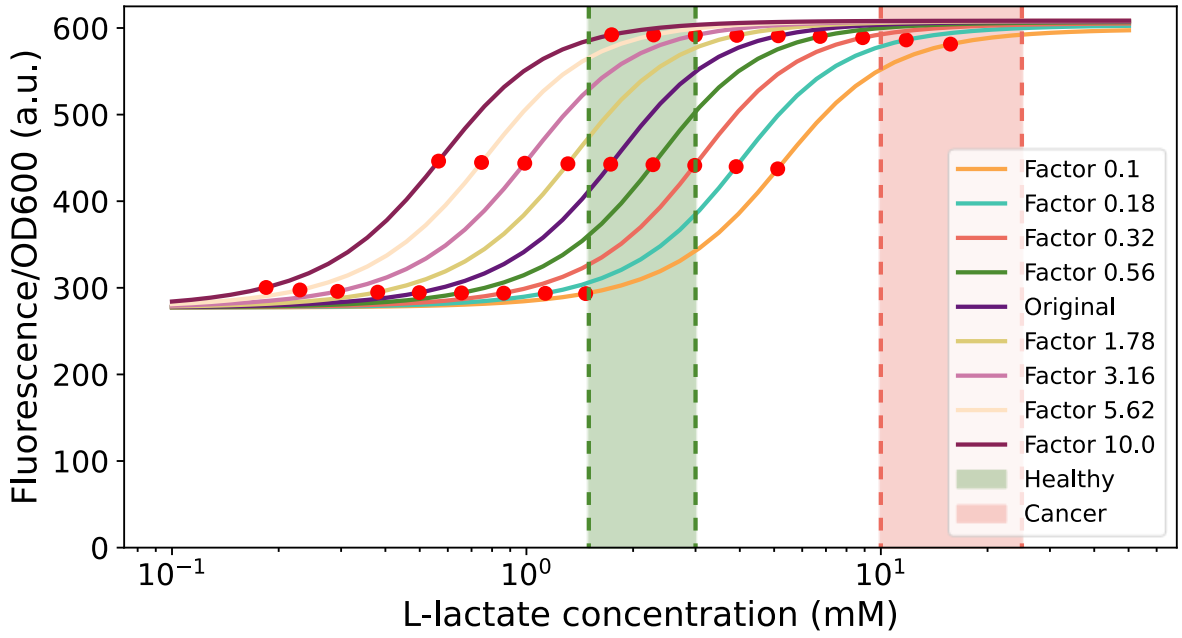

Figure 28: One-at-a-time sensitivity analysis result for alp_k_{act2}, showing what happens to the original dose-response curve (in dark blue) when this parameter is decreased (red line) or increased (purple line). The green and red area highlight the range of healthy and cancerous lactate concentrations respectively. Red dots indicate the EC5, EC50 and EC95 respectively.

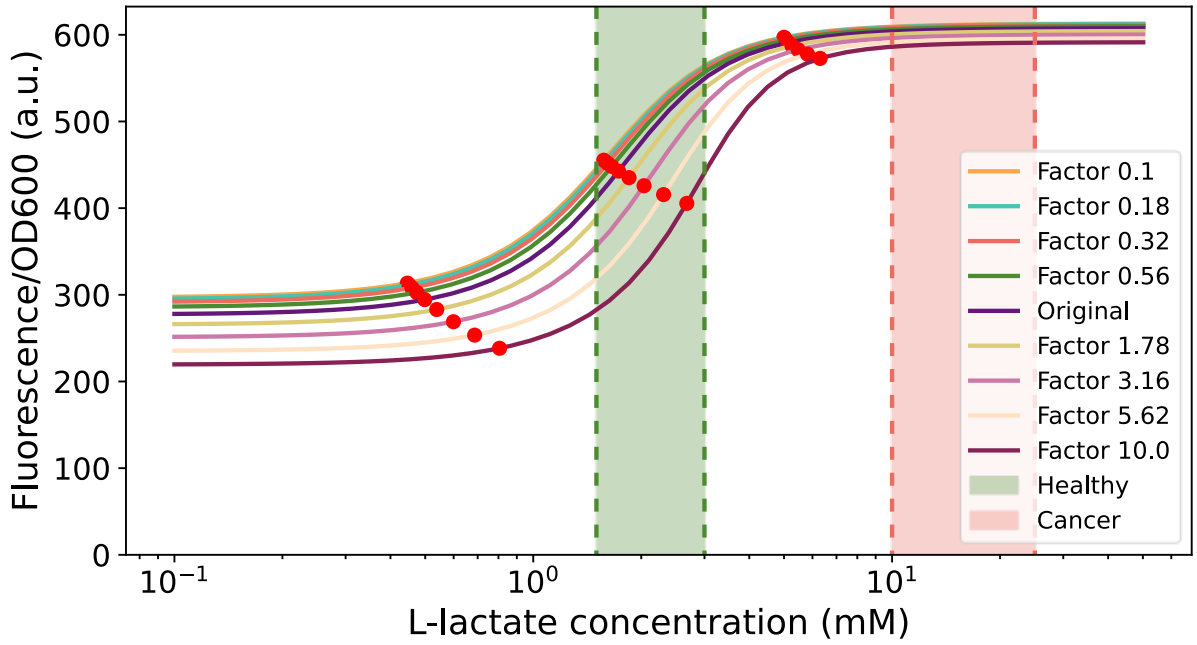

Figure 29: One-at-a-time sensitivity analysis result for alp_{k3}, showing what happens to the original dose-response curve (in dark blue) when this parameter is decreased (orange line) or increased (purple line). The green and red area highlight the range of healthy and cancerous lactate concentrations respectively. Red dots indicate the EC5, EC50 and EC95 respectively.

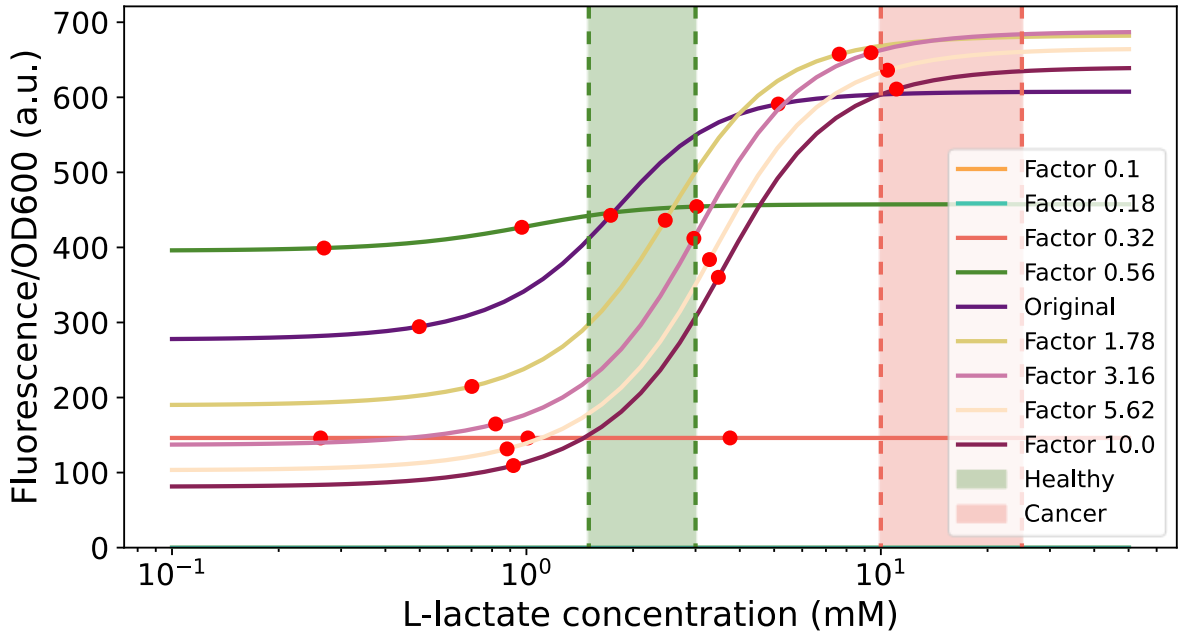

Figure 30: One-at-a-time sensitivity analysis result for cap, showing what happens to the original dose-response curve (in dark blue) when this parameter is decreased (red line) or increased (purple line). The green and red area highlight the range of healthy and cancerous lactate concentrations respectively. Red dots indicate the EC5, EC50 and EC95 respectively.

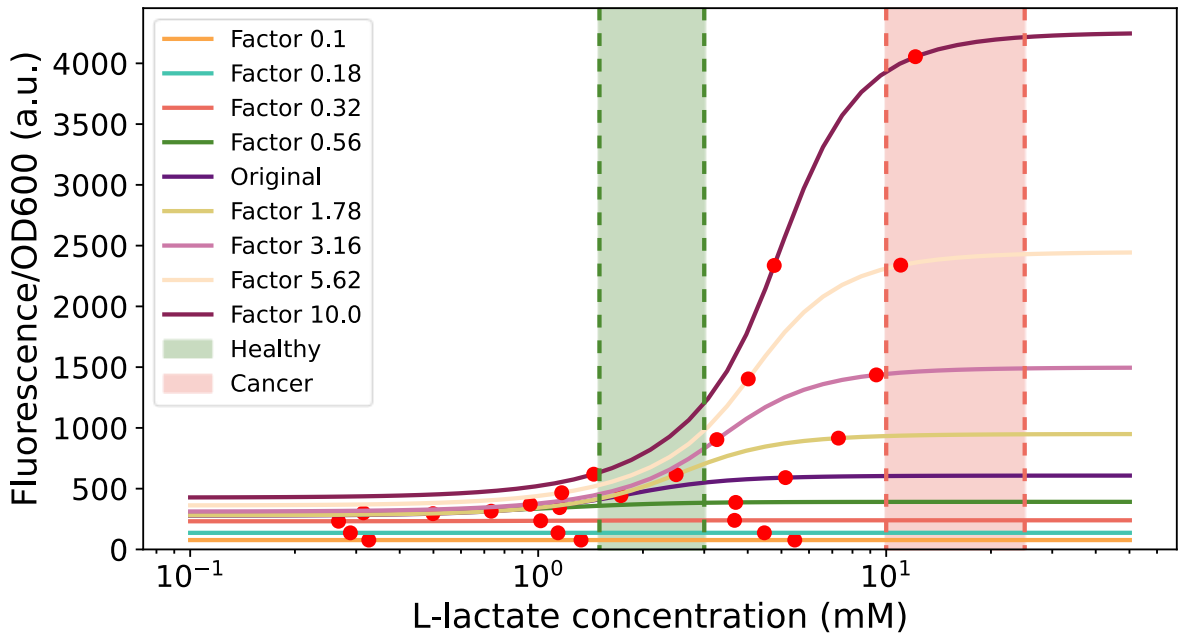

Figure 31: One-at-a-time sensitivity analysis result for copy_nr, showing what happens to the original dose-response curve (in dark blue) when this parameter is decreased (red line) or increased (purple line). The green and red area highlight the range of healthy and cancerous lactate concentrations respectively. Red dots indicate the EC5, EC50 and EC95 respectively.

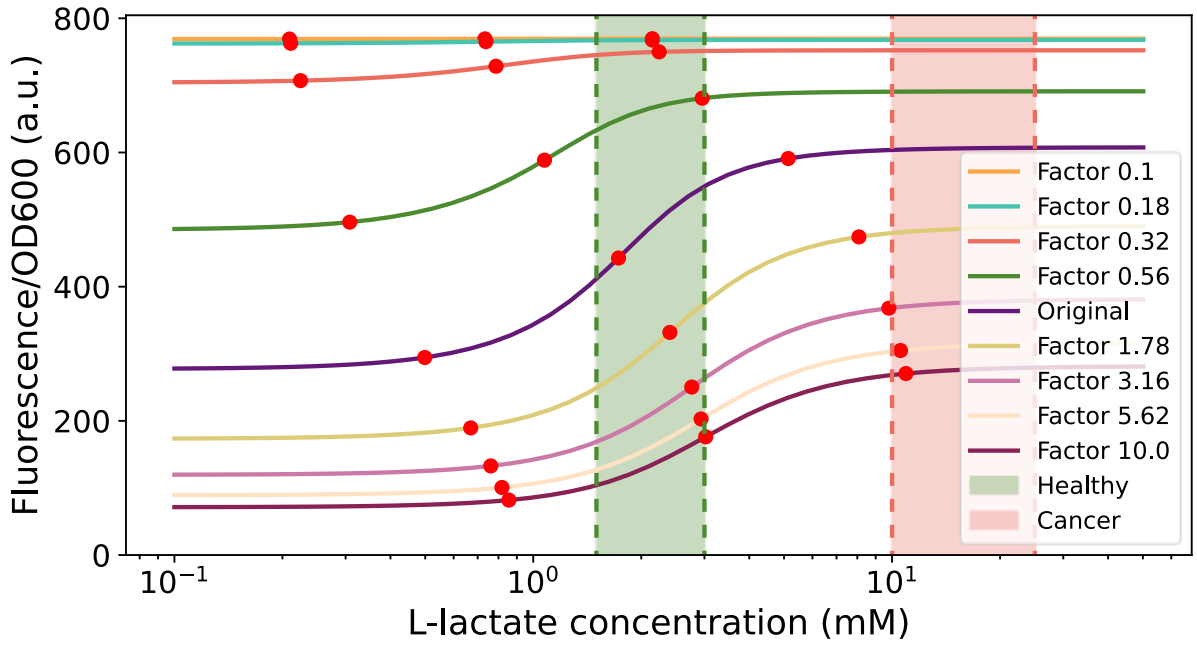

Figure 32: One-at-a-time sensitivity analysis result for k_b_{dcas}, showing what happens to the original dose-response curve (in dark blue) when this parameter is decreased (red line) or increased (purple line). The green and red area highlight the range of healthy and cancerous lactate concentrations respectively. Red dots indicate the EC5, EC50 and EC95 respectively.

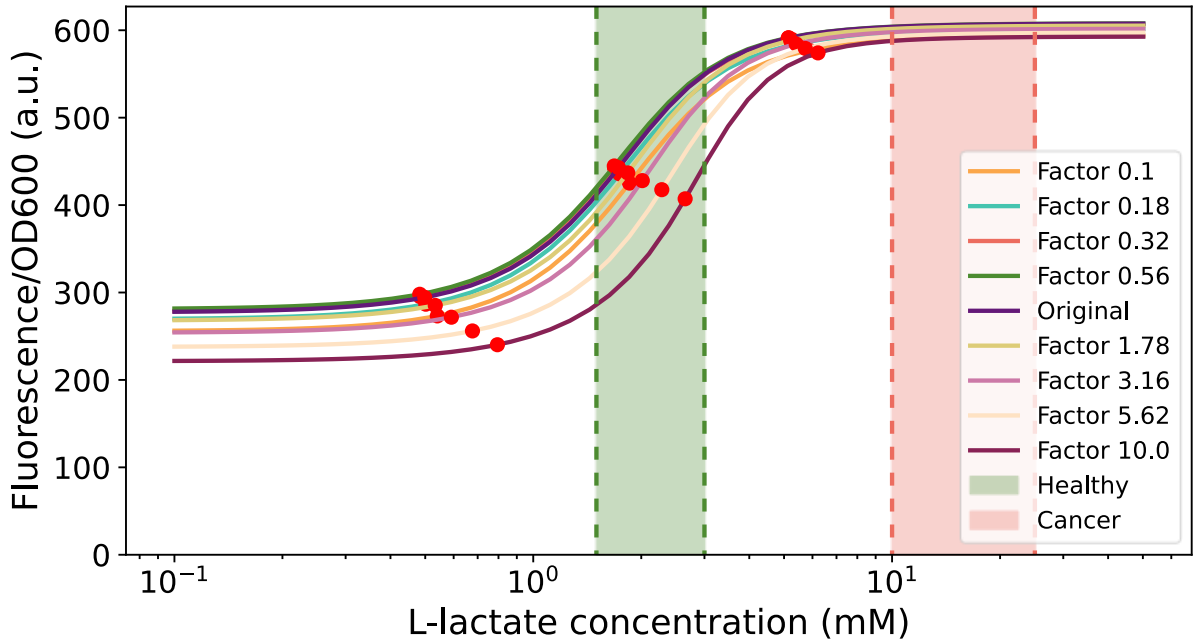

Figure 33: One-at-a-time sensitivity analysis result for k_b_{p3}, showing what happens to the original dose-response curve (in dark blue) when this parameter is decreased (red line) or increased (purple line). The green and red area highlight the range of healthy and cancerous lactate concentrations respectively. Red dots indicate the EC5, EC50 and EC95 respectively.

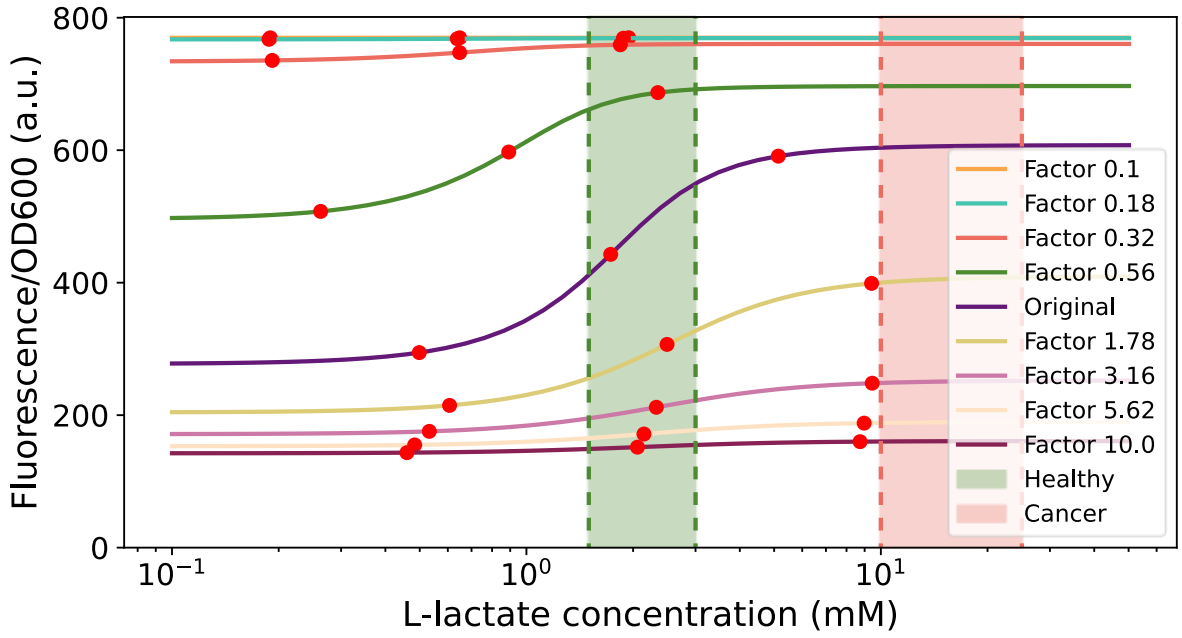

Figure 34: One-at-a-time sensitivity analysis result for k_b_{sgrna}, showing what happens to the original dose-response curve (in dark blue) when this parameter is decreased (red line) or increased (purple line). The green and red area highlight the range of healthy and cancerous lactate concentrations respectively. Red dots indicate the EC5, EC50 and EC95 respectively.

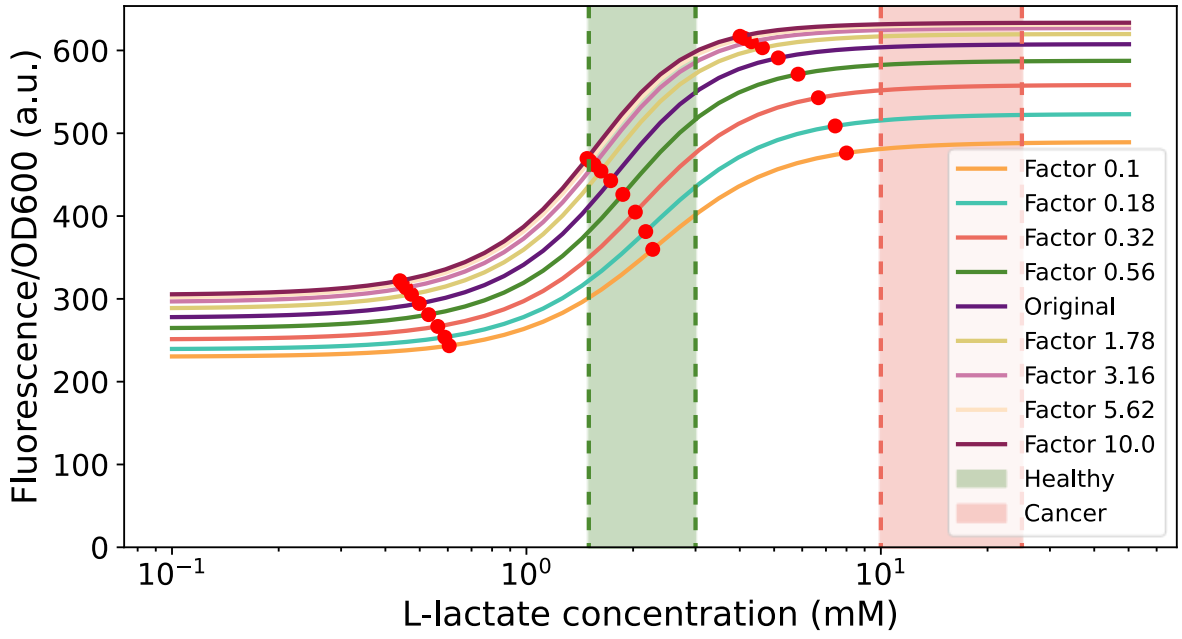

Figure 35: One-at-a-time sensitivity analysis result for $k\_d_{ascascomplex}$, showing what happens to the original dose-response curve (in dark blue) when this parameter is decreased (red line) or increased (purple line). The green and red area highlight the range of healthy and cancerous lactate concentrations respectively. Red dots indicate the EC5, EC50 and EC95 respectively.

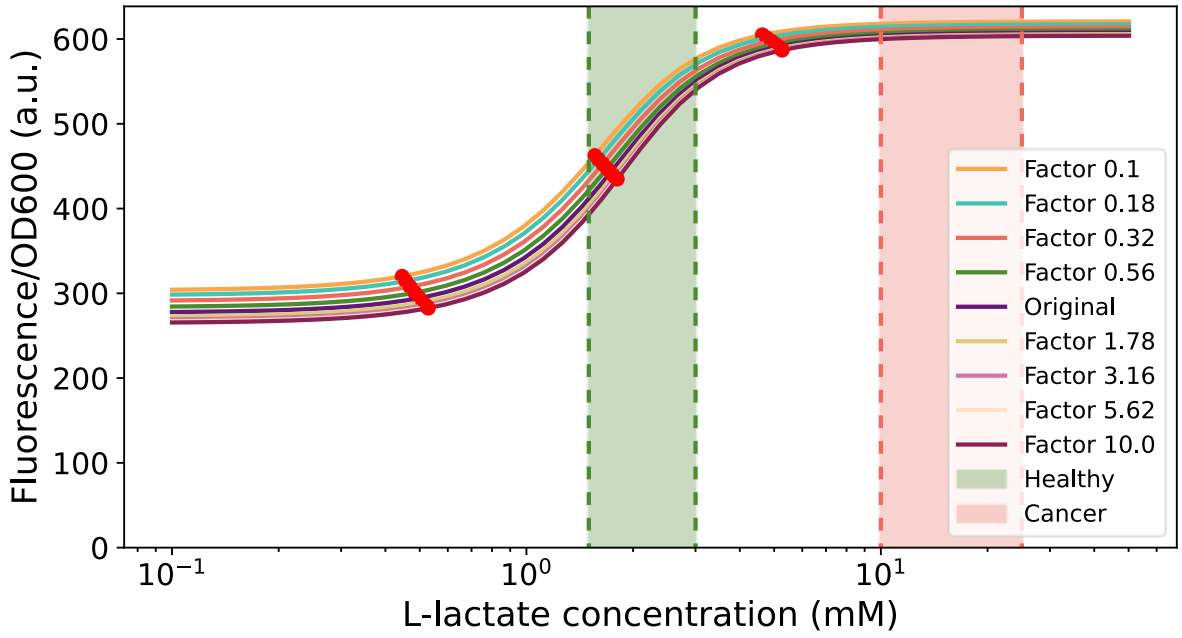

Figure 36: One-at-a-time sensitivity analysis result for $k\_d_{ascomplex}$, showing what happens to the original dose-response curve (in dark blue) when this parameter is decreased (red line) or increased (purple line). The green and red area highlight the range of healthy and cancerous lactate concentrations respectively. Red dots indicate the EC5, EC50 and EC95 respectively.

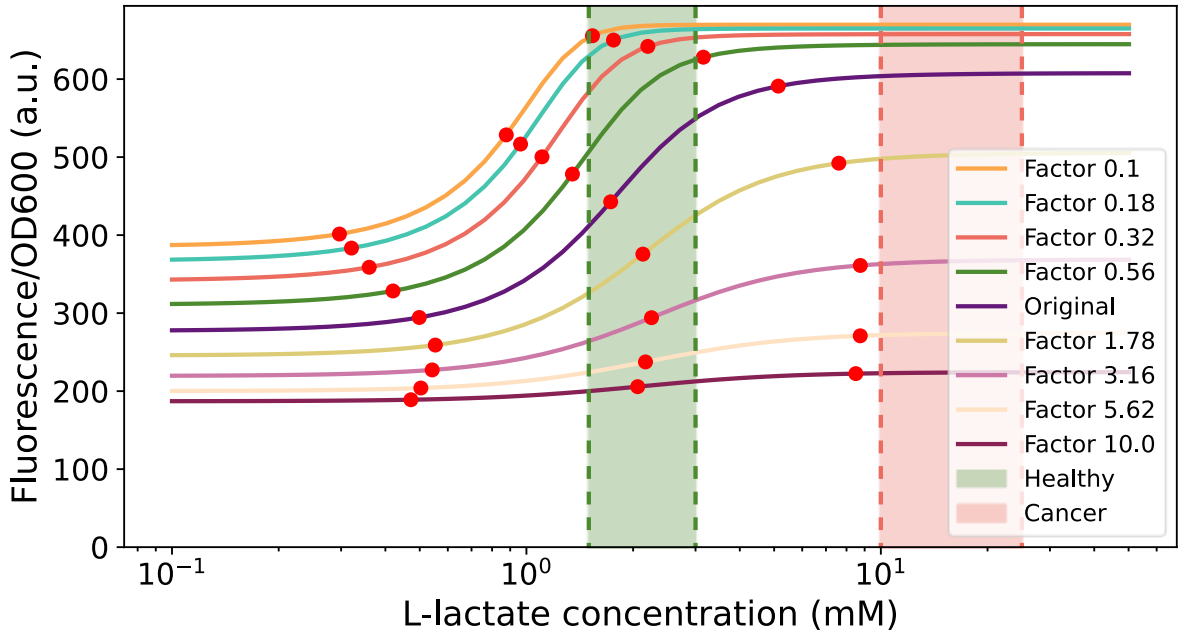

Figure 37: One-at-a-time sensitivity analysis result for k_d_{asrna}, showing what happens to the original dose-response curve (in dark blue) when this parameter is decreased (red line) or increased (purple line). The green and red area highlight the range of healthy and cancerous lactate concentrations respectively. Red dots indicate the EC5, EC50 and EC95 respectively.

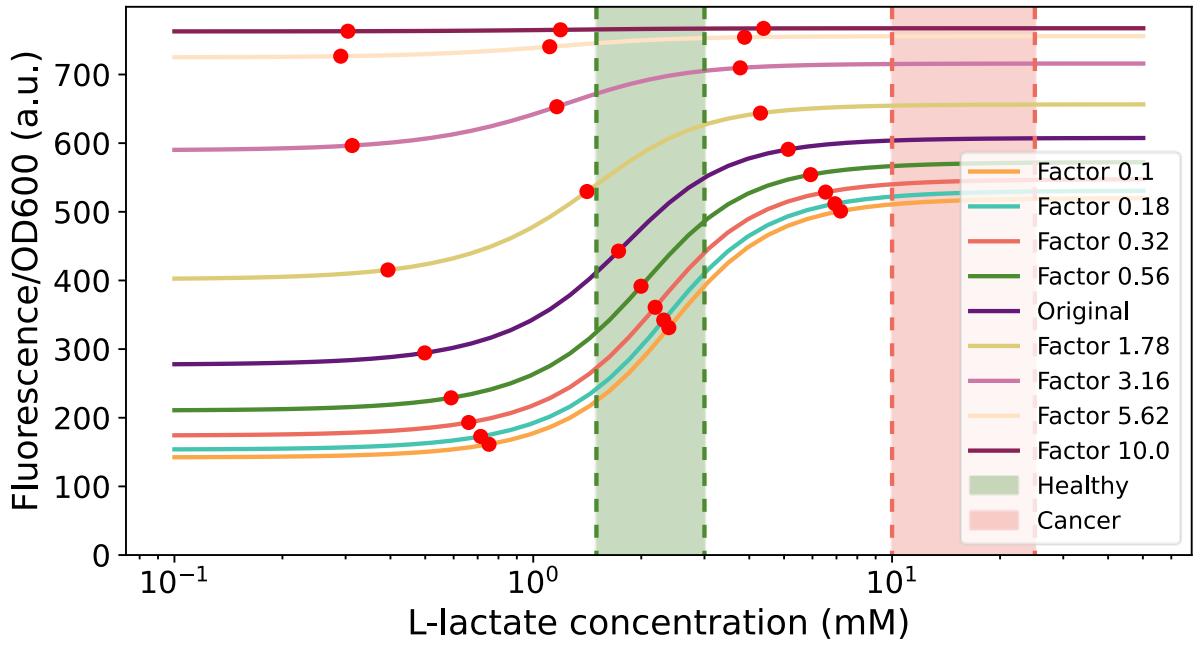

Figure 38: One-at-a-time sensitivity analysis result for $k\_d_{cascomplex}$, showing what happens to the original dose-response curve (in dark blue) when this parameter is decreased (red line) or increased (purple line). The green and red area highlight the range of healthy and cancerous lactate concentrations respectively. Red dots indicate the EC5, EC50 and EC95 respectively.

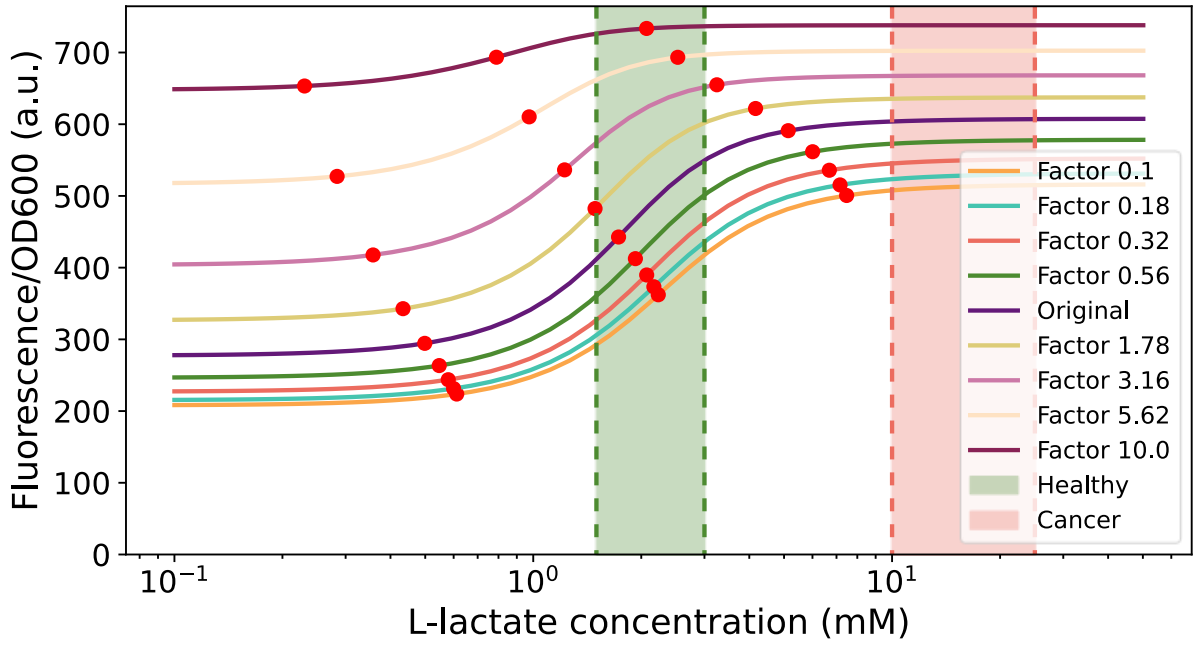

Figure 39: One-at-a-time sensitivity analysis result for k_d_{dcas}, showing what happens to the original dose-response curve (in dark blue) when this parameter is decreased (red line) or increased (purple line). The green and red area highlight the range of healthy and cancerous lactate concentrations respectively. Red dots indicate the EC5, EC50 and EC95 respectively.

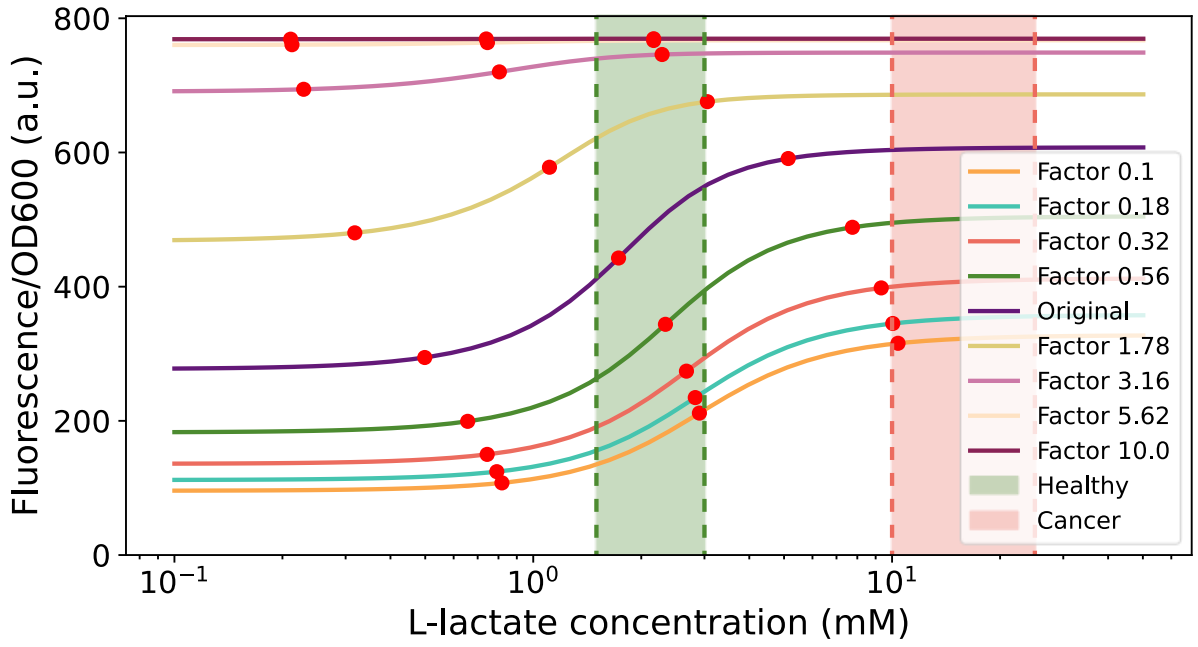

Figure 40: One-at-a-time sensitivity analysis result for $k\_d_{dcasmrna}$, showing what happens to the original dose-response curve (in dark blue) when this parameter is decreased (red line) or increased (purple line). The green and red area highlight the range of healthy and cancerous lactate concentrations respectively. Red dots indicate the EC5, EC50 and EC95 respectively.

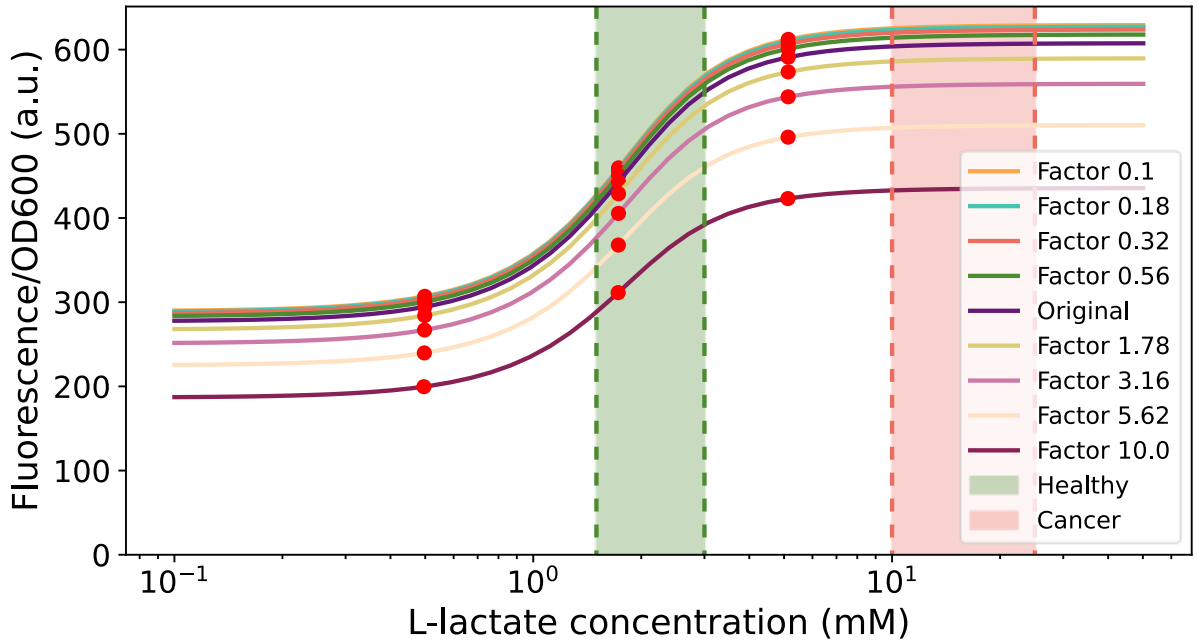

Figure 41: One-at-a-time sensitivity analysis result for k_d_{gfp}, showing what happens to the original dose-response curve (in dark blue) when this parameter is decreased (red line) or increased (purple line). The green and red area highlight the range of healthy and cancerous lactate concentrations respectively. Red dots indicate the EC5, EC50 and EC95 respectively.

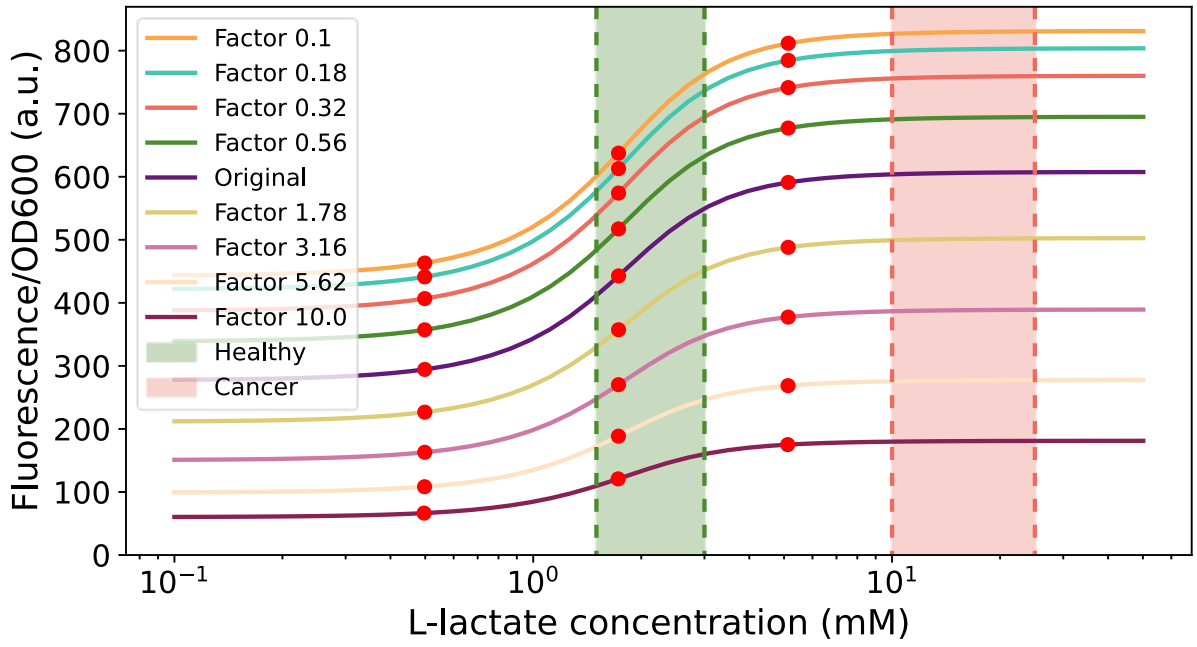

Figure 42: One-at-a-time sensitivity analysis result for $k\_d_{gfpmrna}$, showing what happens to the original dose-response curve (in dark blue) when this parameter is decreased (red line) or increased (purple line). The green and red area highlight the range of healthy and cancerous lactate concentrations respectively. Red dots indicate the EC5, EC50 and EC95 respectively.

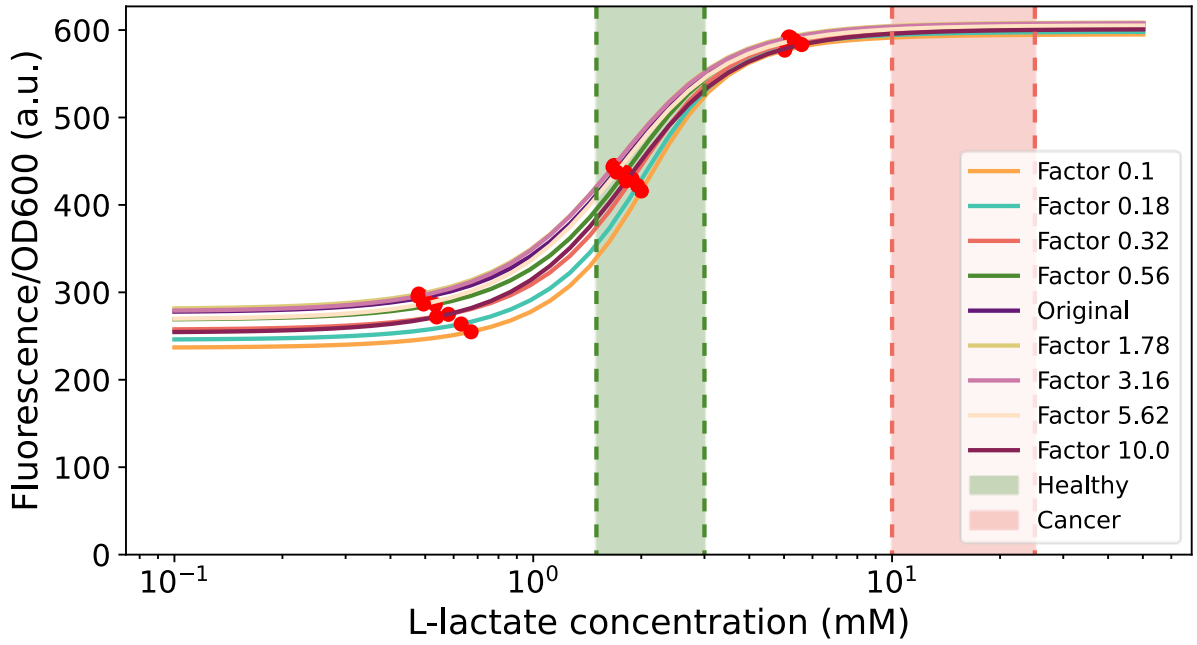

Figure 43: One-at-a-time sensitivity analysis result for k_d_{lldr}, showing what happens to the original dose-response curve (in dark blue) when this parameter is decreased (red line) or increased (purple line). The green and red area highlight the range of healthy and cancerous lactate concentrations respectively. Red dots indicate the EC5, EC50 and EC95 respectively.

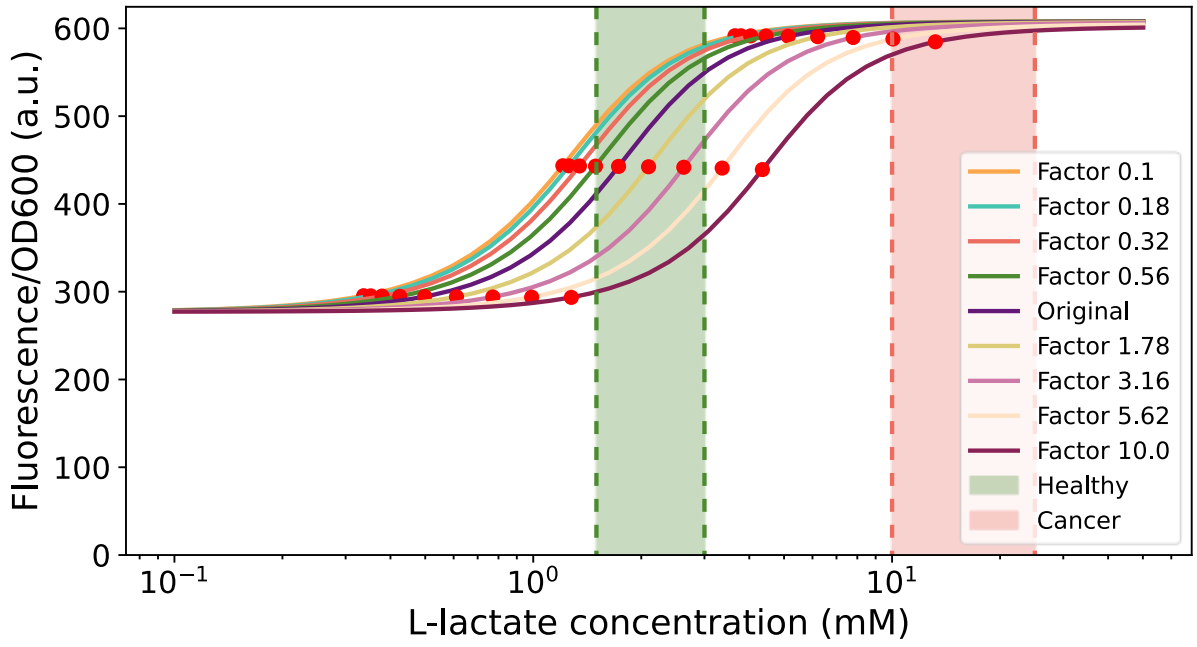

Figure 44: One-at-a-time sensitivity analysis result for $k\_d_{lldrcomplex}$, showing what happens to the original dose-response curve (in dark blue) when this parameter is decreased (red line) or increased (purple line). The green and red area highlight the range of healthy and cancerous lactate concentrations respectively. Red dots indicate the EC5, EC50 and EC95 respectively.

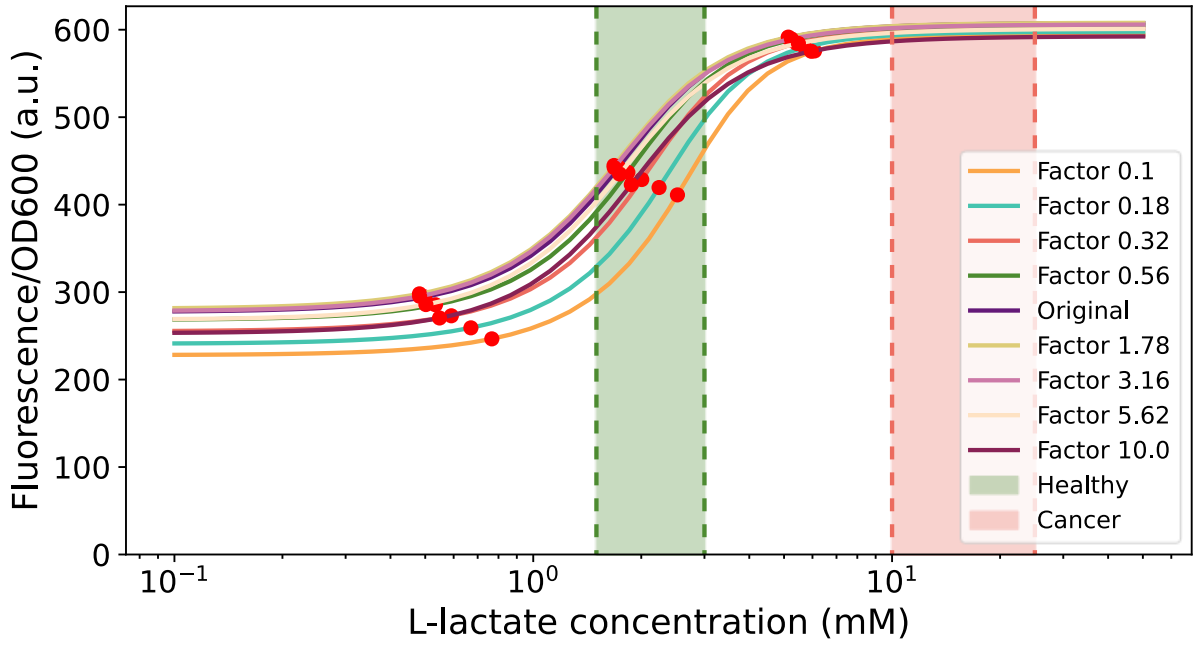

Figure 45: One-at-a-time sensitivity analysis result for $k\_d_{lldrmrna}$, showing what happens to the original dose-response curve (in dark blue) when this parameter is decreased (red line) or increased (purple line). The green and red area highlight the range of healthy and cancerous lactate concentrations respectively. Red dots indicate the EC5, EC50 and EC95 respectively.

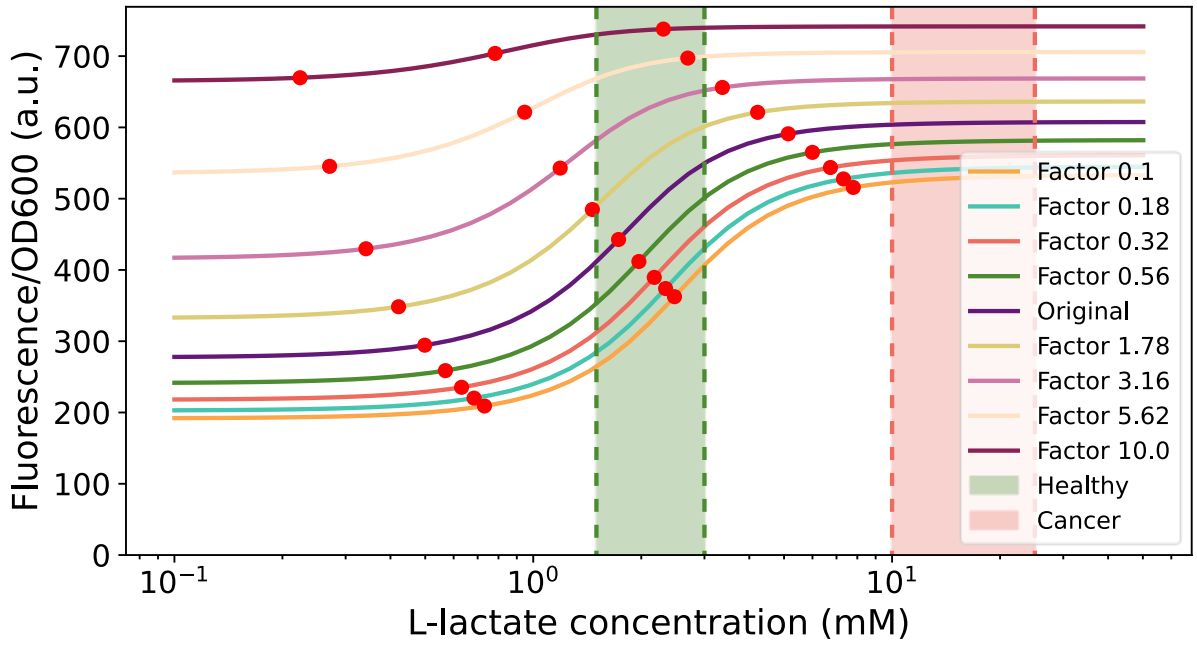

Figure 46: One-at-a-time sensitivity analysis result for k_d_{sgrna}, showing what happens to the original dose-response curve (in dark blue) when this parameter is decreased (red line) or increased (purple line). The green and red area highlight the range of healthy and cancerous lactate concentrations respectively. Red dots indicate the EC5, EC50 and EC95 respectively.

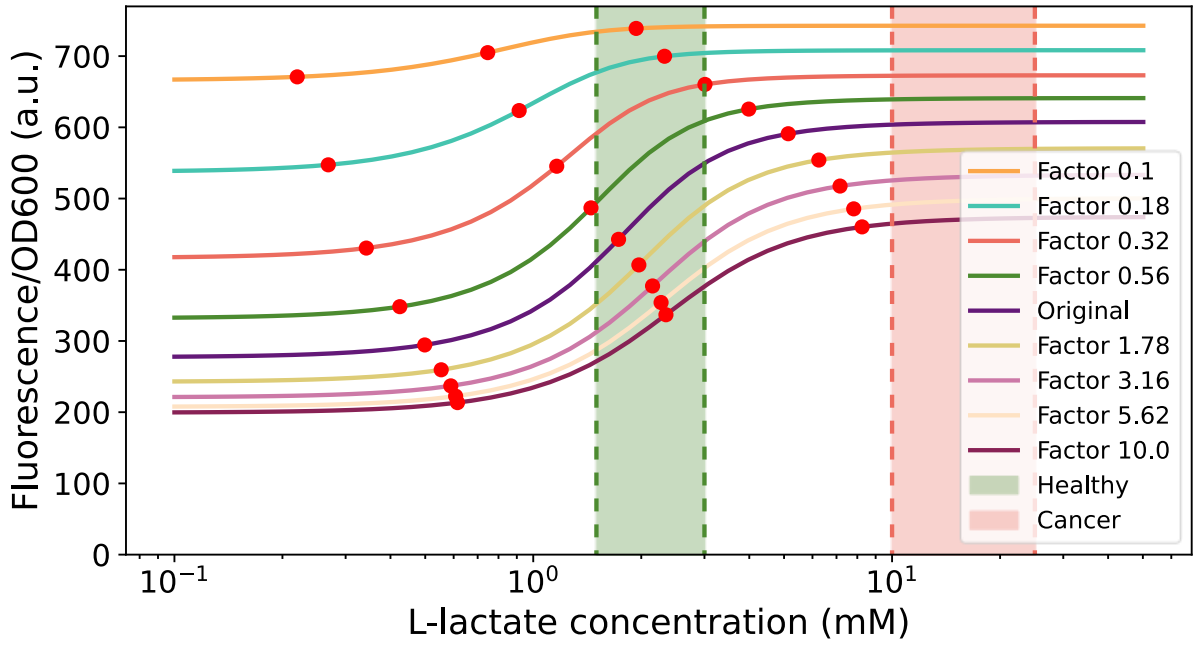

Figure 47: One-at-a-time sensitivity analysis result for $k\_f_{1_{fw}}$, showing what happens to the original dose-response curve (in dark blue) when this parameter is decreased (red line) or increased (purple line). The green and red area highlight the range of healthy and cancerous lactate concentrations respectively. Red dots indicate the EC5, EC50 and EC95 respectively.

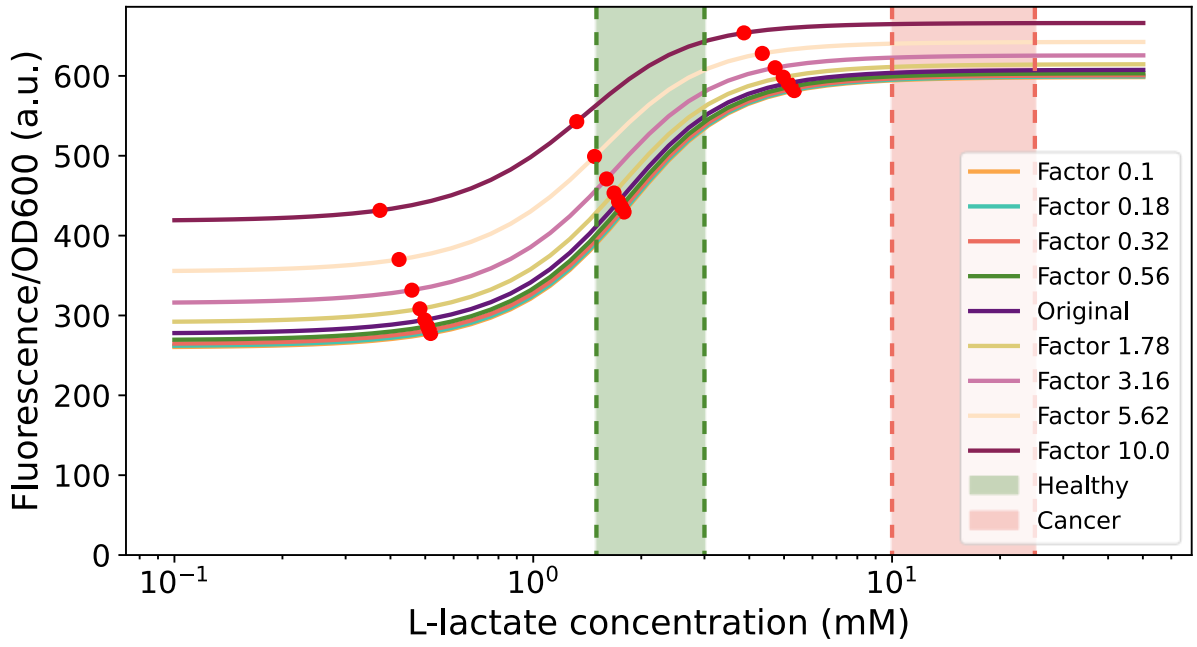

Figure 48: One-at-a-time sensitivity analysis result for $k\_f_{1_{rv}}$, showing what happens to the original dose-response curve (in dark blue) when this parameter is decreased (red line) or increased (purple line). The green and red area highlight the range of healthy and cancerous lactate concentrations respectively. Red dots indicate the EC5, EC50 and EC95 respectively.

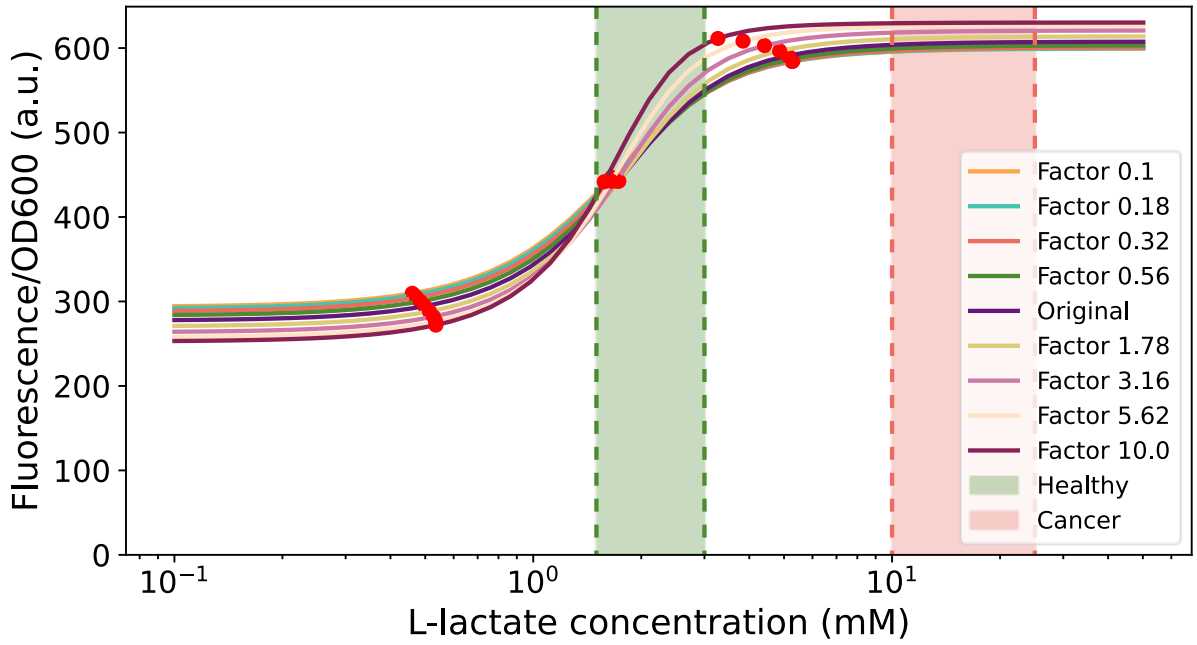

Figure 49: One-at-a-time sensitivity analysis result for $k\_f_{2_{fw}}$, showing what happens to the original dose-response curve (in dark blue) when this parameter is decreased (red line) or increased (purple line). The green and red area highlight the range of healthy and cancerous lactate concentrations respectively. Red dots indicate the EC5, EC50 and EC95 respectively.

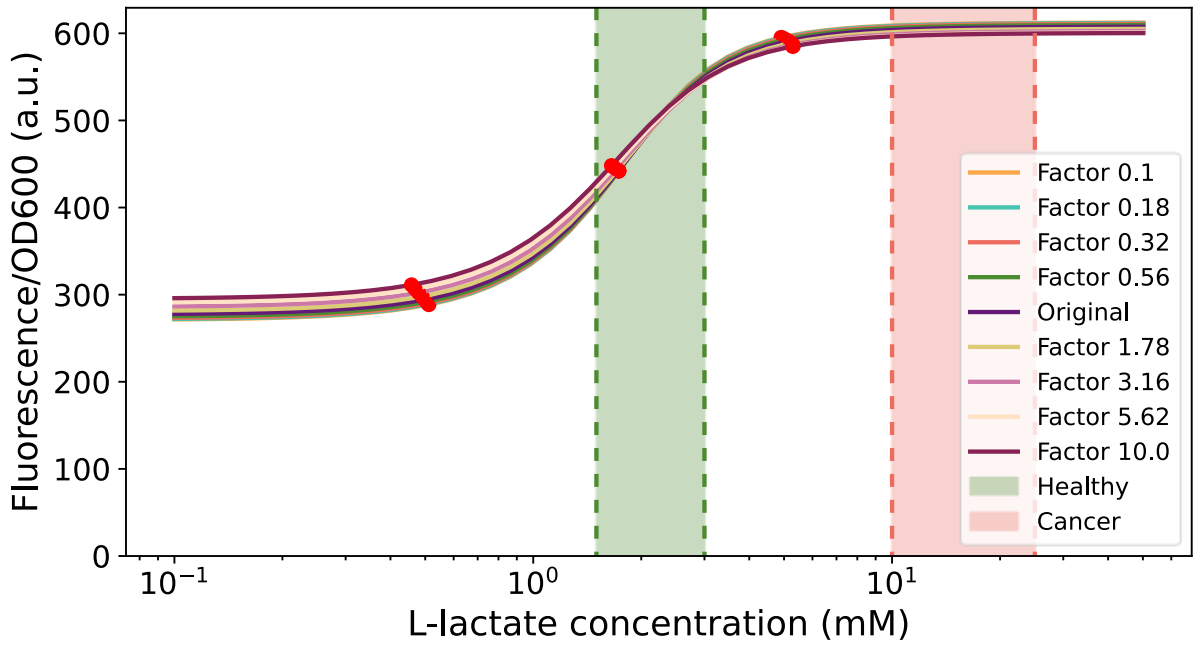

Figure 50: One-at-a-time sensitivity analysis result for $k\_f_{2_{rv}}$, showing what happens to the original dose-response curve (in dark blue) when this parameter is decreased (red line) or increased (purple line). The green and red area highlight the range of healthy and cancerous lactate concentrations respectively. Red dots indicate the EC5, EC50 and EC95 respectively.

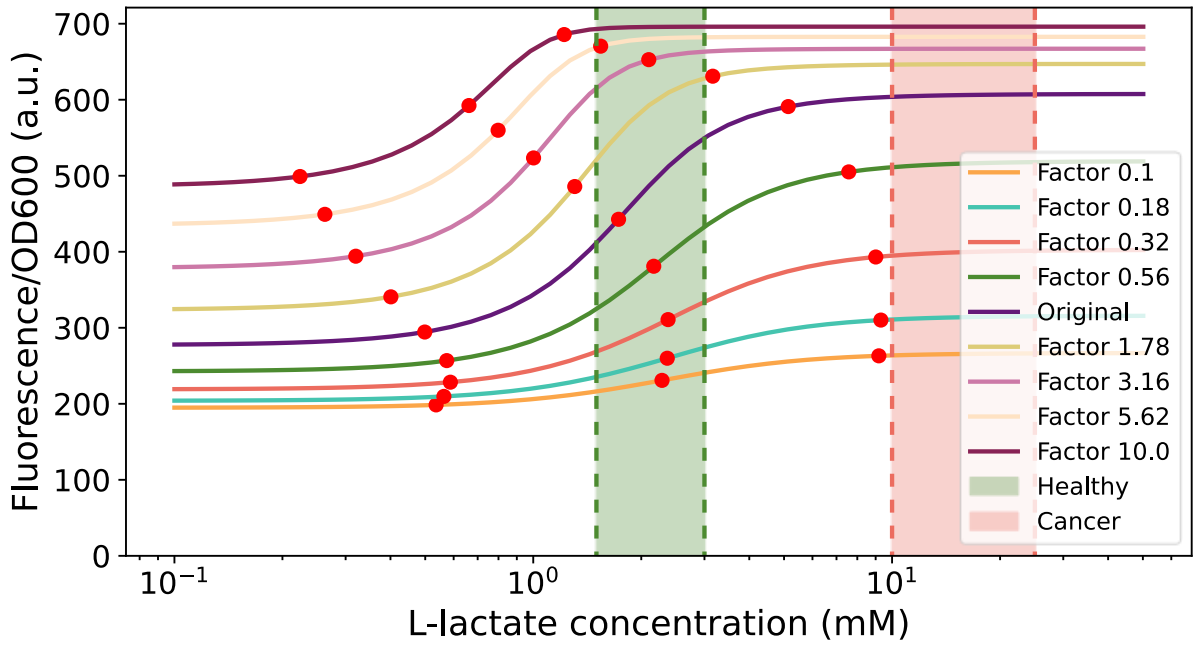

Figure 51: One-at-a-time sensitivity analysis result for $k\_f_{3_{fw}}$, showing what happens to the original dose-response curve (in dark blue) when this parameter is decreased (red line) or increased (purple line). The green and red area highlight the range of healthy and cancerous lactate concentrations respectively. Red dots indicate the EC5, EC50 and EC95 respectively.

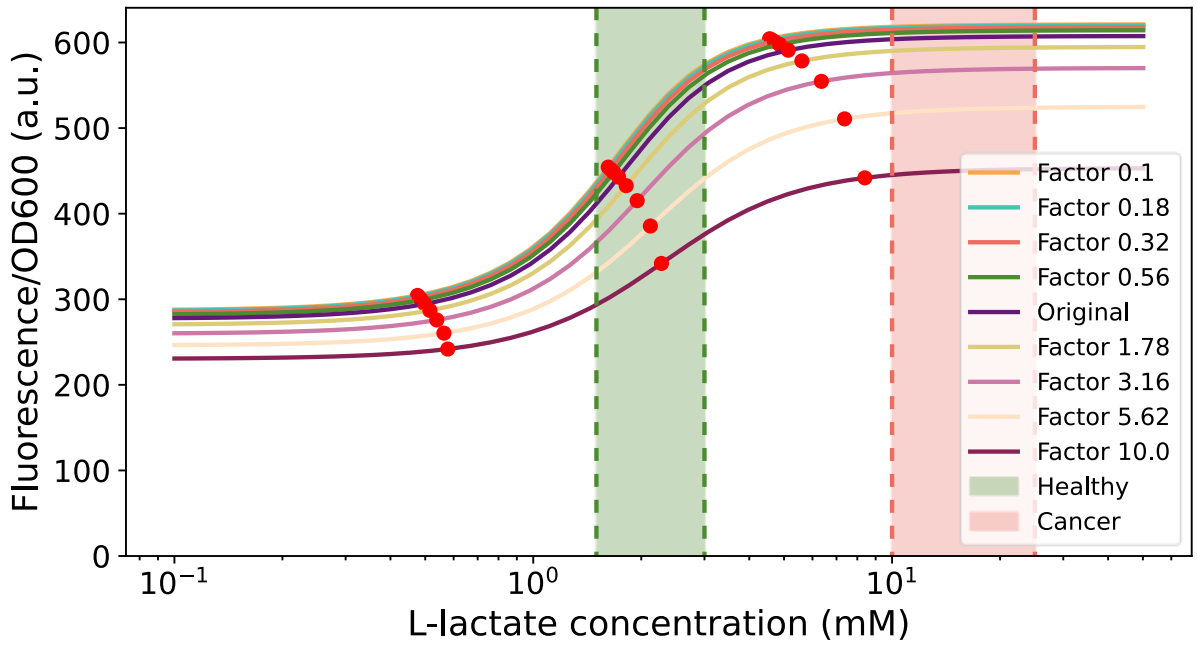

Figure 52: One-at-a-time sensitivity analysis result for $k\_f_{3_{rv}}$, showing what happens to the original dose-response curve (in dark blue) when this parameter is decreased (red line) or increased (purple line). The green and red area highlight the range of healthy and cancerous lactate concentrations respectively. Red dots indicate the EC5, EC50 and EC95 respectively.

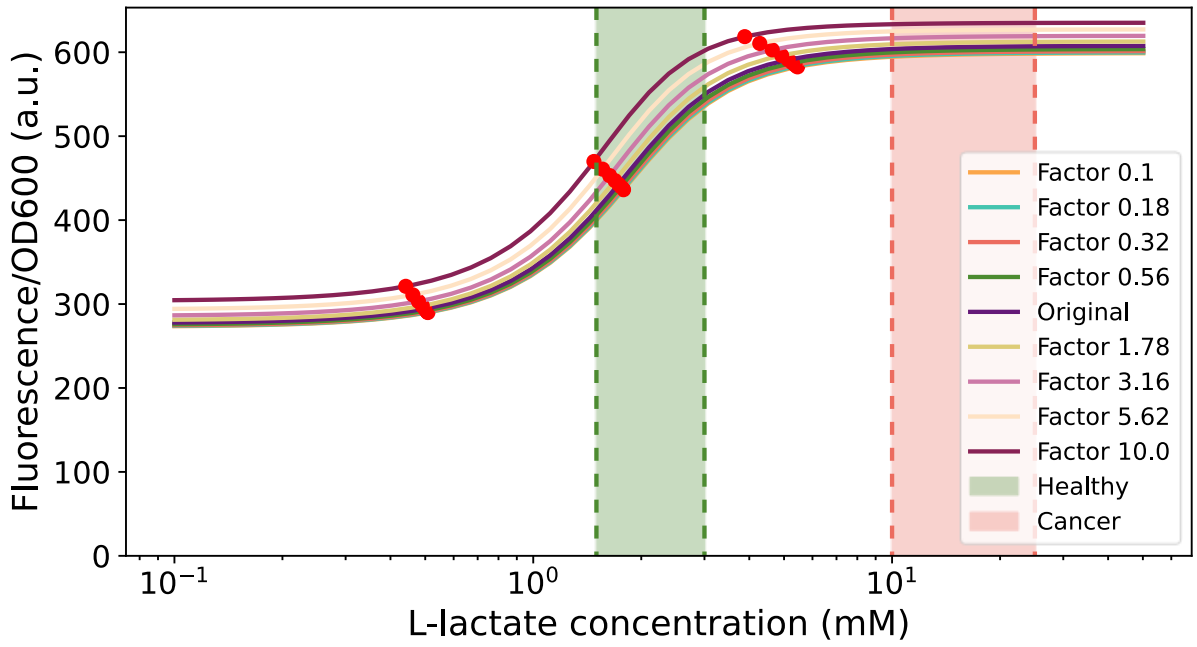

Figure 53: One-at-a-time sensitivity analysis result for $k\_f_{4_{fw}}$, showing what happens to the original dose-response curve (in dark blue) when this parameter is decreased (red line) or increased (purple line). The green and red area highlight the range of healthy and cancerous lactate concentrations respectively. Red dots indicate the EC5, EC50 and EC95 respectively.

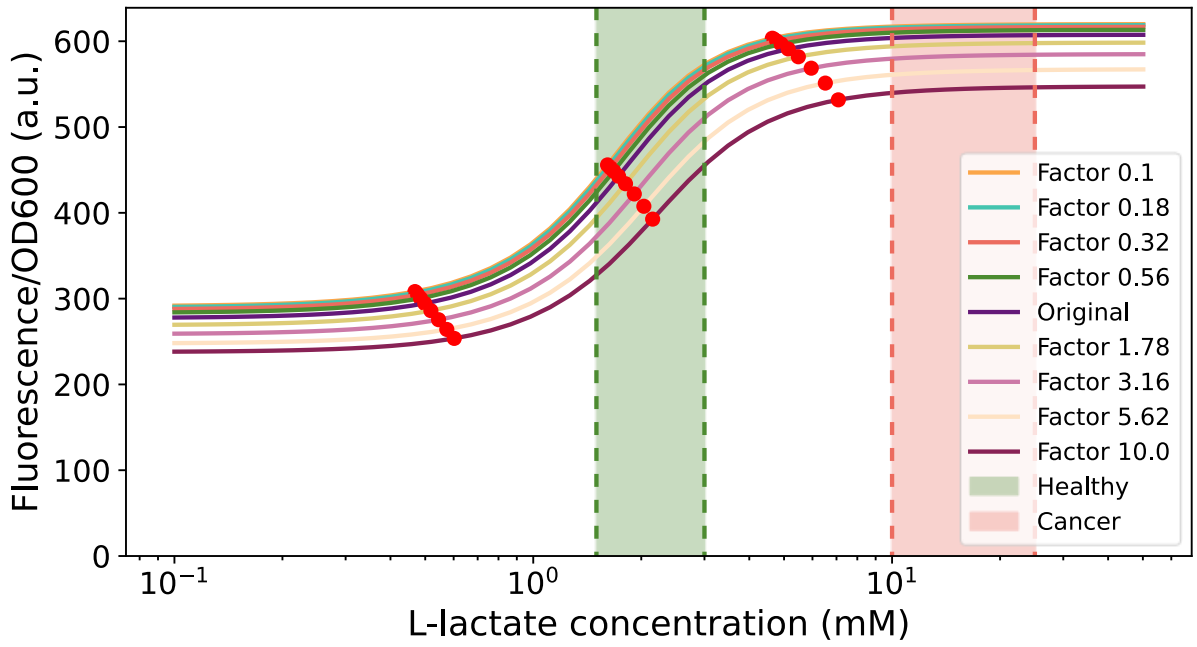

Figure 54: One-at-a-time sensitivity analysis result for $k\_f_{4_{rv}}$, showing what happens to the original dose-response curve (in dark blue) when this parameter is decreased (red line) or increased (purple line). The green and red area highlight the range of healthy and cancerous lactate concentrations respectively. Red dots indicate the EC5, EC50 and EC95 respectively.

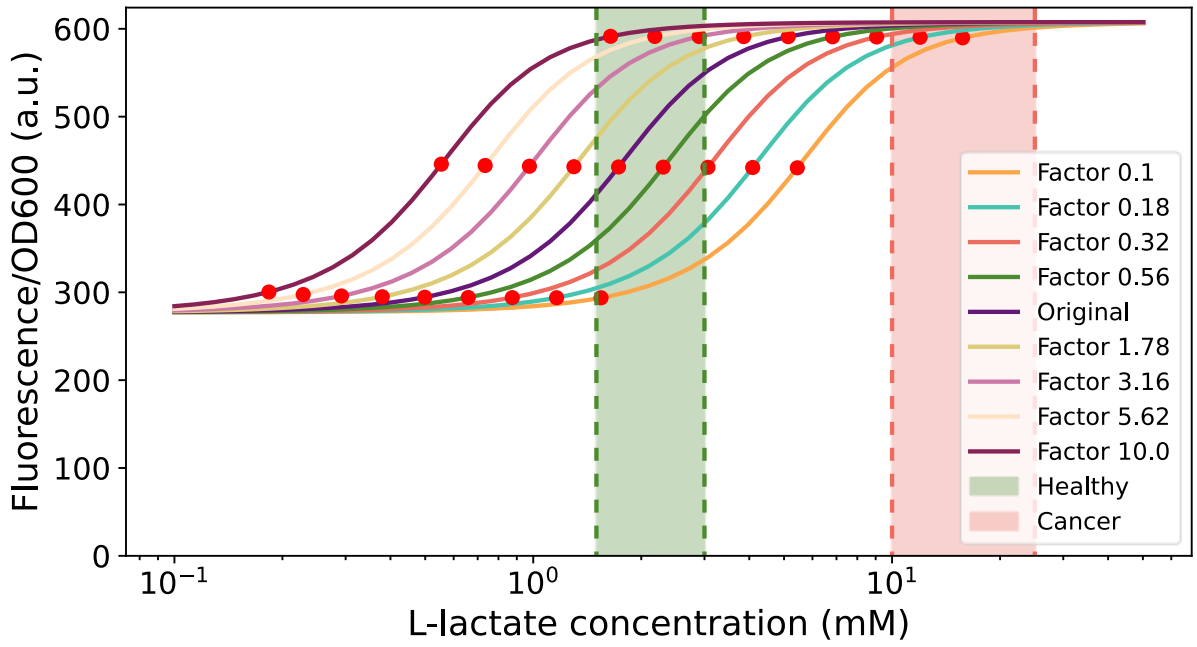

Figure 55: One-at-a-time sensitivity analysis result for $k\_f_{lldrcomplex}$, showing what happens to the original dose-response curve (in dark blue) when this parameter is decreased (red line) or increased (purple line). The green and red area highlight the range of healthy and cancerous lactate concentrations respectively. Red dots indicate the EC5, EC50 and EC95 respectively.

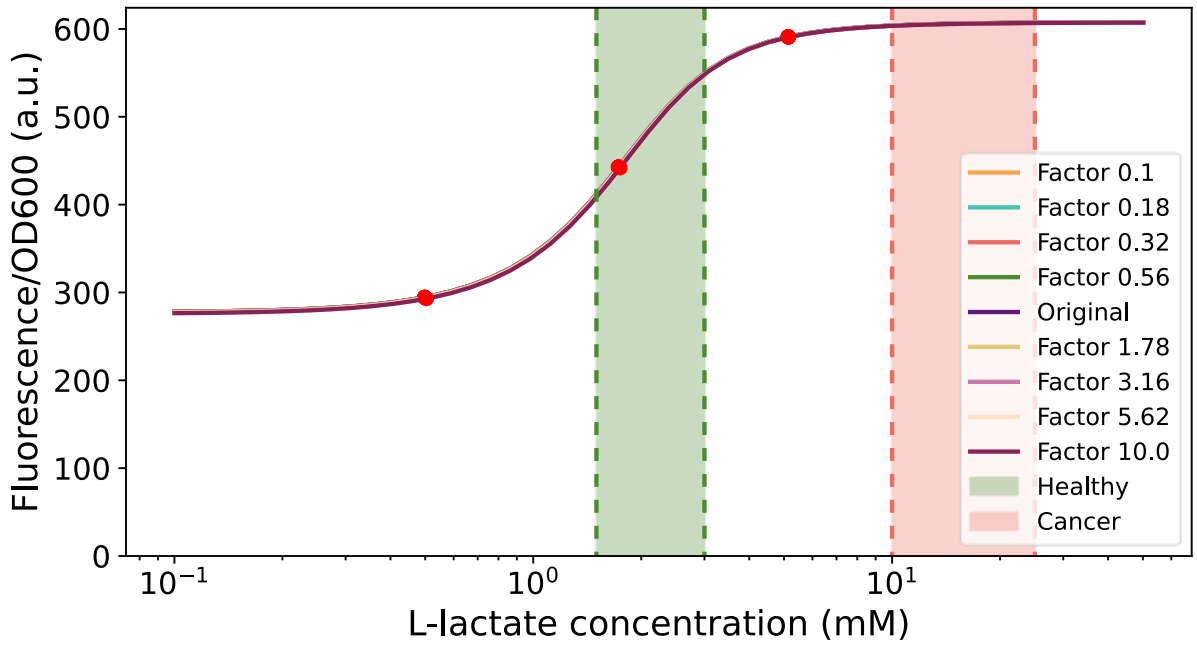

Figure 56: One-at-a-time sensitivity analysis result for k_op_{succ}, showing what happens to the original dose-response curve (in dark blue) when this parameter is decreased (red line) or increased (purple line). The green and red area highlight the range of healthy and cancerous lactate concentrations respectively. Red dots indicate the EC5, EC50 and EC95 respectively.

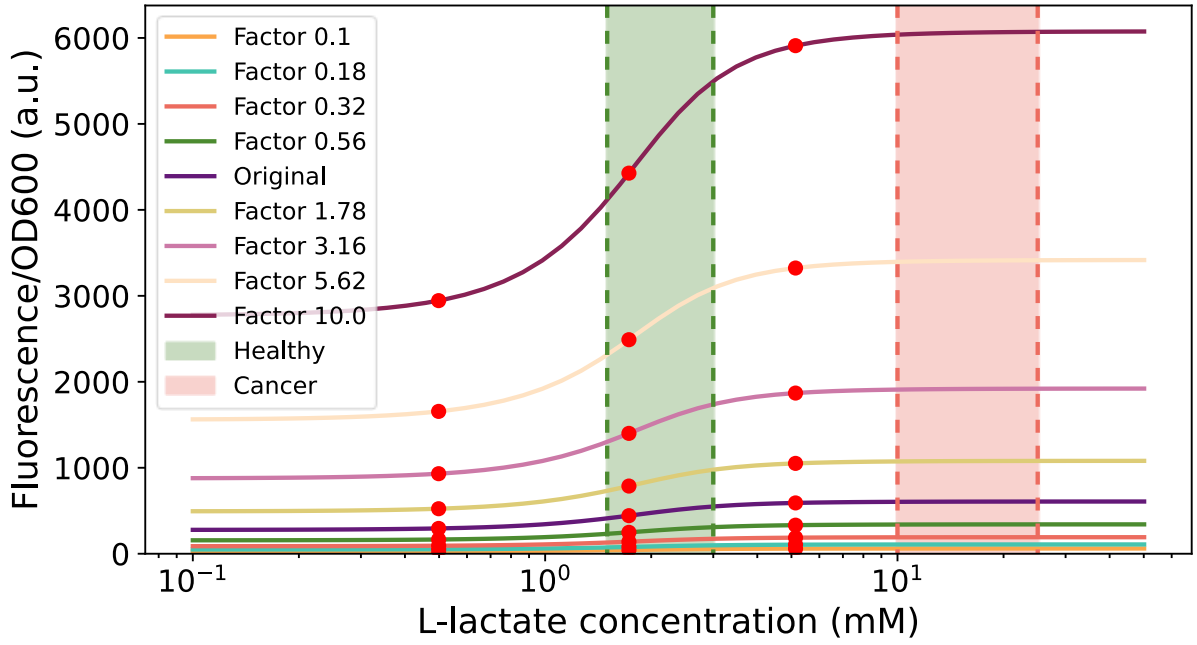

Figure 57: One-at-a-time sensitivity analysis result for $k\_p_{gfpmrna}$, showing what happens to the original dose-response curve (in dark blue) when this parameter is decreased (red line) or increased (purple line). The green and red area highlight the range of healthy and cancerous lactate concentrations respectively. Red dots indicate the EC5, EC50 and EC95 respectively.

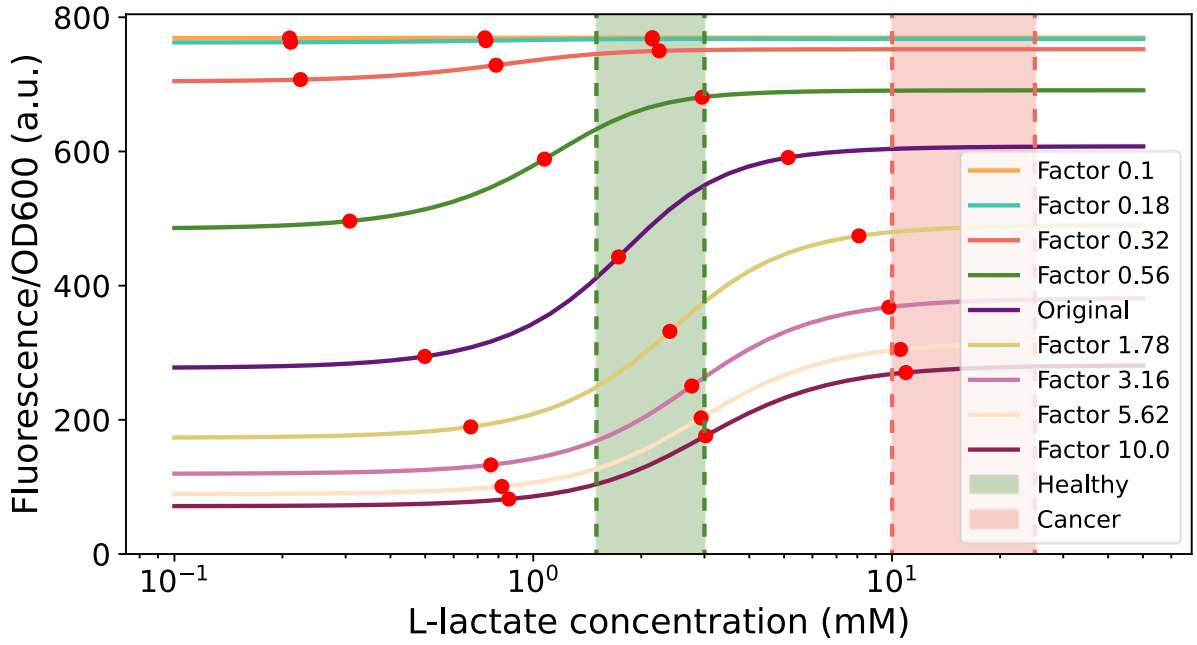

Figure 58: One-at-a-time sensitivity analysis result for k_pt_{dcas}, showing what happens to the original dose-response curve (in dark blue) when this parameter is decreased (red line) or increased (purple line). The green and red area highlight the range of healthy and cancerous lactate concentrations respectively. Red dots indicate the EC5, EC50 and EC95 respectively.

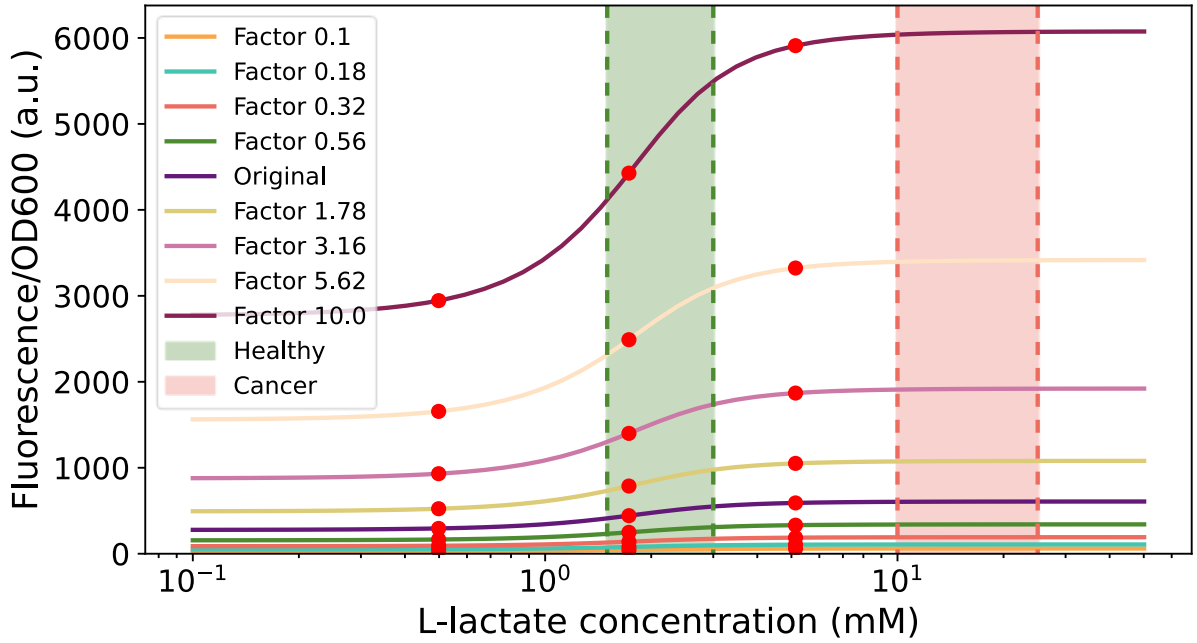

Figure 59: One-at-a-time sensitivity analysis result for k_pt_{gfp}, showing what happens to the original dose-response curve (in dark blue) when this parameter is decreased (red line) or increased (purple line). The green and red area highlight the range of healthy and cancerous lactate concentrations respectively. Red dots indicate the EC5, EC50 and EC95 respectively.

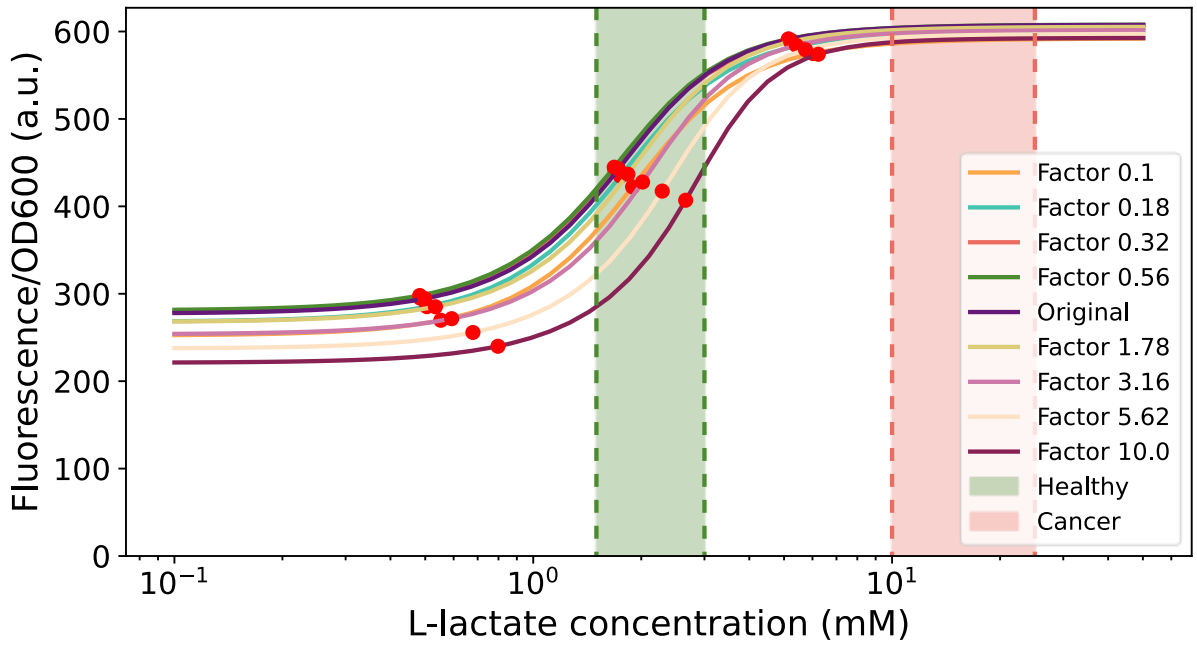

Figure 60: One-at-a-time sensitivity analysis result for k_pt_{lldr}, showing what happens to the original dose-response curve (in dark blue) when this parameter is decreased (red line) or increased (purple line). The green and red area highlight the range of healthy and cancerous lactate concentrations respectively. Red dots indicate the EC5, EC50 and EC95 respectively.

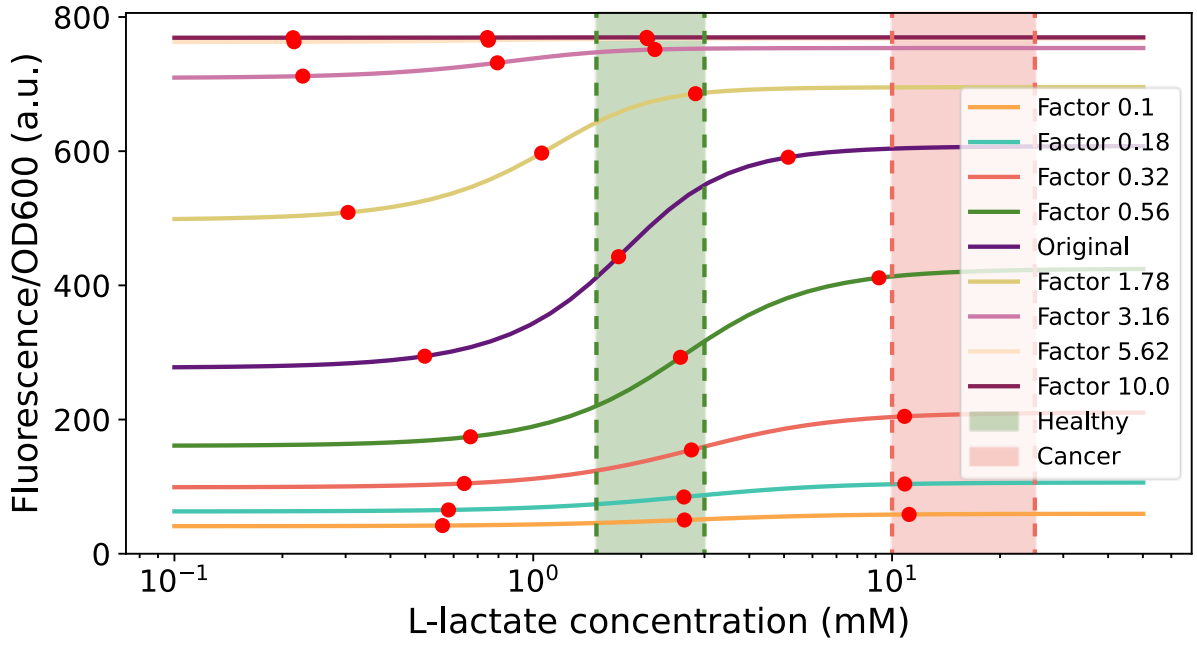

Figure 61: One-at-a-time sensitivity analysis result for kd_{dcas}, showing what happens to the original dose-response curve (in dark blue) when this parameter is decreased (orange line) or increased (purple line). The green and red area highlight the range of healthy and cancerous lactate concentrations respectively. Red dots indicate the EC5, EC50 and EC95 respectively.

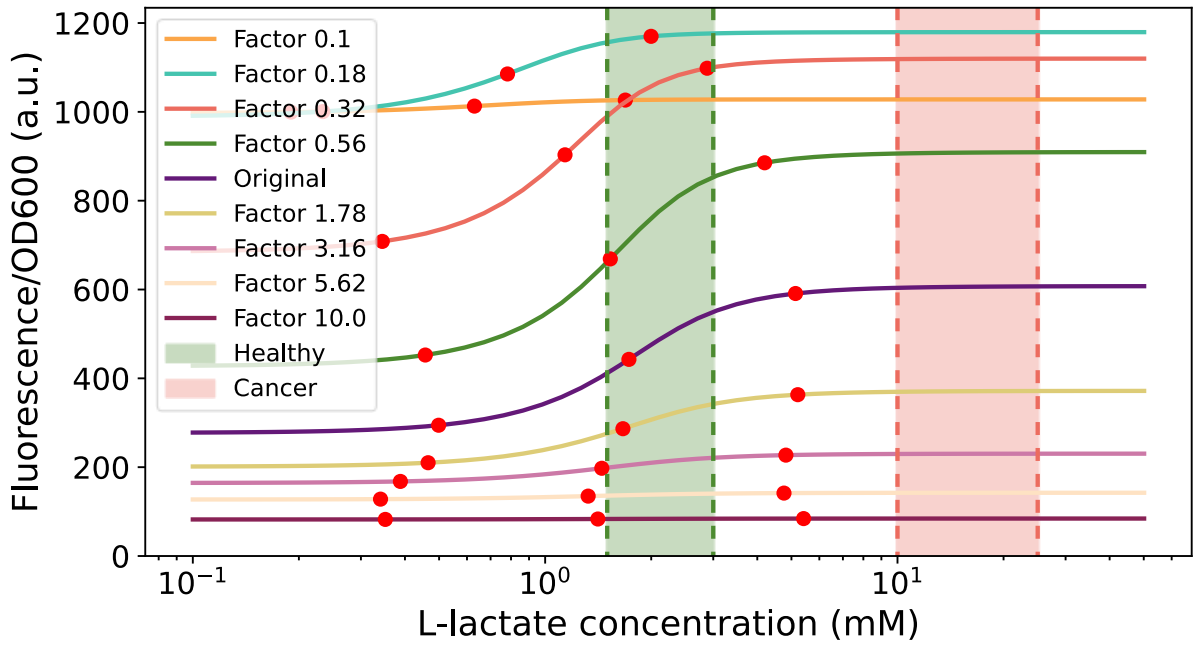

Figure 62: One-at-a-time sensitivity analysis result for μ_{max}, showing what happens to the original dose-response curve (in dark blue) when this parameter is decreased (orange line) or increased (purple line). The green and red area highlight the range of healthy and cancerous lactate concentrations respectively. Red dots indicate the EC5, EC50 and EC95 respectively.

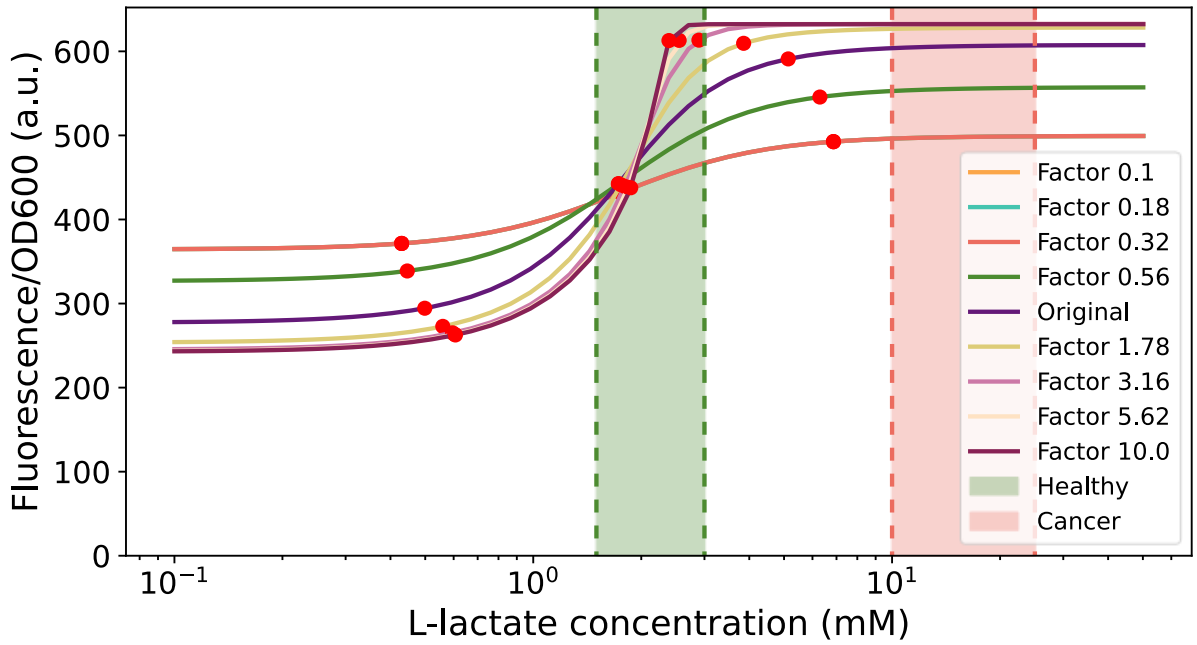

Figure 63: One-at-a-time sensitivity analysis result for $n_{cascomplex}$, showing what happens to the original dose-response curve (in dark blue) when this parameter is decreased (red line) or increased (purple line). The green and red area highlight the range of healthy and cancerous lactate concentrations respectively. Red dots indicate the EC5, EC50 and EC95 respectively.

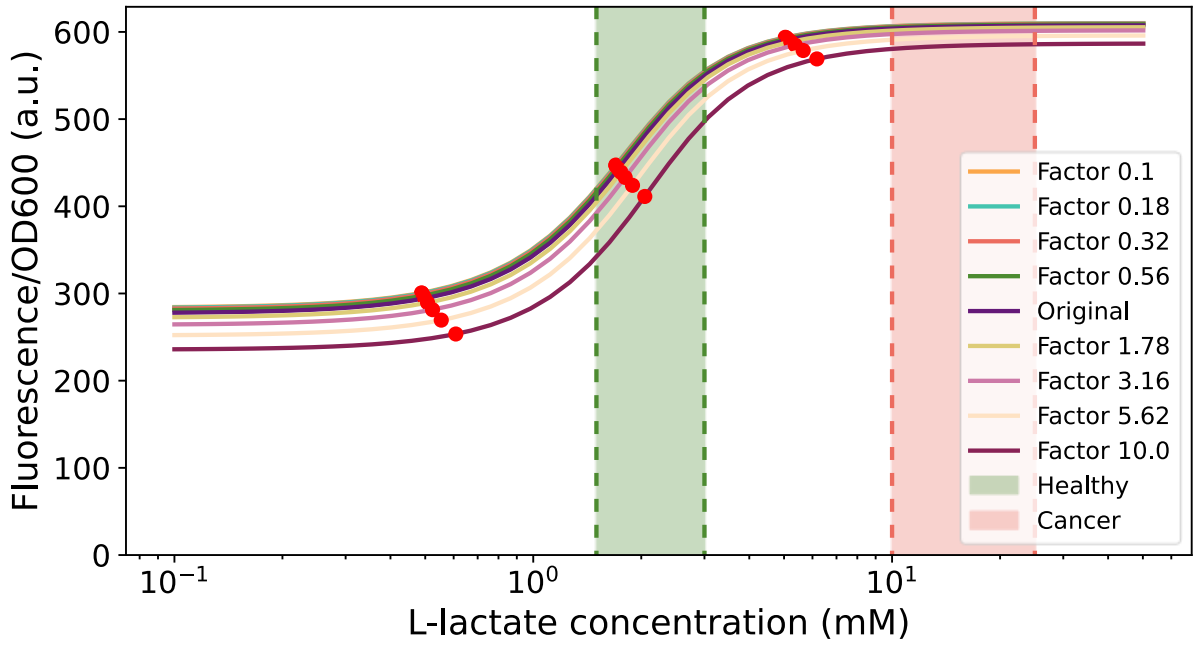

Figure 64: One-at-a-time sensitivity analysis result for γ, showing what happens to the original dose-response curve (in dark blue) when this parameter is decreased (red line) or increased (purple line). The green and red area highlight the range of healthy and cancerous lactate concentrations respectively. Red dots indicate the EC5, EC50 and EC95 respectively.

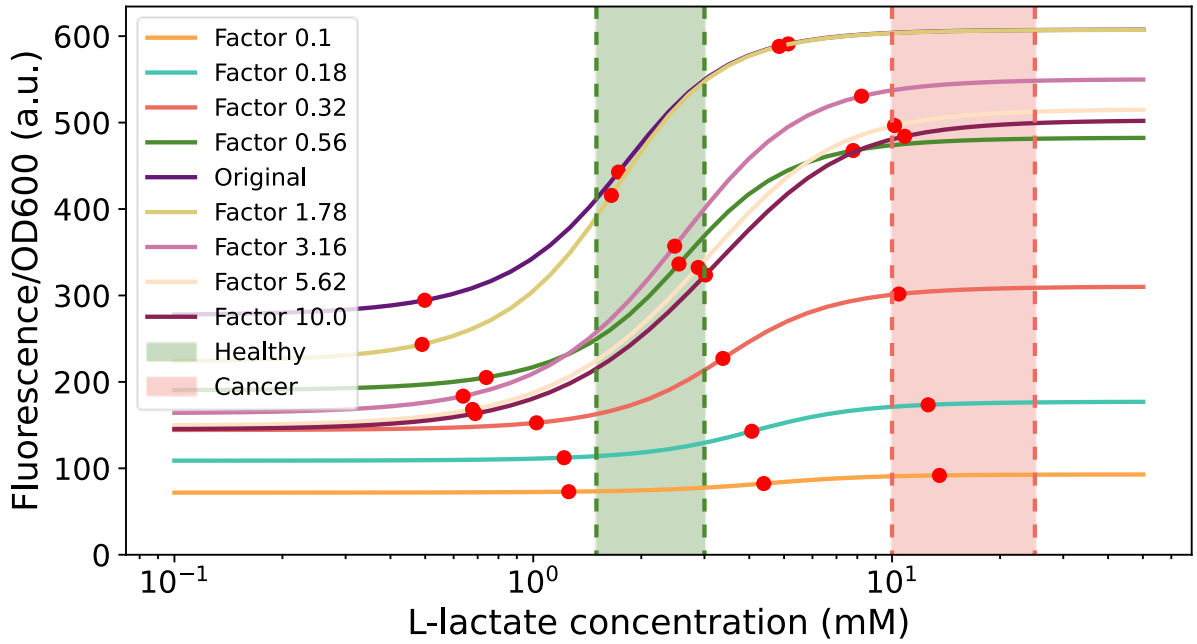

Figure 65: One-at-a-time sensitivity analysis result for σ, showing what happens to the original dose-response curve (in dark blue) when this parameter is decreased (red line) or increased (purple line). The green and red area highlight the range of healthy and cancerous lactate concentrations respectively. Red dots indicate the EC5, EC50 and EC95 respectively.

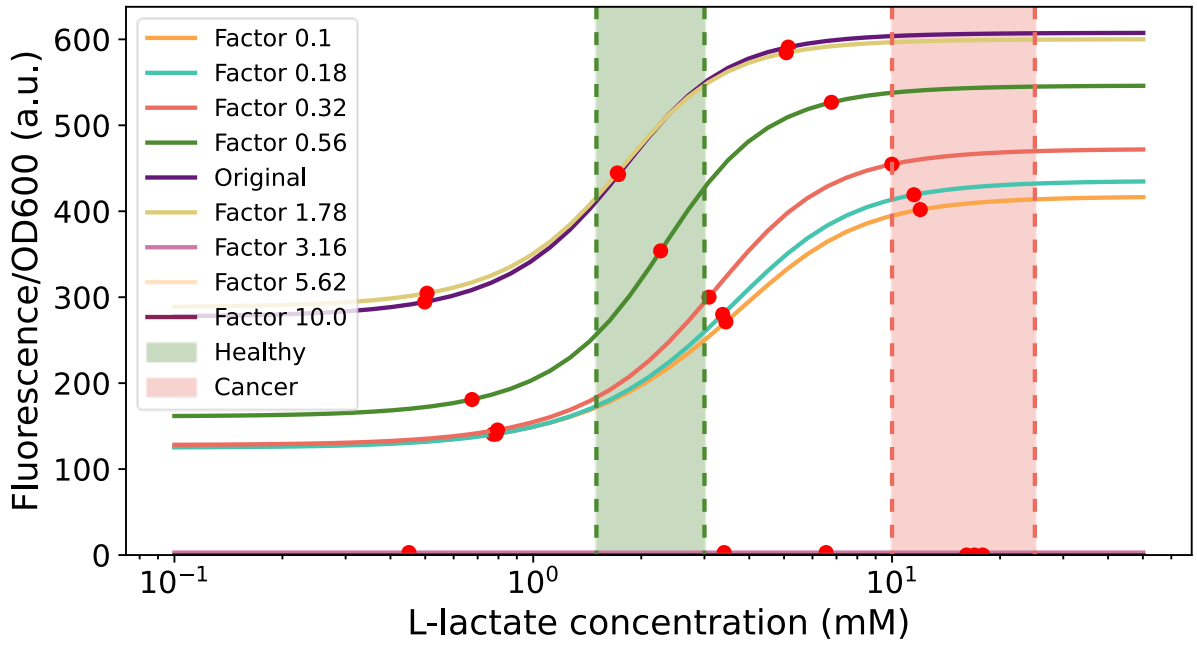

Figure 66: One-at-a-time sensitivity analysis result for t_c, showing what happens to the original dose-response curve (in dark blue) when this parameter is decreased (red line) or increased (purple line). The green and red area highlight the range of healthy and cancerous lactate concentrations respectively. Red dots indicate the EC5, EC50 and EC95 respectively.

Bibliography

[1] Sung H, Ferlay J, Siegel RL, Laversanne M, Soerjomataram I, Jemal A, et al. Global Cancer Statistics 2020: GLOBOCAN Estimates of Incidence and Mortality Worldwide for 36 Cancers in 185 Countries. CA Cancer J Clin 2021;71:209–49. https://doi.org/10.3322/CAAC.21660.

[2] IKNL. National monitoring of the colorectal cancer screening programme in the Netherlands 2021 2022.

[3] Colorectal Cancer: Statistics | Cancer.Net n.d. https://www.cancer.net/cancer-types/colorectal-cancer/statistics (accessed May 2, 2022).

[4] Venkatesh K v., Darunte L, Bhat PJ. Warburg Effect. Encyclopedia of Systems Biology 2013:2349–50. https://doi.org/10.1007/978-1-4419-9863-7_703.

[5] Ho JML, Miller CA, Parks SE, Mattia JR, Bennett MR. A suppressor tRNA-mediated feedforward loop eliminates leaky gene expression in bacteria. Nucleic Acids Res 2021;49. https://doi.org/10.1093/nar/gkaa1179.

[6] Hove H, Mortensen B. Colonic Lactate Metabolism Acidosis and D-Lactic. vol. 40. 1995.

[7] Miller CA, Ho JML, Bennett MR. Strategies for Improving Small-Molecule Biosensors in Bacteria. Biosensors (Basel) 2022;12. https://doi.org/10.3390/BIOS12020064.

[8] Núñez MF, Aguilar J, Baldoma L, Kwon O, Wilson TH, Lin ECC. Transport of L-lactate, D-lactate, and glycolate by the LldP and GlcA membrane carriers of Escherichia coli. Biochem Biophys Res Commun 2002;290:824–9. https://doi.org/10.1006/BBRC.2001.6255.

[9] Goers L, Ainsworth C, Goey CH, Kontoravdi C, Freemont PS, Polizzi KM. Whole-cell Escherichia coli lactate biosensor for monitoring mammalian cell cultures during biopharmaceutical production. Biotechnol Bioeng 2017;114:1290–300. https://doi.org/10.1002/BIT.26254.

[10] Felisa Nu M, Teresa Pellicer M, Badı J, Aguilar J, Baldoma L. The gene yghK linked to the glc operon of Escherichia coli encodes a permease for glycolate that is structurally and functionally similar to L-lactate permease. Microbiology (N Y) 2001;147:1069–77.

[11] Mas-Bargues C, Sanz-Ros J, Román-Domínguez A, Inglés M, Gimeno-Mallench L, el Alami M, et al. Relevance of Oxygen Concentration in Stem Cell Culture for Regenerative Medicine. International Journal of Molecular Sciences 2019, Vol 20, Page 1195 2019;20:1195. https://doi.org/10.3390/IJMS20051195.

[12] Zúñ A, Iga Z, Camacho M, Chang H-J, Fristot E, Mayonove P, et al. Engineered L-Lactate Responding Promoter System Operating in Glucose-Rich and Anoxic Environments. ACS Synth Biology 2021;10:3527–36. https://doi.org/10.1021/acssynbio.1c00456.

[13] Lee YJ, Hoynes-O'Connor A, Leong MC, Moon TS. Programmable control of bacterial gene expression with the combined CRISPR and antisense RNA system. Nucleic Acids Res 2016;44:2462–73. https://doi.org/10.1093/NAR/GKW056.

[14] Specht DA, Cortes LB, Lambert G. Overcoming Leak Sensitivity in CRISPRi Circuits Using Antisense RNA Sequestration and Regulatory Feedback. Cite This: ACS Synth Biol 2022. https://doi.org/10.1021/acssynbio.2c00155.

[15] Santos-Moreno J, Schaerli Y. CRISPR-based gene expression control for synthetic gene circuits 2020. https://doi.org/10.1042/BST20200020.

[16] Zhang R, Xu W, Shao S, Wang Q. Gene Silencing Through CRISPR Interference in Bacteria: Current Advances and Future Prospects. Front Microbiol 2021;12:567. https://doi.org/10.3389/FMICB.2021.635227/BIBTEX.

[17] Snoek T, Chaberski EK, Ambri F, Kol S, Bjørn SP, Pang B, et al. Evolution-guided engineering of small-molecule biosensors. Nucleic Acids Res 2020;48:e3. https://doi.org/10.1093/NAR/GKZ954.

[18] Rubens JR, Selvaggio G, Lu TK. Synthetic mixed-signal computation in living cells. Nat Commun 2016;7. https://doi.org/10.1038/ncomms11658.

[19] Tang SY, Fazelinia H, Cirino PC. AraC regulatory protein mutants with altered effector specificity. J Am Chem Soc 2008;130:5267–71. https://doi.org/10.1021/JA7109053.

[20] Raman S, Rogers JK, Taylor ND, Church GM. Evolution-guided optimization of biosynthetic pathways. Proc Natl Acad Sci U S A 2014;111:17803–8. https://doi.org/10.1073/PNAS.1409523111/SUPPL_FILE/PNAS.1409523111.SAPP.PDF.

[21] Feng XJ, Hooshangi S, Chen D, Li G, Weiss R, Rabitz H. Optimizing genetic circuits by global sensitivity analysis. Biophys J 2004;87:2195–202. https://doi.org/10.1529/BIOPHYSJ.104.044131.

[22] Voit EO, Martens HA, Omholt SW. 150 Years of the Mass Action Law. PLoS Comput Biol 2015;11:e1004012. https://doi.org/10.1371/JOURNAL.PCBI.1004012.

[23] Keller AD. Model genetic circuits encoding autoregulatory transcription factors. J Theor Biol 1995;172:169–85. https://doi.org/10.1006/JTBI.1995.0014.

[24] Aguilera L, Campos E, Giménez R, Badía J, Aguilar J, Baldoma L. Dual role of LldR in regulation of the lldPRD operon, involved in L-lactate metabolism in Escherichia coli. J Bacteriol 2008;190:2997–3005. https://doi.org/10.1128/JB.02013-07.

[25] Klumpp S, Zhang Z, Hwa T. Growth Rate-Dependent Global Effects on Gene Expression in Bacteria. Cell 2009;139:1366–75. https://doi.org/10.1016/j.cell.2009.12.001.

[26] Gutiérrez Mena J, Kumar S, Khammash M. Dynamic cybergenetic control of bacterial co-culture composition via optogenetic feedback. Nature Communications 2022 13:1 2022;13:1–16. https://doi.org/10.1038/s41467-022-32392-z.

[27] Virtanen P, Gommers R, Oliphant TE, Haberland M, Reddy T, Cournapeau D, et al. SciPy 1.0: fundamental algorithms for scientific computing in Python n.d. https://doi.org/10.1038/s41592-019-0686-2.

[28] Rohatgi A. Webplotdigitizer: Version 4.6 2022.

[29] pyDOE · PyPI n.d. https://pypi.org/project/pyDOE/ (accessed December 7, 2022).

[30] Pieters PA, Nathalia BL, van der Linden AJ, Yin P, Kim J, Huck WTS, et al. Cell-Free Characterization of Coherent Feed-Forward Loop-Based Synthetic Genetic Circuits. ACS Synth Biol 2021;10:1406–16. https://doi.org/10.1021/acssynbio.1c00024.

[31] Noh M, Yoo SM, Kim WJ, Lee SY. Gene Expression Knockdown by Modulating Synthetic Small RNA Expression in Escherichia coli. Cell Syst 2017;5:418-426.e4. https://doi.org/10.1016/J.CELS.2017.08.016.

[32] Rosenbaum FP, Poehlein A, Egelkamp R, Daniel R, Harder S, Schlüter H, et al. Lactate metabolism in strictly anaerobic microorganisms with a soluble NAD+-dependent l-lactate dehydrogenase. Environ Microbiol 2021;23:4661–72. https://doi.org/10.1111/1462-2920.15657.

[33] Gorochowski TE, Borujeni AE, Park Y, Nielsen AA, Zhang J, Der BS, et al. Genetic circuit characterization and debugging using RNA-seq. Mol Syst Biol 2017;13:952. https://doi.org/10.15252/MSB.20167461.

[34] Westbrook AM, Lucks JB. Achieving large dynamic range control of gene expression with a compact RNA transcription-translation regulator. Nucleic Acids Res 2017;45:5614–24. https://doi.org/10.1093/NAR/GKX215.